Cysteine biosynthesis and the role of CysE in *Neisseria gonorrhoeae*

A thesis

submitted in partial fulfilment

of the requirements for the degree

of

Master of Science (Research) in Biological Sciences

at

The University of Waikato

by

Keely Elizabeth Ann Oldham

THE UNIVERSITY OF
WAIKATO
Te Whare Wānanga o Waikato

2020

Abstract

Neisseria gonorrhoeae is the causative organism of the sexually transmitted infection (STI), gonorrhoea. Over decades of antibiotic use, the emergence of antibiotic-resistant strains of *N. gonorrhoeae* has dramatically increased and we are facing the reality of almost untreatable gonorrhoea. Combined with increasing incidence, there is an urgent need for new antimicrobial treatments for gonorrhoea infection. The synthesis of the amino acid cysteine is a promising new target for the development of new antimicrobials. Cysteine plays an important role in protein molecules, but also in the synthesis of glutathione for protection against oxidative stress. In addition, cysteine is the key step for the incorporation of sulphur into a variety of cellular constituents. *N. gonorrhoeae* displays unique differences in assimilation of sulphate for the synthesis of cysteine, yet little is known about the synthesis of this important amino acid in *N. gonorrhoeae.*

The first step in the dual-step cysteine biosynthesis pathway is catalysed by the serine acetyltransferase, CysE, an essential gene in *N. gonorrhoeae*. To design inhibitors against this key enzyme we need to elucidate the enzymatic mechanism and the three-dimensional structure. In this thesis, we determine the kinetic parameters and regulation of CysE and present the structure of CysE to 2.01 Å. Biochemical assays demonstrate that CysE has serine acetyltransferase activity and experiences substrate inhibition by acetyl CoA. CysE is also sensitive to feedback inhibition by L-cysteine, which competitively inhibits CysE relative to the substrate L-serine. The structure shows CysE belongs to the left-handed β helix family and adopts a hexameric structure consisting of a dimer of trimers. Our structure reveals the first evidence of domain swapping for a CysE structure, where C-terminal tails domain swap with neighbouring monomers in the crystal lattice. Although an artefact of crystallisation it provides insight into the flexibility of this region.

Collectively the data presented in this thesis represents key advances in our understanding of the uncharacterised cysteine biosynthetic pathway in *N. gonorrhoeae*. Data presented here is the basis for future work using the structure of CysE to guide computational inhibitor design, to identify lead compounds for CysE inhibition, and for the development of new antimicrobials for treatment of gonorrhoea.

Acknowledgements

First of all, I would like to thank my supervisor Dr Joanna Hicks. From teaching me the lab basics, to guiding this project, you have supported me every step of the way. Your enthusiasm for this project and offering me countless opportunities, has made me thoroughly enjoy this project and I'm grateful to be one of your students.

A special thank you to Professor Vic Arcus and Dr Claire Mulholland for taking the time to help me process my structural data and analyse my structures.

Special mention to Dr Emma Summers, for being my crystal wrangler. Without your help those crystals would probably be still sitting in their drops.

Thank you Judith, for being caring and supportive, and keeping the lab running smoothly. And thank you for introducing your lemon-blueberry cake into my life.

Thank you lab family, as you have made what can be a stressful experience, memorable for all the right reasons. From the 3pm coffee trains, to wholesome board game nights, to holidays roaming the southland tussocks, to the catwalks of Queenstown, you guys have been there every step of the way and made coming to the lab everyday a joy.

I would like to thank The University of Waikato and The Waikato Graduate Women Educational Trust for funding me throughout my research.

Lastly, thank you Connor for your support and for also becoming an unwilling expert on my thesis.

Finally, thank you to my family for their unwavering support, plying me with food and always taking an interest in my research. Thank you Nana for always being there. You would be proud.

Table of Contents

List of Figures

List of Tables

List of Equations

Glossary

AcCoA	acetyl coenzyme A
ABC	ATP-binding cassette
Abs	Absorbance
APS	adenosine 5'-phosphosulphate
Arg	arginine, amino acid
Asp	aspartate, amino acid
ASU	asymmetric unit
bp	base pair
BSA	bovine serum albumin
CoA	co-enzyme A
CDC	centre for disease and control prevention
CSC	cysteine synthase complex
C-terminus	Carboxyl end of protein
CysE	serine acetyltransferase
DiANNA	DiAminoacid neural network application
DNA	deoxyribonucleic acid
DTNB	5,5′ -Dithiobis(2-nitrobenzoic acid)/ Ellman’s reagent
ESC	extended spectrum cephalosporin
FPLC	fast protein liquid chromatography
g	times the force of gravity
Glu	glutamate, amino acid

Gly	glycine, amino acid
hexahis tag	hexa-histidine tag
His	histidine, amino acid
HMM	hidden Markov model
IC_{50}	concentration of inhibitor where activity is reduced by 50%
IMAC	immobilised metal affinity chromatography
IPTG	isopropylthio-β-D-galactosidase
K_{av}	gel phase distribution co-efficient
k_{cat}	enzyme rate constant
k_{cat}/K_M	catalytic efficiency constant
K_d	dissociation constant
kDa	kilo Dalton
K_i	inhibitor constant
K_M	Michaelis constant
KO	knockout
LB	Luria Bertani
L-ser	L-serine
LβH	left handed parallel β-helix
Met	methionine
min	minutes
MMK	Michaelis Menten kinetics
MPD	2-methyl-2,4-pentanediol
MQ	milliQ ultrapure water

MR	molecular replacement
MWCO	molecular weight cut off
N-terminus	amino terminus of protein
OAS	*O*-acetylserine
PAGE	polyacrylamide gel electrophoresis
PAP	phosphoadneosylphosphate
PAPS	phosphoadenosylphosphosulphate
PCR	polymerase chain reaction
PDB	protein data bank
PEG	polyethylene glycol
pI	isoelectric point
PLP	pyridoxal-5-phosphate
PMN	polymorphonuclear neutrophil
Pro	proline, amino acid
Q4	quenching buffer
rpm	revolutions per minute
RT	room temperature (22°C)
s	second(s)
SAT	serine acetyltransferase
SDS	sodium dodecyl sulphate
SE	standard error
SEM	standard error of mean
Ser	serine, amino acid

STI	sexually transmitted infection
tNCS	translational non-crystallographic symmetry
TEMED	tetramethylethylenediamine
Tris	tris(hydroxymethyl)aminomethane
V	volts
v/v	volume per volume
Val	valine, amino acid
V_{max}	maximum reaction rate
w/v	weight per volume
WHO	world health organisation
XDS	X-ray detector software

Chapter 1

Introduction

1.1 Introduction

Gonorrhoea is a sexually transmitted infection (STI), caused by the bacterial pathogen *Neisseria gonorrhoeae* (WHO, 2017; Wi *et al.*, 2017). *N. gonorrhoeae* is a gram-negative diplococcus and is spread primarily through sexual contact. In 2016, it was estimated that there were over 85 million cases of gonorrhoea, making it the second most prevalent STI worldwide (Rowley *et al.*, 2019). Since the introduction of antibiotics in the 1940s, *N. gonorrhoeae* has acquired resistance to every single antibiotic used for its treatment. This rapid emergence of antibiotic resistance has created a demand for new antimicrobial treatments, to be able to effectively treat this disease in the future. Targeting amino acid synthesis is a new and promising route for the design of new antimicrobial drugs. The synthesis of the amino acid cysteine is one such route, not only is cysteine an important amino acid for protein function, cysteine synthesis is the primary pathway for the assimilation of sulphur in bacterial cells. However, the cysteine biosynthesis pathway is uncharacterised in *N. gonorrhoeae*. This research investigates the key enzyme for cysteine biosynthesis, CysE, as a potential drug target in *N. gonorrhoeae*.

1.2 Gonorrhoea pathogenesis

N. gonorrhoeae is an obligate human pathogen that has evolved with humans over millennia. One of the key successes of *N. gonorrhoeae* pathogenicity is its ability to mitigate host immune defences. *N. gonorrhoeae* infects mucosal surfaces with the most common site of gonorrhoea infection being the urogenital tract (Wi *et al.*, 2017). However, *N. gonorrhoeae* infection is also commonly found in the anus, nasopharynx and eyes of new born babies whose mothers have been infected with gonorrhoea (Sandstrom, 1987). Gonorrhoeal infection begins with the colonising of the mucosal membrane. *N. gonorrhoeae* adheres to the surface of epithelial cells type via their Type IV pili and opacity (Opa) adhesion like proteins (Edwards & Butler, 2011). The bacteria are internalised into the epithelial cell by endocytosis (Merz & So, 2000; Quillin & Seifert, 2018). *N. gonorrhoeae* then traffics across the

epithelial cell layer and exits at the basolateral end where it is subsequently detected by the immune system (Billker *et al.*, 2002). This prompts immune activation and a localised inflammatory response, mainly a large influx of neutrophils leading to the development of symptoms characteristic of gonorrhoea infection (Hill *et al.*, 1985; Ramsey *et al.*, 1995). However, in a large number of cases gonorrhoeal infection is asymptomatic but still transmissible, with women disproportionally affected compared to men (50 vs.10%) (Workowski & Berman, 2010), leading to persistent gonorrhoeal infection. If left untreated *N. gonorrhoeae* can ascend to the upper urogenital tract, which can lead to serious complications including infertility and pelvic inflammatory disease (Haggerty & Ness, 2006; Stevens & Criss, 2018), and in rare cases disseminate throughout the body causing arthritis (Masi & Eisenstein, 1981). Infection of the nasopharynx is also asymptomatic but transmissible via oral sex (Fifer *et al.*, 2018), but perhaps of more concern is that infection of the nasopharynx is hypothesised to be one of the main routes for acquisition of antimicrobial-resistant genes (Unemo & Nicholas, 2012). *Neisseria* species are naturally transformable and readily obtain DNA from the environment and integrate this into the chromosome (Ochman *et al.*, 2000). This natural transformability also plays a role in the generation of antigenic variation, preventing the immune system from being able to recognise the pathogen and allowing people to experience multiple gonorrhoea infections over their lifetime (Stern *et al.*, 1986; Criss *et al.*, 2005).

1.3 The emergence of antimicrobial-resistant *Neisseria gonorrhoeae*

The rapid emergence of antibiotic-resistant strains of *N. gonorrhoeae* has led to *N. gonorrhoeae* being labelled a high priority pathogen by the World Health Organisation (WHO) (WHO, 2017). Out of all STIs, *N. gonorrhoeae* has the highest levels of antibiotic resistance. Over decades of antibiotic use, *N. gonorrhoeae* has developed resistance to an extensive range of antibiotic classes including; sulphonamides, penicillins, tetracyclines, fluoroquinolones, macrolides and cephalosporins (Figure 1.1) (Unemo & Shafer, 2014; Wi *et al.*, 2017).

The United States (US) Centre for Disease Control and Prevention (CDC), recommends dual antibiotic use to help combat the rise of resistance. The current

recommended dual-therapy is the oral antibiotic azithromycin and the injectable extended-spectrum cephalosporin (ESC), ceftriaxone (Heffernan *et al.*, 2015; Wi *et al.*, 2017; Fifer *et al.*, 2018; Weston *et al.*, 2018). However, even with dual-therapy, frontline antibiotic-resistant strains have emerged both globally and locally (Wi *et al.*, 2017; Eyre *et al.*, 2018; Lee *et al.*, 2018).

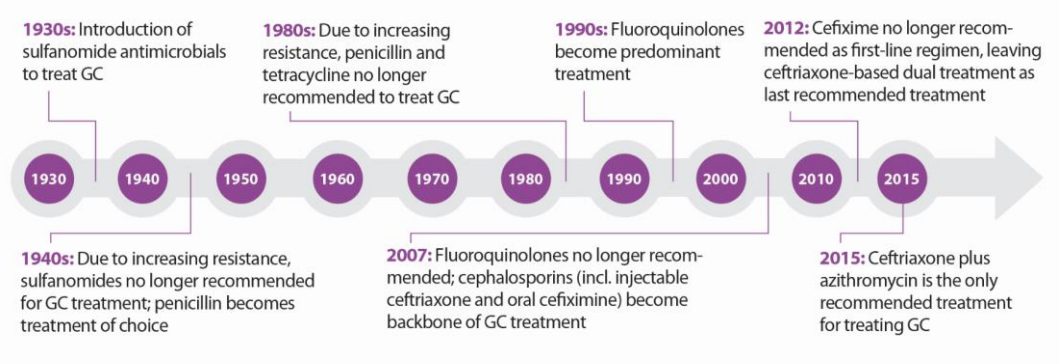

Figure 1.1: Timeline of the emergence of antibiotic-resistant gonorrhoea. Figure from (CDC, 2016).

On a global scale, antibiotic resistance to azithromycin and ceftriaxone are on the rise (Unemo & Shafer, 2014; Fifer *et al.*, 2018; George *et al.*, 2019) and *N. gonorrhoeae* has now achieved 'super-bug' status (WHO, 2017). In 2018, strains in the UK were isolated that were completely resistant to both azithromycin and ceftriaxone (Eyre *et al.*, 2018; Jennison *et al.*, 2019). These patients required hospitalisation for three days for treatment with last resort intravenous antibiotics. While there have been no cases of treatment-resistant gonorrhoea in New Zealand, resistance to azithromycin and ceftriaxone have been detected in several district health boards (Lee *et al.*, 2018; ESR, 2019). A recent study tested the antimicrobial susceptibility of 400 New Zealand *N. gonorrhoeae* isolates and demonstrated that around 10 and 4% of isolates, displayed decreased susceptibility to azithromycin and ceftriaxone, respectively (Lee *et al.*, 2018). Combined with increasing global incidence rates of gonorrhoea, there is a very real possibility that azithromycin and ceftriaxone-resistant gonorrhoea will be encountered in New Zealand. Subsequently, *N. gonorrhoeae* has been titled a 'high priority pathogen' by the WHO with research desperately needed to develop vaccines to reduce the spread of gonorrhoea, and new treatments for antimicrobial-resistant gonorrhoea infections (WHO, 2017). We need new antimicrobial targets for the design of new antibiotics.

Once such approach is through targeting pathways and mechanisms that are essential for infection and survival of *N. gonorrhoeae*.

One new and promising area of antimicrobial research is targeting amino acid biosynthesis pathways (Campanini *et al.*, 2015). The sulphur assimilation and cysteine biosynthetic pathways have been investigated for development of antimicrobials for treatment of persistent pathogens, such as the tuberculosis causing bacterium, *Mycobacterium tuberculosis*, and we hypothesise these are also a valid target in *N. gonorrhoeae*.

1.4 Oxidative stress and the role of L-cysteine in the cell

L-cysteine is the primary method of making environmental sulphur available to the cell. Cysteine is used to make a host of vital biomolecules such as iron-sulphur cluster proteins, biotin and co-enzyme A (Kredich, 2008). Cysteine is also required for reducing agents, including thioredoxin and glutathione, which are essential for mitigating intracellular oxidants (Carmel-Harel & Gisela., 2000; Kredich, 2008).

One of the main challenges for bacteria, in particular pathogens, is evasion of the host immune system and mitigation of the hostile host environment, which is where *N. gonorrhoeae* excels (Quillin & Seifert, 2018). *N. gonorrhoeae* encounters two major sources of oxidative stress; oxidative stress produced by commensal *Lactobacillus* species, and the host immune system. The immune system exerts this primarily through polymorphonuclear neutrophils (PMNs) (Seib *et al.*, 2006).

Lactobacilli are one of the predominant commensals of the female urogenital tract (Eschenbach *et al.*, 1989). *Lactobacillus* species have been shown to prevent the colonisation of *N. gonorrhoeae* (Eschenbach *et al.*, 1989). *Lactobacillus* species secrete hydrogen peroxide, which in turn inhibits growth of *N. gonorrhoeae* (St Amant *et al.*, 2002). *Lactobacilli* also secrete lactate, which lowers pH and promotes aerobic respiration, leading to the endogenous production of reactive oxygen species (ROS) (Seib *et al.*, 2006).

In gonorrhoea infection, one of the main oxidative challenges is from the host immune system. During colonisation of the surface of the cell epithelia, outer membrane vesicles (OMVs) and lipooligosaccharide (LOS) are released by *N. gonorrhoeae*, and bind to nucleotide-binding oligomerisation domain (NOD) and toll-like receptors (TLRs) on dendritic cells and macrophages (Liu *et al.*, 2006). This binding triggers the release of chemokines and cytokines (Kawasaki & Kawai, 2014). The release of cytokines recruits PMNs to the site of infection (Borregaard, 2010). Here, PMNs phagocytose *N. gonorrhoeae*, which are exposed to large amounts of oxidative stress from the neutrophil mediated oxidative burst (rapid release of ROS) (El-Benna *et al.*, 2016). While phagocytosis is an effective method for killing bacteria, *N. gonorrhoeae* has evolved the ability to survive this process and hijack these PMNs (Simons *et al.*, 2005). The purulent exudate typical of symptomatic gonorrhoea infection, largely consists of PMNs infected with *N. gonorrhoeae* (Hill *et al.*, 1985). For *N. gonorrhoeae* to be able to mitigate this oxidative stress would require effective intracellular reducing systems, and for the most part, the compounds that make up these systems are derived from L-cysteine.

Glutathione is derived from L-cysteine and is synthesised by glutathione reductase. Glutathione's role in the cell is to scavenge free radicals and prevent unwanted oxidation of the cellular contents (Meister & Anderson, 1983). Glutathione levels are one of the main mechanisms to mitigate oxidative stress encountered during infection. Glutathione levels have been reported to be three-fold greater in *N. gonorrhoeae* compared to *E. coli* (15 vs. 5 mM) (Archibald & Duong, 1986). Glutathione synthesis systems are present in *N. gonorrhoeae* (Hicks & Mullholland, 2018), but the bacteria lack glutathione transportation systems (Seib *et al.*, 2006). Given that there are no transporters present, glutathione synthesis is reliant on the cysteine biosynthesis pathway (Hicks & Mullholland, 2018).

1.5 Sulphate import, reduction and cysteine biosynthesis in *Neisseria* species

The *de novo* biosynthesis of L-cysteine is conserved across both bacterial and higher plant species. This is the predominant pathway for making inorganic sulphur available to the organism. There is a large degree of genome similarity between *Neisseria meningitidis* and *N. gonorrhoeae* (90%) (Hicks & Mullholland, 2018),

however there are key differences in terms of sulphate assimilation and cysteine synthesis, between these pathogenic *Neisseria* species, which will be addressed in this section.

1.5.1 Active transport of sulphate

Cysteine biosynthesis begins with the importation and successive reduction of sulphate inside the cell. There are two main classes of sulphate transporter proteins, the major facilitator superfamily (MFS) and ATP-binding cassette (ABC) superfamily (Guédon & Martin-Verstraete, 2007). Sulphate is actively imported into the cell by these transporters. In pathogenic *Neisseria* species (*N. meningitidis* and *N. gonorrhoeae*), genomic analysis showed that *N. gonorrhoeae* possesses only one sulphate uptake system, belonging to the ABC transporter superfamily (Figure 1.2) (Hicks & Mullholland, 2018). This is composed of a transporter permease (*cysW*), an ATP-binding protein (*cysA*), periplasmic sulphate-binding protein (*sbp*) and a sulphate permease (*cysU)* (Kertesz, 2001; Hicks & Mullholland, 2018). c*ysU* is present in both pathogenic *Neisseria* species except for *N. gonorrhoeae* strain FA1090 (Hicks & Mullholland, 2018). Previous research has shown that the sbp transporter is able to transport sulphate (Kredich, 2008) and given that *N. gonorrhoeae* is able to grow on thiosulphate as a sole sulphur source (Le Faou, 1984), this suggests that sbp is able to transport thiosulphate in *N. gonorrhoeae* (Hicks & Mullholland, 2018).

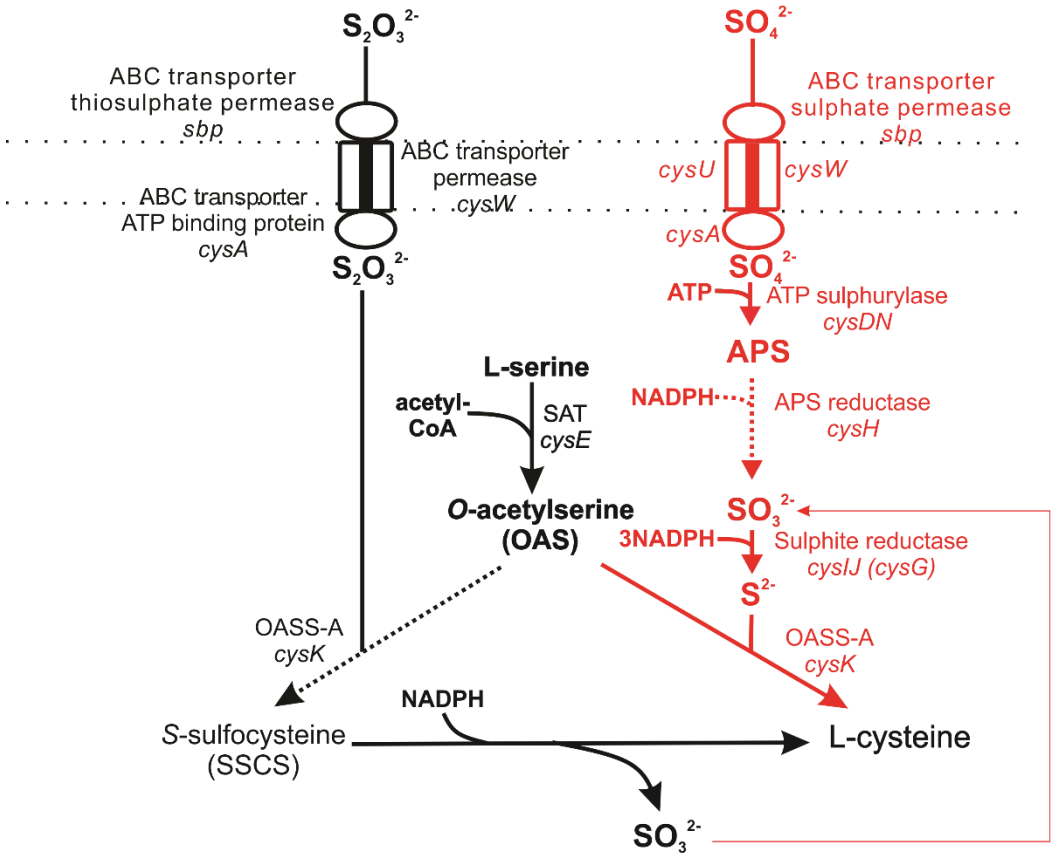

Figure 1.2: Sulphate assimilation and cysteine biosynthetic pathways in *Neisseria* species. Sulphate importation and reduction pathway (red) is non-functional in *N. gonorrhoeae*. Both pathways are functional in *N. meningitidis.* Figure from (Hicks & Mullholland, 2018).

Reduction of sulphate

Once imported into the cell, sulphate is primed for incorporation into L-cysteine through successive reduction to sulphide (Figure 1.2). In *E. coli*, sulphate is initially reduced to adenosine 5'-phosphosulphate (APS) by the multi-enzyme complex ATP sulfhydrylase (cysDN). For the majority of bacteria, APS is reduced to phosphoadenosylphosphosulphate (PAPS) by ATP-kinase (cysC), and then is reduced by PAPS reductase (cysH), to sulphite and phosphoadenosylphosphate (PAP) (Kredich, 2008). Uniquely, in *Neisseria* both reactions are carried out by a single enzyme, APS reductase (also denoted as cysH), which reduces APS directly to sulphite (Figure 1.2) (Rusniok *et al.*, 2009). The final step in the sulphate reduction pathway is the reduction of sulphite to sulphide, by sulphite reductase (cysIJ) (Kredich, 2008). Sulphide is then incorporated with O-acetylserine to form L-cysteine.

Analysis of *Neisseria* genomes revealed that the completeness and arrangement of the sulphate reduction pathway varies (Hicks & Mullholland, 2018). In *N. meningitidis*, the genes for both import and reduction of sulphate are controlled under a single operon *cysGHDNJI*. In all *N. gonorrhoeae* strains examined, a 3.5 kb deletion between genes *cysG* and *cysN* is present, removing *cysH* and *cysD* from the operon (Figure 1.3) (Hicks & Mullholland, 2018). These genes are not found elsewhere in the *N. gonorrhoea*e genome (Hicks & Mullholland, 2018). The genes *cysIJ*, encoding the sulphite reductase are present in the *N. gonorrhoeae* genome, but are non-functional due to an in-frame stop codon present in each coding sequence (Figure 1.3). The deletion of *cysD* and *cysH* would prevent the ability *N. gonorrhoeae* to reduce sulphate and the in frame stop codons in *cysIJ* would prevent the reduction of sulphite to sulphide rendering this pathway non-functional in *N. gonorrhoeae*. Previous research by Le Faou (1984), investigated the sulphur requirements of pathogenic *Neisseria*, and demonstrated that *N. gonorrhoeae* is unable to grow on sulphate as the sole source of sulphur. This is consistent with the non-functional sulphate reduction pathway in *N. gonorrhoeae* described above and differs from commensal *Neisseria* species and *N. meningitidis* which can grow on sulphate as a sole sulphur source. Previous growth experiments demonstrated that *N. gonorrhoeae* can grow on media supplemented with thiosulphate, in the absence of L-cysteine (Le Faou, 1984), which suggests that the ABC transporter complex is able to import both thiosulphate and sulphate (Hicks & Mullholland, 2018).

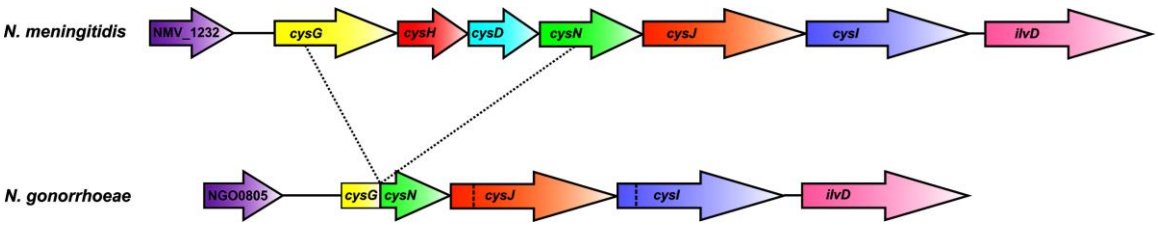

Figure 1.3: Comparison of sulphate reduction operons in *Neisseria* species. Dotted lines represent a deletion between *cysG* and *cysN* in *N. gonorrhoeae*, which results in the deletion of *cysH* and *cysD* and the partial truncation of *cysG* and *cysN*. Direction of arrows indicate direction of transcription. Dashed lines represent areas of homology. Figure from (Hicks & Mullholland, 2018).

1.5.3 Transport of L-cysteine and L-cystine

While *de novo* cysteine synthesis is well conserved across bacteria, bacteria can also obtain L-cysteine directly from the environment. Under oxidative conditions,

the majority of L-cysteine will be in its oxidised form L-cystine (two L-cysteine molecules connected by a disulphide bond) (Ohtsu *et al.*, 2010). In *Neisseria* species, L-cysteine and L-cystine are actively imported into the cell via ABC-transporters. *N. gonorrhoeae* has ABC transporters for both L-cysteine (*ngo2011-2014*), and L-cystine (*ngo0372-0374*) (Bulut *et al.*, 2012; Hicks & Mullholland, 2018). Interestingly, homology searches of the *N. meningitidis* genome revealed the presence of only the L-cystine transporter. Comparison of the *N. gonorrhoeae* and *N. meningitidis* genomes (90% sequence homology), revealed the complete deletion of the L-cysteine ABC transporter operon (Figure 1.4) from *N. meningitidis*. Further searching demonstrated that these genes were not present elsewhere in the *N. meningitidis* chromosome (Hicks & Mullholland, 2018). This suggests *N. meningitidis* either relies on L-cystine and *de novo* cysteine synthesis to meet L-cysteine demands, or has a different transporter for L-cysteine (Hicks & Mullholland, 2018). This difference might be due to differences in cysteine/cysteine availability, between the host infections sites of *N. gonorrhoeae* and *N. meningitidis*.

Across bacteria, the ability to import L-cysteine and L-cystine is well conserved, particularly in pathogens. The advantage of being able to import L-cysteine/L-cystine from the environment, is it requires less energy compared to *de novo* synthesis of L-cysteine (Takahashi *et al.*, 2018). However, transportation alone would not be ideal in a cysteine/cystine deplete or oxidative environment, and therefore justifies the need for *de novo* synthesis of L-cysteine.

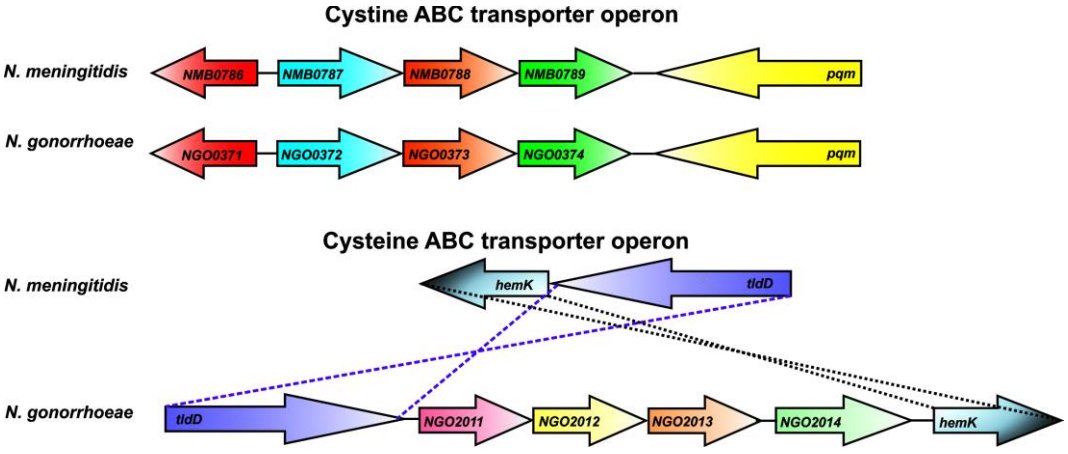

Figure 1.4: Comparison of L-cysteine and L-cystine transporters in pathogenic *Neisseria* species. L-cystine transporter operons are present in both *Neisseria* species. L-cysteine ABC transporter operon is only present for *N. gonorrhoeae* and not in *N. meningitidis*. Direction of arrows indicate direction of transcription. Dashed lines represent areas of homology. Figure from (Hicks & Mullholland, 2018).

1.5.4 Cysteine biosynthesis

The cysteine biosynthesis pathway is a two-step reaction, catalysed by serine acetyltransferase (SAT) and *O*-acetylsulfhydrylase (OASS), which have been denoted as CysE and CysK/CysM (isoforms of OASS), respectively. CysE catalyses the acetylation of L-serine, forming *O*-acetylserine and CoA. Finally, *O*-acetylserine undergoes a condensation reaction, catalysed by CysK with sulphide to form L-cysteine (Figure 1.5). The two-step pathway is regulated at the first step by feedback inhibition with L-cysteine (Figure 1.5).

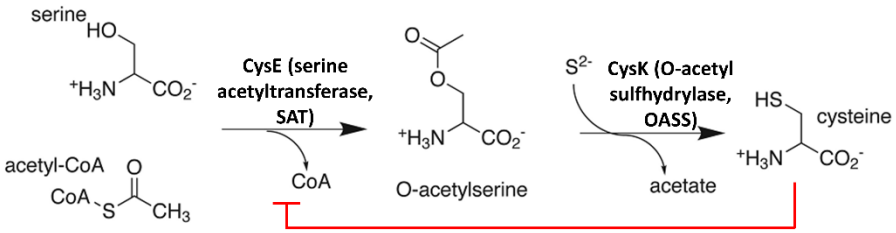

Figure 1.5: CysE and CysK reaction pathway for cysteine biosynthesis. Red line demonstrates cysteine feedback inhibition of CysE. Figure adapted from (Yi *et al.*, 2013).

CysE is a member of the left-handed β helix family and is well conserved across bacteria (Johnson *et al.*, 2005). CysE is an essential gene in *N. gonorrhoeae* (Remmele *et al.*, 2014) and while is non-essential in *N. meningitidis*, the *cysE* deletion strain grows poorly in media and has increased sensitivity to antibiotics (Capel *et al.*, 2016). The primary method of preventing high concentrations of L-cysteine, which is toxic to bacteria, is via feedback inhibition of CysE, a mechanism which is also well conserved across bacteria (Johnson *et al.*, 2004; Benoni *et al.*, 2017b).

There are two isoforms of *O*-acetylsulfhydryalase, OASS-A and OASS-B, which have been denoted as CysK and CysM, respectively (Kredich, 2008). OASS belong to the cysteine synthase superfamily and utilises pyridoxal 5'-phosphate (PLP) as a cofactor. In *S. typhimurium*, both OASS isoforms are present, but CysM was shown to be expressed under anaerobic conditions, while CysK expressed under aerobic conditions (Tai *et al.*, 1993). CysM differs from CysK as it able to directly utilise thiosulphate to create S-sulfocysteine (Tai *et al.*, 1993), which is then reduced to L-cysteine. Most bacteria have both CysK (OASS-A) and CysM (OASS-B) isoforms for the synthesis of cysteine using sulphide or thiosulphate respectively.

Neisseria species are unique in that they have only one OASS isoform with greatest homology to CysK (OASS-A), that utilises sulphide for the synthesis of cysteine (Hicks & Mullholland, 2018). This raises interesting questions regarding the role of CysK in *N. gonorrhoeae*, as the bacterium lacks the ability to reduce sulphate to sulphide and relies on thiosulphate for the synthesis of cysteine, a substrate that is usually used by the alternate OASS isoform CysK. While OASS is not an essential gene for pathogenic *Neisseria* species (Remmele *et al.*, 2014), it has been shown to be important for cell invasion in *N. meningitidis* (Capel *et al.*, 2016).

1.6 Regulation of cysteine biosynthesis

1.6.1 The cysteine synthase complex

The flux of sulphur through the cysteine biosynthesis pathway is regulated at the protein level in two ways: feedback inhibition by the pathway product, L-cysteine, and the formation of the cysteine synthase complex (CSC). This bienzyme complex was first discovered during purification of CysE and CysK from *S. typhimurium* (Kredich & Tomkins, 1966; Kredich *et al.*, 1969). Evidence of CSC formation has been confirmed in bacterial species, including *E. coli* (Mino *et al.*, 1999; Benoni *et al.*, 2017b) and *Haemophilus influenzae* (Salsi *et al.*, 2010), as well as plants (Yi *et al.*, 2013). Gel filtration chromatography and fluorometric studies have demonstrated that the stoichiometry of the CSC is composed of a 3:2 protomer ratio, consisting of one CysE hexamer and two dimers of CysK (Figure 1.6) (Kredich *et al.*, 1969; Wang & Leyh, 2012; Benoni *et al.*, 2017b). The C-terminal tail of CysE inserts into the active site of CysK to inhibit its activity.

The formation of the CSC is ultimately controlled by sulphur availability. As a part of the CSC, CysE loses sensitivity to inhibition by L-cysteine, and catalytic activity increases as a result of reduction of substrate inhibition by L-serine (Benoni *et al.*, 2017b). Contrastingly, in the CSC, CysK activity becomes almost completely inhibited (Saito *et al.*, 1995). The CSC is dissociated by millimolar amounts of CysE product *O*-acetylserine (Kredich *et al.*, 1969; Wang & Leyh, 2012) *O*-acetylserine can then non-enzymatically isomerise, forming *N*-acetylserine, which can bind to transcriptional regulator CysB and promote expression of sulphate assimilatory genes, but when sulphur is available, sulphide promotes association of the CSC (Droux *et al.*, 1998; Zhao *et al.*, 2006). Hence, the CSC acts as form of regulation in response to sulphur availability in the environment.

The binding of the CysE C-terminal peptide into the active site of CysK has been confirmed through fluorometric spectroscopy peptide binding studies, which monitored a blue shift in emission (500 nm) by CysK co-factor, pyridoxal 5'-phosphate (PLP) (Campanini *et al.*, 2005). The complex has also been shown to protect CysE from cold inactivation and proteolytic degradation (Mino *et al.*, 2001). Combined, the CSC is an important regulatory element of the cysteine biosynthetic pathway and to date is uncharacterised in *N. gonorrhoeae*.

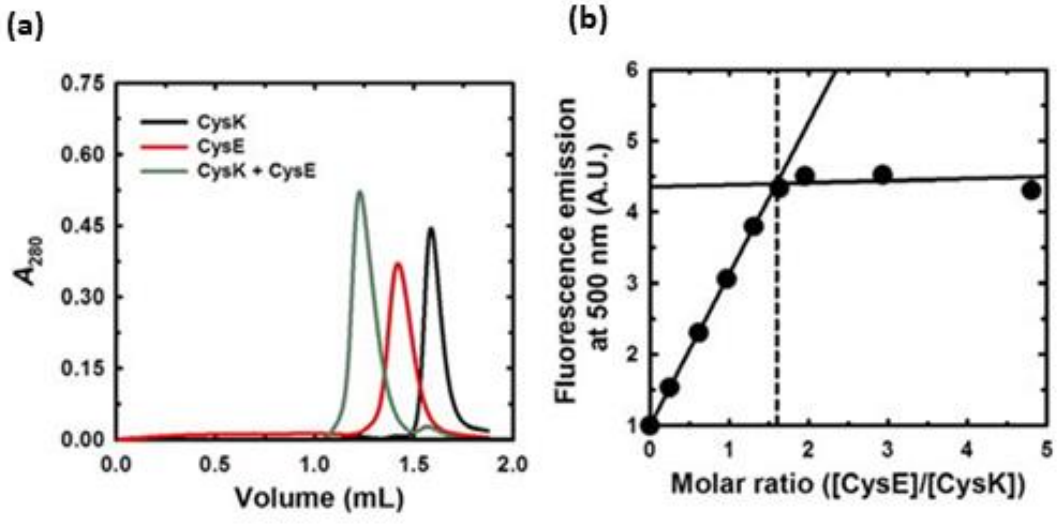

Figure 1.6: Analysis of the cysteine synthase complex from *E. coli*. (a) Example of gel filtration chromatograph of CSC, CysE and CysK. (b) Formation of the CSC through monitoring PLP emission at 500 nm with increasing [CysE/CysK] molar ratio. Figure adapted from (Benoni *et al.*, 2017b).

There is no structure of the CSC to date, however there is crystal structure of CysK from *H. influenzae*, with a ten amino acid CysE C-terminal peptide bound in the active site (Huang *et al.*, 2005). Exploration of the key residues required for binding was determined by screening a tetrapeptide library, where binding ability was monitored by CysK activity and PLP fluorescence (Campanini *et al.*, 2005). The authors demonstrated that a C-terminal isoleucine is essential for binding and inhibition of CysK. This residue has been shown to be well conserved across CSC forming organisms (Huang *et al.*, 2005; Salsi *et al.*, 2010; Benoni *et al.*, 2017b).

Using Clustal Omega (Madeira *et al.*, 2019) we generated a sequence alignment of five sequences for bacterial CysE homologues and were analysed using ESPript 3.0 (Figure 1.7)(Robert & Gouet, 2014). CysE from *N. gonorrhoeae* shows moderate sequence similarity to the compared CysE homologues (57%, with the exception of *N. meningitidis*, 97%). Here we see that the C-terminus four peptide fragment, GDGI, is well conserved between *Yersinia pestis*, *E. coli* and *S. typhimurium*. In *Neisseria* species this peptide sequence is DFMI. Due to conservation of the C-terminal isoleucine we expect CysE from *N. gonorrhoeae* to form the CSC. Given that there are key differences in the sulphate assimilation pathways between *N. gonorrhoeae* and other bacteria, characterisation of the CSC would provide further insight into sulphur assimilation and synthesis of L-cysteine in *N. gonorrhoeae*.

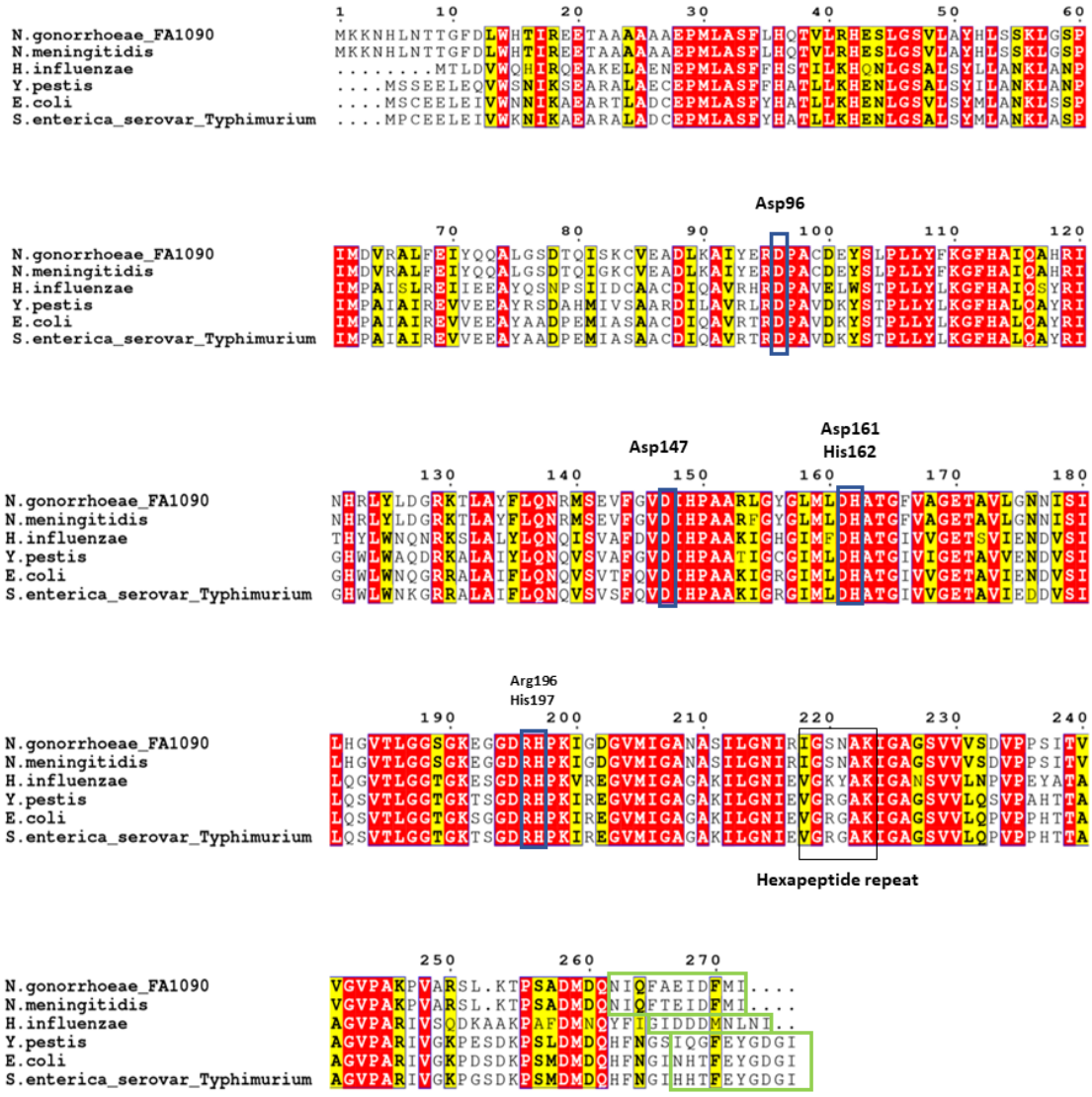

Figure 1.7: CysE peptide sequence alignment. The *N. gonorrhoeae* FA1090 CysE peptide sequence was aligned to the following CysE homologues; *N. meningitidis* (97% sequence similarity); *H. influenzae* (54.8% sequence similarity); *Y. pestis* (57% sequence similarity); *E. coli* (57.4% sequence similarity) and *S. typhimurium* (57% sequence similarity). Highly conserved residues are highlighted in red, and less conserved residues are highlighted in yellow. Active site residues for CysE are surrounded by a blue box. Example of hexapeptide repeat highlighted in black box. The last ten residues of C-terminal tail are surrounded by a green box. Sequence alignment created using Clustal Omega. Figure created using ESPript 3 (Robert & Gouet, 2014).

1.6.2 Transcriptional regulation of sulphate assimilation and cysteine biosynthesis

Transcriptional regulation of the cysteine regulon is controlled by the master regulator CysB. CysB is a tetramer and a member of the LysR family of transcription factors (Henikoff *et al.*, 1988). Within the CysB N-terminal domain is a helix-turn-helix motif which allows DNA binding (Pabo & Sauer, 1984). CysB

positively regulates the sulphate assimilatory and cysteine synthesis genes, in the presence of cysteine pathway intermediate, *N*-acetylserine (isoform of *O*-acetylserine) (Ostrowski & Kredich, 1989; Hryniewicz & Kredich, 1991). The CysE product *O*-acetylserine is unstable and rapidly and non-enzymatically forms the isoform *N*-acetylserine. The proposed mechanism for CysB-mediated activation is binding of *N*-acetylserine produces a conformational change in CysB, which then binds to CysB binding regions and recruits RNA polymerase (Hicks & Mullholland, 2018). Investigation of CysB regulation in *S. typhimurium* demonstrated that CysB upregulated expression of sulphate assimilation genes *cysJIH*, *cysK* and *cysP* (Ostrowski & Kredich, 1989). CysB also negatively autoregulates its own transcription through binding upstream of its own promoter (Jagura-Burdzy & Hulanicka, 1981; Ostrowski & Kredich, 1991). Hicks and Mullholland (2018) identified the presence of the DNA binding repeat for CysB (CCGTTG-N_{17}-CAACGG) in the *cysB* promoter region in both *N. gonorrhoeae* and *N. meningitidis*. However, these binding sites could not be confirmed at the start of the sulphate reduction regulon or cysteine biosynthetic genes in *N. gonorrhoeae*. This could be due low conservation of CysB binding sequences.

cysB is an essential gene in *N. gonorrhoeae* (Remmele *et al.*, 2014). During *in vivo* infection, *cysB* expression was downregulated compared to growth on media (McClure *et al.*, 2015). Transcriptional regulation of the cysteine regulon is particularly important for pathogenic bacteria, as the success of infection is dependent on the ability of the organism to rapidly adapt to and overcome host defences. The only gene in the sulphate assimilation and cysteine biosynthesis regulon not under CysB transcriptional regulation is *cysE*, which is constitutively expressed (Jones-Mortimer *et al.*, 1968; Kredich, 1971). However, CysE experiences regulation at the enzyme level, with feedback inhibition by L-cysteine and formation of cysteine synthase complex.

1.7 CysE

1.7.1 Structural characteristics of CysE

The serine acetyltransferase (SAT), CysE, belongs to the left-handed parallel β-helix (LβH) family. LβH proteins are defined by a hexapeptide tandem repeat, consisting of [LIV]-[GAED]-X_2-[STAV]-X, that gives rise to a left handed β-barrel, which is a unique structural feature of these proteins (Raetz & Roderick, 1995). SATs are composed of two structural domains: an amino-terminal (N-terminal) α-helical domain and an LβH carboxyl-terminal (C-terminal) domain. The LβH domain is structured like triangular prism, which fit with two other monomers, to form a trimer (Johnson *et al.*, 2005). The resulting trimer dimerises to forms a hexamer through hydrophobic interactions at the N-terminal face of each trimer (Pye *et al.*, 2004). SATs are unique as they are the only acyltransferase to adopt a hexameric conformation, instead of the more common trimeric arrangement (Johnson *et al.*, 2005). This higher oligomeric state allows for pathway regulation through formation of the CSC (Mino *et al.*, 1999; Wirtz & Hell, 2006; Benoni *et al.*, 2017b), which has been shown to not form in a rare trimeric form of SAT from *Entamoeba histolytica* (Kumar *et al.*, 2011).

To date there are only six bacterial CysE structures deposited in the Protein Data Bank (PDB). Independent of sequence similarity there is good structural conservation between bacterial and plant CysE proteins (Olsen *et al.*, 2004; Yi *et al.*, 2013). Structures include CysE in the apo, L-serine (substrate), CoA (product) and L-cysteine (inhibitor) bound forms (Figure 1.8). Both L-serine and L-cysteine bind in the bottom of the CysE active site, above the extended β-loop. Comparison of structures with L-serine and CoA bound, demonstrates that the thioester group from CoA is in close proximity to L-serine bound in the active site, supporting the proposed mechanism of serine acetyltransferases.

The C-terminal tail of the CysE monomer that binds to CysK to form the CSC has also been implicated in L-cysteine inhibition. Deletion of the C-terminal tail reduces L-cysteine sensitivity (increased K_i for L-cysteine) (Mino *et al.*, 1999). The C-terminal tail is often unmodelled in apoenzyme structures, but adopts a folded conformation for L-cysteine bound structures, which is visible for CysE proteins from *E. coli*, *H. influenzae, Y. pestis* and *Glycine max* (soybean) (Pye *et al.*, 2004) (Olsen *et al.*, 2004) (Kim *et al.*, 2006; Yi *et al.*, 2013). We can observe this in Figure 1.8, where the folded C-terminal tails are present in the cysteine bound structure (Figure 1.8c), but are undefined for L-serine and CoA-bound structures (Figure 1.8a and b). In this folded conformation the C-terminal tail competes directly with the binding site of acetyl CoA/CoA. This structural evidence supports the competitive inhibition mechanism for L-cysteine relative to acetyl CoA seen in inhibition assays (Hindson & Shaw, 2003);(Hindson, 2003; Johnson *et al.*, 2004), making L-cysteine a competitive inhibitor for both L-serine and acetyl CoA.

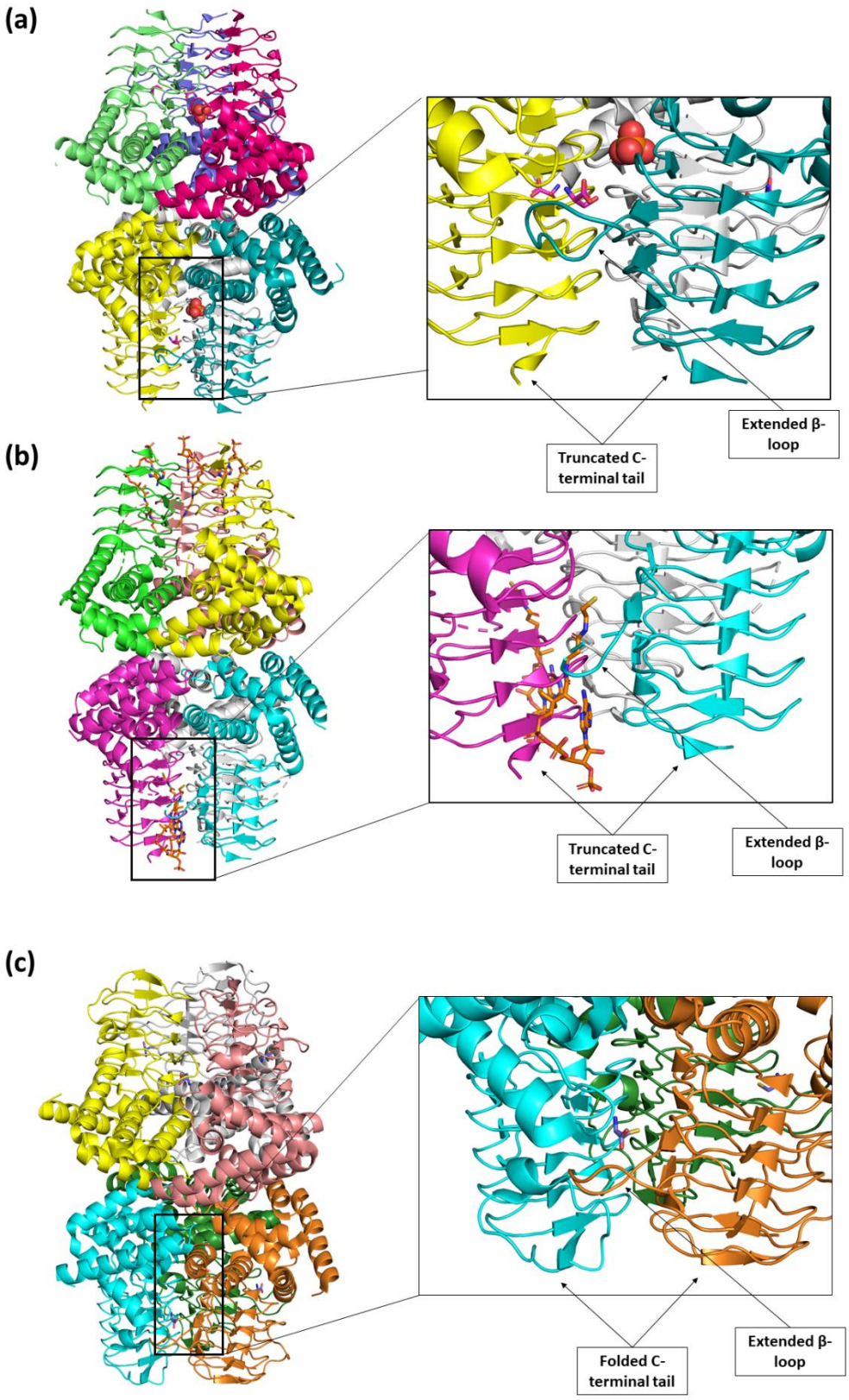

Figure 1.8: Comparison of L-serine, CoA and L-cysteine CysE binding sites. (a) Structure of L-serine bound to CysE from soybean *Glycine max* (4N6B). L-serine represented as pink sticks. Phosphate represented as spheres (b) Structure of CysE with CoA bound from soybean *Glycine max* (4N69). CoA represented as orange sticks (c) Structure of CysE with L-cysteine bound from *E. coli* (1T3D). L-cysteine represented as purple sticks. Images generated using PyMOL.

Members of the left handed parallel β-helix (LβH) family, including CysE, have a conserved histidine in the active site (Johnson *et al.*, 2005). The proposed mechanism for the acetyl-transfer reaction of CysE, is by a general acid-base catalysis, where the histidine, alongside a conserved aspartate act to form a catalytic triad with substrate L-serine. (Pye *et al.*, 2004; Johnson *et al.*, 2005). In *E. coli* this aspartate residue (Asp143) is positioned, in close proximity (2.8 Å) to the well conserved histidine (His158), which is predicted to transform the histidine into a strong base (Figure 1.9, Figure 1.10) (Pye *et al.*, 2004). His158 activates the β-hydroxyl group of L-serine, for nucleophilic attack on the acetyl thioester of acetyl CoA, through acting as a base and accepting a hydrogen from the hydroxyl group (Figure 1.10). The nucleophilic attack on acetyl CoA forms a ternary complex between the enzyme, L-serine and acetyl CoA (E:L-serine:acetylCoA), before the histidine behaves as a general acid and donates a hydrogen to the sulphur group of acetyl CoA, leading to collapse of the complex and product release (Figure 1.10) (Pye *et al.*, 2004; Johnson *et al.*, 2005). The CysE active site from *E. coli* with L-cysteine bound, has been used here to illustrate the co-ordination of the active site residues. Ternary intermediate modelling by (Pye *et al.*, 2004), demonstrated that the carboxylic acid and amine group of L-serine would interact with the same active site residues as L-cysteine, allowing prediction of the reaction mechanism of CysE. The importance of these active site residues for catalysis has been demonstrated using site directed mutagenesis (Guan *et al.*, 2008). The results from solvent deuterium isotope effect studies, would suggest that the generation of the E:L-serine:acetylCoA is the rate-limiting step of this reaction (Quinn & Sutton, 2011).

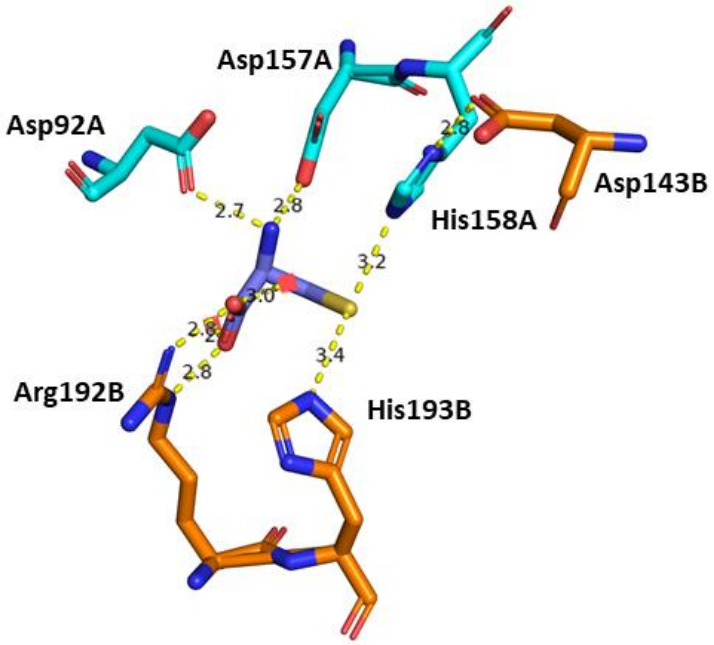

Figure 1.9: Active site residues from CysE from *E. coli* with L-cysteine (1T3D). Hydrophilic interactions denoted as dashed yellow lines. Distances are in angstroms. Active site residues are denoted as sticks, coloured based on which chain they reside on, with chain A coloured cyan and chain B coloured orange. L-cysteine is denoted as purple sticks. Figure generated in PyMOL

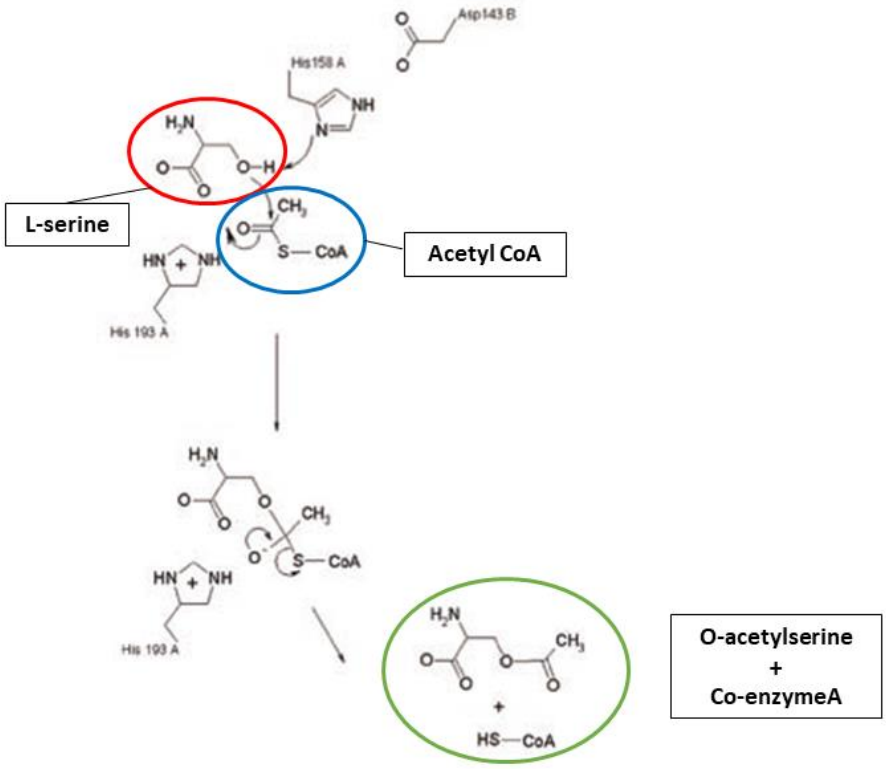

Figure 1.10: Reaction mechanism for CysE from *E.coli*. Substrates L-serine and acetyl CoA, are highlighted in red and blue, respectively. Reaction products *O*-acetylserine and co-enzyme A ae highlighted in green. Figure adapted from (Pye *et al.*, 2004).

1.7.2 CysE kinetic mechanism

The kinetics of CysE homologues from both bacteria and plants have been studied extensively. As CysE utilises two substrates for product formation there are two possible catalytic mechanisms: sequential and ping-pong. In a ping-pong mechanism, one of the products is released before all substrates have bound, generating an enzyme intermediate in the process. In a sequential kinetic mechanism, both substrates bind to the enzyme, before product(s) are released. This mechanism can be random, where both forms of substrate binding and product release occur or ordered where both substrates bind, and product(s) are released in a specific order. Both mechanisms generate a ternary complex (enzyme:substrateA:substrateB) (Fersht, 2017). Initial research hypothesised a ping-pong reaction mechanism for CysE (Leu & Cook, 1994). However, a combination of equilibrium isotope exchange experiments (Hindson & Shaw, 2003) and collection of Lineweaver-Burk plots (Hindson & Shaw, 2003; Johnson *et al.*, 2004; Benoni *et al.*, 2017b) overwhelmingly supports a sequential binding mechanism and formation of the ternary complex in Figure 1.10. The exact type of sequential mechanism reported for CysE does vary, with a random sequential mechanism reported for CysE from *E. coli* (Hindson & Shaw, 2003) and an ordered binding mechanism reported for CysE from *H. influenzae* (Johnson *et al.*, 2004), where acetyl CoA binds first, followed by L-serine (Figure 1.11).

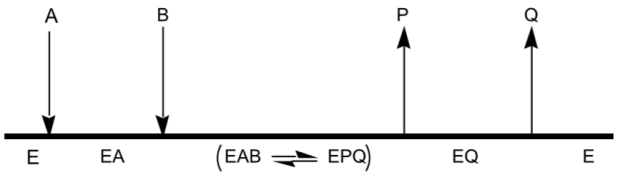

Figure 1.11: Ordered sequential mechanism for CysE from *Haemophilus influenzae*. The scheme here depicts that acetyl CoA is the first substrate to bind (A) and L-serine the second substrate to bind (B) and the product co-enzyme A is the first to leave (P) followed by product *O*-acetylserine (Q). A = acetyl CoA, B = L-serine, EAB = enzyme and substrates complex, EPQ = enzyme and products complex, P = co-enzyme A, Q = *O*-acetylserine. Figure from (Johnson *et al.*, 2004).

1.8 CysE as a drug target

Targeting the cysteine biosynthesis pathway has garnered interest regarding developing new antimicrobials, as cysteine biosynthesis pathways has been shown to be important for pathogen virulence and antibiotic resistance. As mammals synthesise L-cysteine through the reverse-transsulphuration of methionine obtained from diet, they do not have possess this reductive sulphate assimilation pathway, making this a promising target for drug development (Thomas & Surdin-Kerjan, 1997; Hicks & Mullholland, 2018). Research into developing inhibitors has already begun for targeting CysK isoforms for pathogenic bacteria including *S. typhimurium* (Spyrakis *et al.*, 2013) and *M. tuberculosis* (Brunner *et al.*, 2016)

A transcriptomic study showed that *cysE* (NGO_1423) is an essential gene in *N. gonorrhoeae* MS11 (Remmele *et al.*, 2014). The authors used genome wide transposon-mediated mutagenesis to knockout and determine the essentiality of genes. Essentiality was tested by growing gene-deletion strains on GCB plates supplemented with L-cysteine. The essentiality of *cysE* demonstrates that for *N. gonorrhoeae*, L-cysteine requirements cannot be met solely from the import of cysteine from the environment.

CysE has been evaluated as a drug target in *E. coli*. Inhibitors were identified through computational screening, and the most promising inhibitor was confirmed through inhibitor assays as a moderate inhibitor with an inhibition constant (K_i) of 72 µM (Turnbull & Surette, 2010). Together, this information supports our project aims to biochemically characterise CysE, and in turn use this information for future computational-inhibitor screening and inhibitor design.

The regulation of cysteine biosynthesis has not been well studied in *N. gonorrhoeae*. *N. gonorrhoeae* lacks the necessary transporters for glutathione uptake, and it is hypothesised that cysteine biosynthesis is responsible for the synthesis of glutathione (Seib *et al.*, 2006). Although, *N. gonorrhoeae* has cysteine and cystine transporters, it is likely that to maintain high intracellular concentrations of glutathione and given the essentiality of both *cysB* and *cysE*, *N. gonorrhoeae* likely relies on *de novo* cysteine synthesis to meet these high L-cysteine demands.

Although *N. gonorrhoeae* cannot grow on sulphate as it lacks the ability to reduce sulphate to sulphide (by virtue of genome deletions and in frame stop codons) it is able to grow on thiosulphate as the sole source of sulphur. We suggest that *N. gonorrhoeae* has a different, yet functional cysteine biosynthetic pathway, and as an essential part of that, a functional serine acetyltransferase for step one in the synthesis of cysteine. Genome searches and sequence comparisons identified an annotated and likely functional serine acetyltransferase in *N. gonorrhoeae* FA1090.

1.9 Research Objectives

The aim of this research is to characterise a key enzyme in the *N. gonorrhoeae* cysteine biosynthetic pathway, CysE (EC 2.3.1.30). Characterisation of the biochemical and biophysical properties of CysE from *N. gonorrhoeae* guide future research for the development of new antimicrobials and will improve our understanding of the pathogenicity of *N. gonorrhoeae*. The following objectives were set to achieve this:

Objective 1:

Investigate the serine acetyltransferase activity and L-cysteine inhibition of CysE from *N. gonorrhoeae*. This will involve development of a kinetic assay to measure SAT activity and subsequent characterisation of Michaelis Menten kinetics, reaction mechanism and L-cysteine inhibition.

Objective 2:

Determine the three dimensional structure of CysE using protein crystallisation and X-ray diffraction. We will collect an apoenzyme structure, as well as structures complexed with either substrate (acetyl CoA and L-serine), and with product feed-back inhibitor L-cysteine.

Objective 3:

Characterise the cysteine synthase complex from *N. gonorrhoeae*. This will involve purification of CysK alongside CysE, forming the CSC and biophysically characterising the stoichiometry of the complex and biochemical activity of CysE as a part of the complex.

Chapter 2

Biochemical characterisation of CysE

2.1 Introduction

CysE is a key enzyme in the biosynthesis of cysteine in bacteria and plants. It catalyses the first step of the two-step cysteine synthesis reaction (Figure 1.2). CysE is a serine acetyltransferase (SAT, EC:2.3.1.30) and is a member of the left-handed β-helix (LβH) acyltransferase family. SATs catalyse the acyl transfer from acetyl CoA to the β-hydroxyl group of L-serine forming, O-acetylserine and co-enzyme A (Figure 1.5) (Pye *et al.*, 2004; Johnson *et al.*, 2005). In the second step of the cysteine synthesis reaction the activated form of L-serine, *O*-acetylserine, undergoes a condensation reaction with sulphide, catalysed by *O*-acetylserine sulfhydrylase (OASS, CysK, EC:2.5.1.47)(Kredich *et al.*, 1969). CysE itself is regulated by feedback inhibition by the pathway product, L-cysteine (Hindson, 2003; Johnson *et al.*, 2004; Kumar *et al.*, 2014; Benoni *et al.*, 2017b). Sequence alignment of CysE homologues with CysE from *N. gonorrhoeae*, shows conservation of key secondary structures and the active site residues, His162 and Asp147 (His158 and Asp143 in *E. coli*), which form the catalytic triad with substrate L-serine, enabling acyl transfer (Figure 1.7 and Figure 1.10). Given that these active site residues are present, we predict that CysE from *N. gonorrhoeae* will have serine acetyltransferase activity.

SATs and related LβH acyltransferases are a relatively well studied family of enzymes. CysE enzymes from other bacteria have an ordered sequential mechanism, with acetyl CoA binding ahead of L-serine (Johnson *et al.*, 2004; Benoni *et al.*, 2017b). Initially CysE from *E. coli* was shown to have a random-order sequential mechanism (Hindson, 2003; Hindson & Shaw, 2003), but more recent research by Benoni *et al.* (2017b) and Johnson *et al.* (2004), measuring CysE activity using a direct assay (monitoring absorbance at 232 nm), suggests an ordered mechanism in keeping with the majority of characterised CysE homologues.

The cysteine biosynthetic pathway is feedback inhibited by L-cysteine binding to CysE. L-cysteine competes directly with L-serine for the active site of the enzyme displaying competitive inhibition (Johnson *et al.*, 2004). This mechanism of inhibition appears to be well conserved across the CysE family (Hindson, 2003; Johnson *et al.*, 2004). Analysis of co-crystallised crystal structures of CysE with L-cysteine, shows L-cysteine bound in the L-serine binding pocket located in the CysE active site (Pye *et al.*, 2004; Kim *et al.*, 2006), supporting the observation of L-cysteine being a competitive inhibitor relative to L-serine (Kredich & Tomkins, 1966; Johnson *et al.*, 2004). Interestingly, L-cysteine has also being reported to be a competitive inhibitor relative to acetyl CoA (Johnson *et al.*, 2004). This is due to L-cysteine inducing a conformational change in the C-terminal tail, which precludes acetyl CoA from binding to the acetyl CoA binding site (Yi *et al.*, 2013). This is thought to be part of the mechanism to prevent the unwanted acetylation of L-cysteine, given that it is isostructural to L-serine.

We propose that CysE is a good target for the design of new antimicrobials to treat antimicrobial-resistant *N. gonorrhoeae.* Inhibitor design relies on not only structural characterisation of the enzyme, but also a detailed understanding of the enzyme's kinetics and reaction mechanism. This chapter biochemically characterises CysE to understand the Michaelis Menten kinetics, mechanism of action and the mechanism of inhibition by L-cysteine. There are two published assays to measure CysE activity. The first is a coupled continuous assay where 5,5-Dithiobis(2-nitrobenzoic acid) (DTNB) is used to measure CoA production at 412 nm (Kredich & Tomkins, 1966). The second is a direct continuous assay where the depletion of acetyl CoA is measured at 232 nm over the course of the assay. The direct continuous assay as in (Chronis & Krishnan, 2004) was used for the kinetic characterisation of CysE in this chapter. Although activity is measured at a low wavelength, this simple assay gives a direct readout of CysE activity, whereas a coupled assay has the potential to induce error with the reaction of CoA with DTNB been a limiting factor in the reaction.

2.2 Materials and Methods

2.2.1 Cloning of CysE for expression in *Escherichia coli*

The *cysE* gene NGO_1423 was codon optimised for *E. coli* and ordered from Geneart (Thermo Fisher) (Appendix A). The synthetic *cysE* construct was cloned into expression vector pET28b with an N-terminal hexahistidine-tag, between Ndel and Xhol restriction sites by Dr Joanna Hicks (The University of Waikato). The NGO_1423 pET28b plasmid was checked by DNA sequencing before transformation into *E. coli* BL21 (DE3) for protein expression. Positive transformants were selected for by growing overnight at 37°C, Luria-Bertani (LB)-agar (Appendix A2) supplemented with 50 $\mu g.ml^{-1}$ kanamycin.

2.2.2 Long-term storage of BL21 CysE expression strains

Seeder cultures were prepared from positive transformants, by inoculating a single colony from a transformation plate into 10 ml of LB broth supplemented with 50 $\mu g.ml^{-1}$ kanamycin and incubated at 37°C, shaking at 200 rpm, overnight.

Glycerol stocks were prepared from seeder cultures, 0.5 ml of seeder culture and 0.5 ml of sterile 50% glycerol (w/v) were combined and stored at -80°C.

2.2.3 CysE expression cultures

Large scale expression cultures were prepared by inoculating 10 ml of seeder culture (prepared as per section 2.2.2) into 1 L of LB broth, supplemented with 50 $\mu g.ml^{-1}$ kanamycin. Cultures were incubated at 37 °C, 200 rpm until the culture reached log phase of growth (optical density at A_{600} = 0.5-0.7), at which point protein expression was induced by the addition of 1 ml of 0.75 M isopropylthio-β-D-galactosidase (IPTG) (final concentration 0.75 mM). Cultures were returned to 37°C, 200 rpm and incubated overnight.

Expression cultures were centrifuged at 4,600*g* for 20 min at 4°C, after which the supernatant was discarded. The remaining cell pellet was resuspended in 25 ml of lysis buffer (50 mM Tris pH 8.0, 200 mM NaCl, 20 mM imidazole). The resuspended culture was transferred to a 50 ml falcon tube and centrifuged for a further 20 min at 4,600*g*, 4°C. After centrifugation, the supernatant was discarded, and the pellet was stored at -80°C.

2.2.4 Purification of CysE

CysE was isolated and purified using immobilised metal affinity chromatography (IMAC) and gel filtration chromatography. Protein solubility was assessed using SDS-PAGE gel electrophoresis. Oligomeric state was measured using gel filtration chromatography and native-PAGE gel electrophoresis.

2.2.4.1 Immobilised metal affinity chromatography

Frozen CysE cell pellets (section 2.2.3) were thawed at room temperature. Cell pellets were resuspended by vortexing in 25 ml of lysis buffer (50 mM Tris pH 8.0, 200 mM NaCl, 20 mM imidazole), and one cOmplete™, Mini, EDTA-free Protease Inhibitor Cocktail tablet (Roche, Switzerland) was added to inhibit cellular proteases. Cells were lysed using a Misonix sonicator on setting four (microtip probe (5-50 ml volume)). Cells were sonicated on ice for 5 min, in alternating 30 s bursts, with 30 s intervals of no sonication, (2.5 min of sonication in total).

The sonicated lysate was centrifuged at 20,000*g* for 20 min at room temperature. The supernatant was filtered through 1.2, 0.45 and 0.2 µm filters. IMAC purification was carried out using either an AKTÄ Purifier fast protein liquid chromatography (FPLC) system (GE Life Sciences, New Zealand) or an NGC FPLC system (BioRad). The same method for IMAC and gel filtration was used for either FPLC system. The filtered supernatant was manually loaded onto a HisTrap™ HP 5 ml column (GE Life Sciences, New Zealand) that was pre-equilibrated in lysis buffer. The column was attached to the FPLC and flushed with 20 ml of lysis buffer at 2 ml.min^{-1}. The concentration of elution buffer (50 mM Tris pH 8.0, 200 mM NaCl, 1 M imidazole) was gradually increased to 50%, over 25 ml, to elute the HexaHis-tagged CysE.

2.2.4.2 Gel filtration chromatography

At room temperature (22°C), IMAC peak fractions were concentrated in a 10,000 Da MWCO Amicon® spin concentrator at 3,600*g* for 20 min, or until the volume of protein concentrate was reduced to 0.75 ml. The concentrate was loaded onto a Enrich 650 analytical gel filtration column (Bio-Rad Laboratories, USA), pre-equilibrated in gel filtration buffer (50 mM Tris pH 8.0, 100 mM NaCl) with a flow rate of 1 ml.min^{-1}. Concentrated protein was manually loaded into the injection loop

of the FPLC for injection onto the column. After sample injection 28 ml of gel filtration buffer was run at 1 ml.min^{-1} through the column. Fractions of eluted protein were collected and stored at room temperature.

2.2.4.3 SDS and native-PAGE gel electrophoresis

Native-PAGE gels were used for both native-PAGE and SDS-PAGE gel electrophoresis. This was accomplished by addition of SDS to sample loading buffer and running buffer. Native-PAGE gels were composed of both a resolving and stacking layer, at 12 and 5% polyacrylamide, respectively. All gels were made in house in a multi-gel caster (Hoefer). The resolving layer was prepared by mixing the "Resolving layer" components listed in Table 2.1, and filling the gel caster, leaving a three cm gap at top of the gel plate. Isopropanol was then applied to the top of the gel (3 ml) and was left until the resolving layer had polymerised (30 min). Once set, the isopropanol layer was carefully removed, the stacking layer was prepared by combining "Stacking Layer" components listed in Table 2.1 and filling to the top edge of the gel caster. A ten well comb was inserted into the top of each gel, before leaving to set at room temperature for 30 min. Gels were stored at 4°C for up to four weeks.

Protein samples were prepared for gel-loading by mixing 15 µl of sample with 5 µl of 4x SDS loading dye (also known as Quench, Q4) (Appendix B). 20 µl of sample was loaded per well, along with 10 µl of Precision Plus Protein™ ladder (Bio-Rad Laboratories, USA) per gel. The gels were run in 1 x Tris-Glycine SDS-PAGE running buffer (Appendix B) at a constant 150 V, until the loading dye migrated to the end of the resolving gel, where it was reduced to 100 V. The gel was run until the dye migrated to the end of the gel.

Protein bands were visualised by staining in Coomassie Fairbanks stain (Appendix B). Gels and stain were heating by microwaving for 30 s, followed by five min incubation at room temperature with agitation (120 rpm). Stained gels were rinsed with distilled water and left in destaining solution (10% acetic acid) overnight. Destained gel bands were visualised using an Omega Lum™ gel imager (Aplegen, USA).

Table 2.1: Components for five native-PAGE gels. Ammonium persulphate (APS) stock solution was prepared fresh weekly.

Component	**12% Resolving layer (ml)**	**8% Stacking layer (ml)**
Resolving buffer (1.5 M Tris pH 8.8)	7.5	-
Stacking buffer (1 M Tris pH 6.8)	-	1.6
30% Polyacrylamide/Bis (375:1) (v/v)	10.0	2.125
10% APS (w/v)	0.15	0.063
10% TEMED	0.015	0.0063
MQH_20	10.35	8.625

2.2.4.4 Measuring the oligomeric state of CysE

Previously, the Enrich650 gel filtration column (Bio-Rad Laboratories, USA) was calibrated in gel filtration buffer (50 mM Tris pH 8.0, 200 mM NaCl) using Gel Filtration Standards (Bio-Rad Laboratories, USA), by Dr Joanna Hicks. The calibration curve can be found in Appendix B.2. The molecular weight of CysE was calculated taking the peak elution volume ($V_{e)}$ and calculate the K_{av} gel phase distribution co-efficient using Equation 2.1, where V_o is the column void volume and V_c is the total column volume: The calibration standard curve relating K_{av} and molecular weight was used to determine the molecular weight of CysE from the calculated K_{av}.

Equation 2.1: Formula for calculating gel phase distribution co-efficient

$$K_{av} = \frac{V_e - V_o}{V_c - V_o}$$

2.2.4.5 Measuring protein concentration Nanodrop™

Protein concentration was determined by Nanodrop™ 2000 (Thermofisher, USA) measuring absorbance at 280 nm. This protein quantification method works by

measuring the absorbance of tryptophan residues (280 nm). Protein concentration was calculated using Beer-Lambert law (Equation 2.2), where absorbance readings were corrected by dividing the Nanodrop™ reading (1 Abs = 1 $mg.ml^{-1}$) by the molar absorption co-efficient of the CysE protein, ($\mathcal{E}$ = 0.555 L mol^{-1}/cm^{-1}) as determined by ProtParam (Gasteiger *et al.*, 2005).

Equation 2.2: Beer-Lambert equation. A= absorbance, $\mathcal{E}$ = molar absorption co-efficient (L mol^{-1}/cm^{-1}), l = pathlength (cm) and c = concentration ($molL^{-}$).

$$A = \varepsilon cl$$

2.2.4.6 Disulphide bond prediction

Disulphide prediction for CysE was carried out using DiANNA 1.1 (Ferrè & Clote, 2006).

2.2.5 Kinetic assay parameters

CysE was purified by IMAC and gel filtration chromatography as per sections 2.2.4.1 and 2.2.4.2. Protein concentration was measured by absorbance at 280 nm using a Nanodrop™ (section 2.2.4.5). All CysE protein used in assays was purified the same day. All assays were carried out in gel filtration buffer (50 mM Tris pH 8.0, 100 mM NaCl). Master stocks for both substrates L-serine and acetyl CoA, were prepared in gel filtration buffer (50 mM Tris pH 8.0, 100 mM NaCl). An enzyme working stock of 0.134 $mg.ml^{-1}$ (5.3 nM, CysE monomer 31.6 kDa) was prepared at the beginning of the assay and stored at room temperature (22°C) before and for the duration of the assays.

2.2.5.1 Assay parameters

Assay data was collected using the same gel filtration buffer (50 mM Tris pH 8.0, 100 mM NaCl). Assays were carried out in a 500 µl quartz cuvette, with total assay volume of 400 µl. Assay components

Table 2.2: CysE kinetic assay setup. Concentrations of substrate were varied by adjusting the volume of substrate master stock added, unless the volume to be added was less than 4 µl or greater than 40 µl, and then a more dilute or concentrated stock was used, respectively. This was done to prevent lowering the overall temperature of the assay, as substrate stocks were stored on ice for the duration of the assays. Amount of enzyme used for each reaction was kept constant (0.00156 $mg.ml^{-1}$).

Component	Volume (µl)
Buffer	315-387
L-serine	4-40
Acetyl CoA	4-40
Enzyme	5
Total	400

All substrate stocks were prepared in assay gel filtration buffer (50 mM Tris pH 8.0, 100 mM NaCl). Acetyl CoA stock aliquots were stored following manufacturer's instructions at -80°C, to prevent unwanted hydrolysis of acetyl CoA to co-enzyme A. Stocks were thawed at room temperature and stored short-term on ice for assays. Acetyl CoA was purchased as a powdered tri-lithium salt from Roche (MW = 827.5 $g.mol^{-1}$) and stored as a powder at 4°C. L-serine stocks were also prepared and stored at -80°C.

Serine acetyltransferase activity of CysE was monitored via depletion of substrate acetyl CoA at 232 nm ($\Delta\varepsilon_{232}$ = 4500 M^{-1} cm^{-1}, absorbance of thioester bond) using an adapted method from (Chronis & Krishnan, 2004). Absorbance at 232 nm was recorded at 0.125 s intervals for 30 s using a ThermoSpectronic Heλios spectrophotometer (ThermoScientific, USA). Initial velocity data (Δ Absorbance/second) was derived from linear regression analysis of the first ten seconds of the reaction (unless otherwise stated). The catalytic rate (ΔAbsorbance/second) of CysE can be calculated directly from the depletion of acetyl CoA by dividing the rate by -1, as one mol of acetyl CoA is used to make one mol of *O*-acetylserine. All datapoints were collected in duplicate, unless otherwise stated. All assays were conducted at room temperature (22°C).

2.2.5.2 Michaelis Menten analysis

The Michaelis constant (K_M) is the concentration of substrate required for an enzyme to produce half its maximum theoretical rate (V_{max}) (Fersht, 2017). K_M is a measure of the affinity of the enzyme for the substrate of interest. Hence, when an enzyme has a low K_M for a substrate, the enzyme has a high affinity for the substrate and will require lower concentrations of substrate before the enzyme's binding sites become saturated. If an enzyme has a high K_M for a substrate, this indicates that the substrate has a low affinity for the substrate and higher concentrations will be needed for saturation (Fersht, 2017). Approximate values of V_{max} can be achieved under saturating concentrations of substrate. This is a theoretical value that can be never reached in a practical setting but is denoted as being the rate where the concentration of substrate is2 x K_M (V_{max} = 2 x K_M).

The K_M and V_{max} were calculated for each substrate by varying the concentration of the substrate of interest, while keeping the other at saturating concentrations, so that it is not rate limiting. Saturating conditions are defined as concentrations 2 x K_M, and greater L-serine Michaelis Menten curves were collected over a range of L-serine concentrations (0.1-200 mM). Acetyl CoA Michaelis Menten plots were collected over a range of acetyl CoA concentrations (0.1-1 mM). Both Michaelis Menten plots were collected at fixed saturating conditions of the other substrate.

K_M and V_{max} were determined by non-linear regression fit of the Michaelis Menten equation (Equation 2.3) using GraphPad Prism (version 8.2.0, Windows, GraphPad Software, La Jolla California USA,).

Equation 2.3: The Michaelis Menten equation. S = substrate, K_M = Michaelis constant, v = rate, v_{max} = theoretical maximum rate.

$$v = \frac{v_{max}[S]}{K_M + [S]}$$

Enzyme catalytic efficiency was measured by calculating the catalytic constant (k_{cat}) and the specificity constant k_{cat}/K_M. K_{cat} is a measure of the amount of product being formed over time, per unit of enzyme (s^{-1}). This is calculated by dividing the V_{max} rate ($M.s^{-1}$), by the molar concentration of hexameric enzyme. The catalytic efficiency k_{cat}/K_M ($M^{-1}s^{-1}$) was calculated by dividing the k_{cat} (s^{-1}) by the K_M (M). Catalytic efficiency values were calculated for each substrate.

2.2.5.3 CysE inhibition assays

L-cysteine inhibition assays were measured using a modified assay method from section 2.2.5.1. Modifications included the addition of L-cysteine (final concentration, 0.01-40 µM) to the assay mixture before initiating the reaction by the addition of enzyme.

Cysteine stocks (0.1 and 1.0 mM) were made up fresh in gel filtration buffer (50 mM Tris pH 8.0, 100 mM NaCl) and stored on ice throughout preparation and assays to prevent unwanted oxidation of L-cysteine to L-cystine.

2.2.5.4 Substrate inhibition

Substrate inhibition was measured through non-linear regression fit of the substrate inhibition Equation 2.4 using GraphPad Prism (version 8.2.0, Windows, GraphPad Software, La Jolla California USA,).

Equation 2.4: Substrate inhibition equation. S = substrate, K_i = inhibition constant, K_M = Michaelis constant, v = rate, v_{max} = theoretical maximum rate.

$$v = \frac{v_{max}\,[S]}{K_M[S](\frac{1+[S]}{K_i})}$$

2.2.5.5 Measuring cysteine inhibition parameters

The concentration of inhibitor that reduces enzyme rate by half (IC_{50}) were calculated by fitting the "log [inhibitor] vs. normalised response" (Equation 2.5) to rate data ($mM.s^{-1}$) using GraphPad Prism (version 8.2.0, Windows, GraphPad Software, La Jolla California USA,). GraphPad calculated IC_{50} from plotting rate against logarithms of increasing concentrations of L-cysteine

Equation 2.5: Equation for determining IC_{50} of L-cysteine. I = inhibitor concentration, v = rate, v_0 = rate with no inhibitor present, v/v_o = normalised rate.

$$\frac{v}{v_o} = \frac{100}{(1+10^{([\mathrm{I}]-\log IC50)})}$$

For characterising the inhibition type of L-cysteine, it was decided due to time constraints to investigate the inhibition mechanism of only one substrate during this thesis. We decided to investigate the K_i and type of inhibition L-cysteine displayed relative to L-serine, as L-cysteine has been shown to bind directly to the active site

of our enzyme, and so we believe would be a good model for guiding novel inhibitor design.

Before characterising the type of inhibition exhibited by L-cysteine on L-serine, the K_i was estimated by, plotting the reciprocal rate against increasing concentrations of inhibitor, to create a Dixon plot (Equation 2.6) (Dixon, 1953). The rate was calculated by monitoring rate over increasing concentrations of L-cysteine, at fixed concentrations of L-serine and saturating concentrations of acetyl CoA (0.45 mM). Rate data was collected at L-serine concentrations of 1,3 and 10 mM. When plotted the data forms a straight line. Linear regression analysis was fitted for each L-serine concentration and the intercept of these points were plotted. The K_i can be derived from the x-coordinate of the intersection of these lines.

Equation 2.6: Dixon plot equation. K_i = inhibition constant, S= substrate, v = rate, V_{max} = theoretical maximum rate, I = inhibitor.

$$\frac{1}{v} = \frac{K_M + [S]}{V_{\max}[S]} + [I]\frac{(\frac{K_M}{K_i} + \frac{[S]}{K_i})}{V_{max}[S]}$$

To determine the inhibition type of L-cysteine, Michaelis Menten plots were collected and fitted using Equation 2.7. Rates were collected with varying concentrations of L-serine (1, 3 and 10 mM) and at fixed concentrations of L-cysteine (0.5x, 1x, 2x and 4x K_i) of L-cysteine, at saturating conditions of acetyl CoA and varying the concentrations of L-serine.

Equation 2.7: Competitive inhibition model. K_M = Michaelis constant, K_{Mobs} =observed K_M when inhibitor is present, S = substrate, v = rate, v_{max} = theoretical maximum rate, Ki = in inhibition constant, I = inhibitor.

$$v = \frac{v_{max}[S]}{K_{Mobs} + [S]}$$

Where

$$K_{Mobs} = K_M(\frac{1 + [I]}{K_i})$$

2.3 Results and Discussion

2.3.1 Expression and purification of CysE

To successfully characterise CysE from *N. gonorrhoeae* we need to purify soluble and active protein. Prior to the start of this MSc research, Dr Joanna Hicks had cloned CysE and optimised protein expression and purification (Section 2.2.1 and 2.2.3). During assay development we encountered enzyme stability issues, but we were able to optimise our purification and assay method to mitigate this.

CysE was successfully purified by IMAC and gel filtration chromatography. The IMAC purification chromatogram in Figure 2.1a show that CysE elutes at ≈ 45% elution buffer (450 mM of imidazole). The corresponding SDS-PAGE gel of the IMAC fractions, demonstrates that the majority of *E. coli* protein present in the supernatant is removed during IMAC purification (Figure 2.1b). This results in relatively pure CysE protein of approx. 32 kDa (Figure 2.1b, blue arrow) consistent with the predicted molecular weight of the CysE monomer (31.6 kDa, calculated as per section 2.2.4.5). Fractions containing IMAC purified CysE (Figure 2.1, green bar) were concentrated for gel filtration purification (Figure 2.1a) as per section 2.2.4.2.

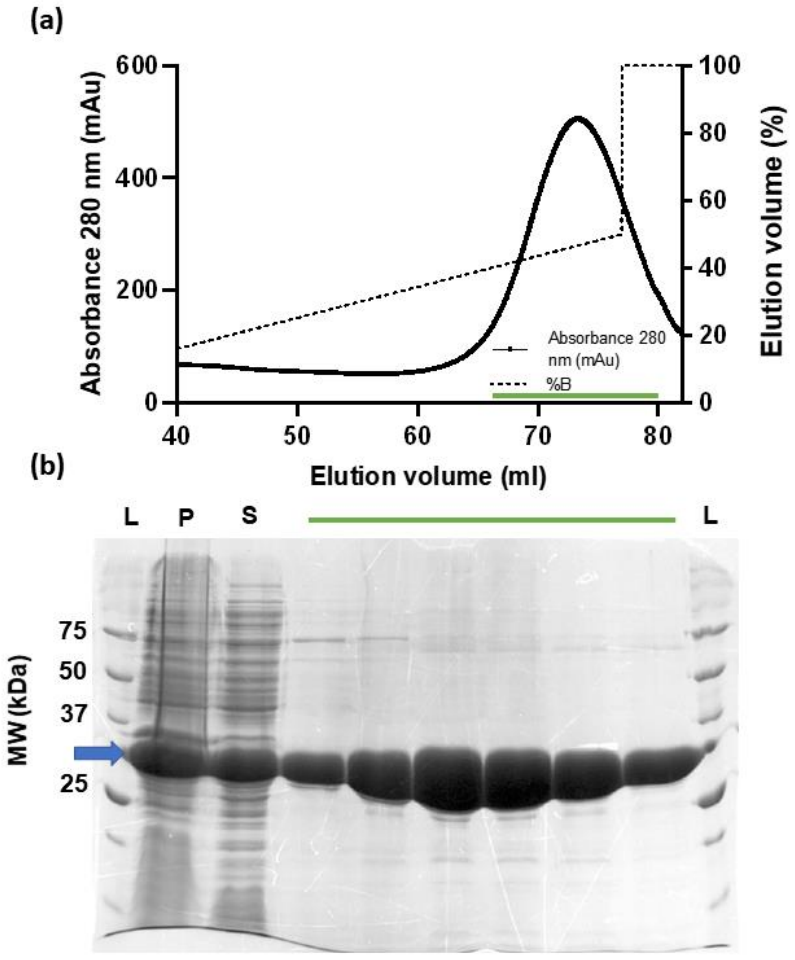

Figure 2.1: IMAC purification of CysE at room temperature. (a) IMAC chromatogram of A_{280} nm shows volume (left X-axis) and concentration of elution buffer (%B right X-axis). Data from 0-40 ml has being excluded for scaling purposes. (b) 12% SDS-PAGE gel of CysE IMAC purification. CysE protein is labelled with a blue arrow and is present in all samples (the insoluble pellet (P), soluble supernatant (S) and IMAC fractions (green bar)). Molecular weights of Precision Plus Protein Standards (L) in kDa are labelled. Purification was carried out at room temperature.

IMAC-purified CysE underwent a final purification step via gel filtration chromatography (section 2.2.4.2). CysE eluted as a single peak from an ENrich 650 analytical gel filtration column with an elution volume of 12.56 ml (Figure 2.2a, orange bar). Using the ENrich 650 calibration curve (Appendix B.1.2), the apparent molecular weight from the elution volume is 193.8 kDa. The predicted molecular weight of the CysE monomer is 31.6 kDa, which suggests that CysE elutes as a hexamer (6 x 31.6 kDa = 189.6 kDa). No protein was present in the void volume of the column (10.56 ml) indicating that CysE did not aggregate and remained soluble during purification. The corresponding SDS-PAGE of the gel filtration column show pure CysE protein of approximately 32 kDa (Figure 2.2b).

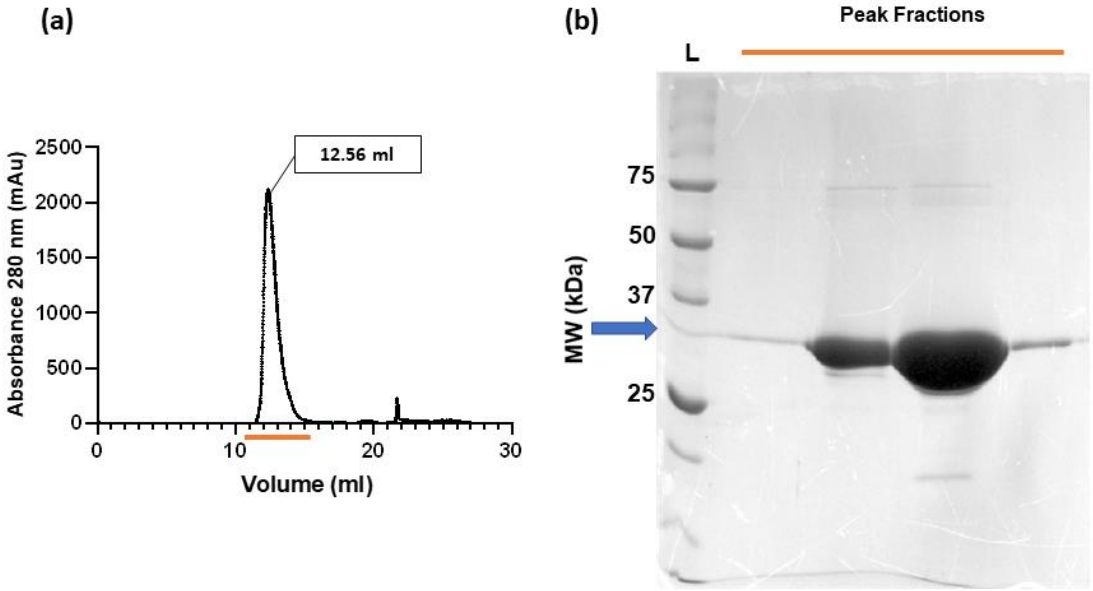

Figure 2.2: Gel filtration purification of CysE. (a) Enrich 650 gel filtration chromatogram shows the elution of a large peak at 12.56 ml (b) 12% SDS-PAGE analysis shows high yield and purity of CysE (orange bar). CysE protein band is labelled with a blue arrow. Molecular weights of Precision Plus Protein Standards (L) in kDa are labelled. Purification was carried out at room temperature.

2.3.2 Assay optimisation

We developed an assay to measure the activity of CysE from *N. gonorrhoeae*, based on the method for characterising CysE activity from soybean (Chronis & Krishnan, 2004). All assays were carried out in gel filtration/ assay buffer (50 mM Tris pH 8.0, 100 mM NaCl) at 22°C. Assays were set up as per section 2.2.5.1. All raw data used is listed in Appendix B.3.

Initially trial assays were collected to determine the appropriate amount of enzyme to collect initial velocity data for Michaelis Menten kinetics. Enzyme concentration was optimised to have sufficient linear initial velocity to measure during the assay (10 s). Assays were set up using concentrations of 0.1 mM and 1 mM acetyl CoA, and L-serine, respectively, based on saturating substrate concentrations for soybean CysE, reported by (Chronis & Krishnan, 2004). The following concentrations of CysE were trialled: 0.00156, 0.0031 or 0.0625 $mg.ml^{-1}$. Rates were monitored for 5 min (Figure 2.3a) but initial velocity was examined from the first 30 s of the assay (Figure 2.3b). The enzyme concentration, 0.0625 $mg.ml^{-1}$, was deemed to be too

high as the reaction reaches completion within the ten seconds, making it impossible to measure the initial velocity (Figure 2.3a). This prompted trialling 1:20 and 1:40 dilutions, 0.031 and 0.0156 $mg.ml^{-1}$ respectively. Rate curvature within the first ten seconds is present for 0.0031 $mg.ml^{-1}$, but further dilution to 0.00156 $mg.ml^{-1}$ eliminated this. The initial velocity (ΔAbs/s) calculated from the first ten seconds of each concentration was plotted (Figure 2.4). Here both lower concentrations show that initial velocity is dependent on enzyme concentration and increases linearly with increasing enzyme concentration. Hence, it was decided that a final CysE concentration of 0.00156 $mg.ml^{-1}$ would be used for the collection of Michaelis Menten kinetics.

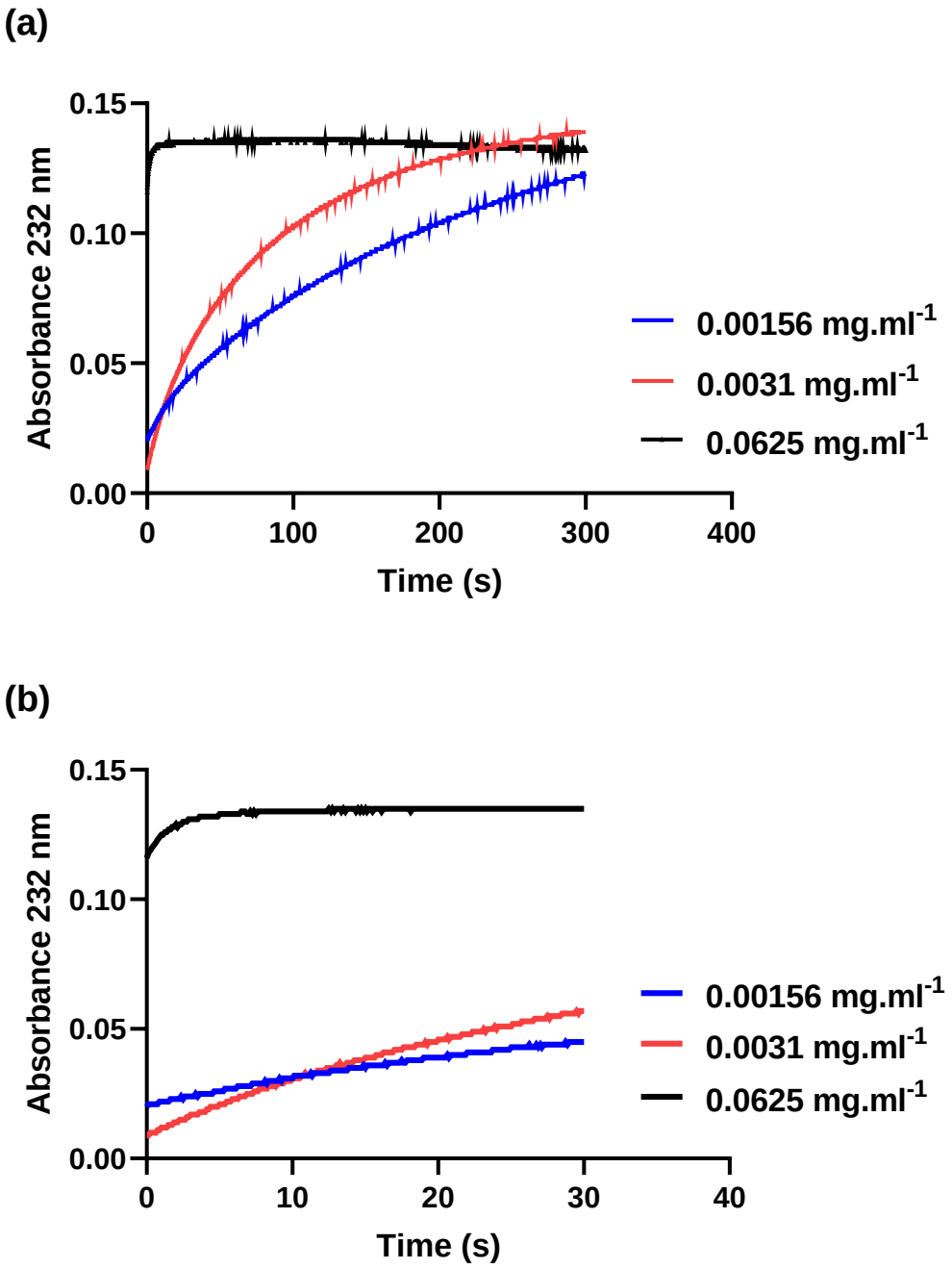

Figure 2.3: Dependence of rate on CysE concentration. Monitoring CysE activity at 232 nm with varying concentrations of enzyme. (a) CysE activity monitored by depletion of absorbance at 232 nm for 5 min. (b) First 30 s from plot (a), was used to visualise the linear region. Final enzyme concentrations trialled 0.00156, 0.0031 and 0.0625 mg.ml^{-1}. All assays were initiated with 5 µl of enzyme. Absorbance plotted represent single replicates. Raw untransformed data used to create plot (a) in Appendix B.3.

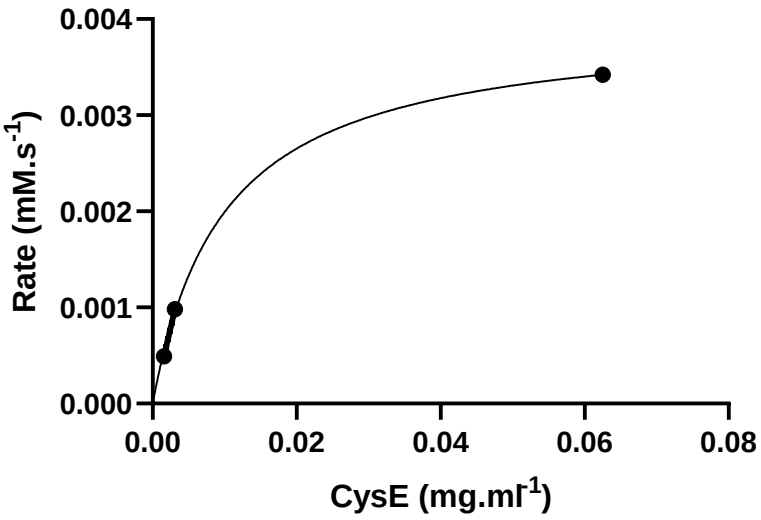

Figure 2.4: Rate dependence on concentration of CysE. Rates were calculated from the first ten seconds of the reaction. Rates are plotted for 0.00156, 0.0031 and 0.06250 mg.ml^{-1}. Single replicates were collected. Linear regression fitted for enzyme concentrations 0.00156 and 0.0031 mg.ml^{-1}. Non-linear regression curve fitted for all enzyme concentrations.

Initial activity assays were collected by varying the concentration of L-serine and acetyl CoA. Initial assay data (data not shown) demonstrated that CysE activity increased linearly at concentrations greater than 0.1 mM acetyl CoA and 1 mM L-serine, indicating that saturating substrate concentrations taken from(Chronis & Krishnan, 2004) are not saturating for CysE from *N. gonorrhoeae*. These results prompted us to collect initial velocity data at higher concentrations of each substrate to determine approximate saturating concentrations to use for collection of Michaelis Menten curves.

We collected preliminary data varying concentrations of the substrates L-serine and acetyl CoA, but over the course of several hours, we observed a slow steady decrease in enzyme activity (Figure 2.5). Further investigation demonstrated that this drop in activity only occurred when the CysE enzyme stock was stored on ice and did not occur when a sample of that enzyme stock was stored at room temperature (Figure 2.5).

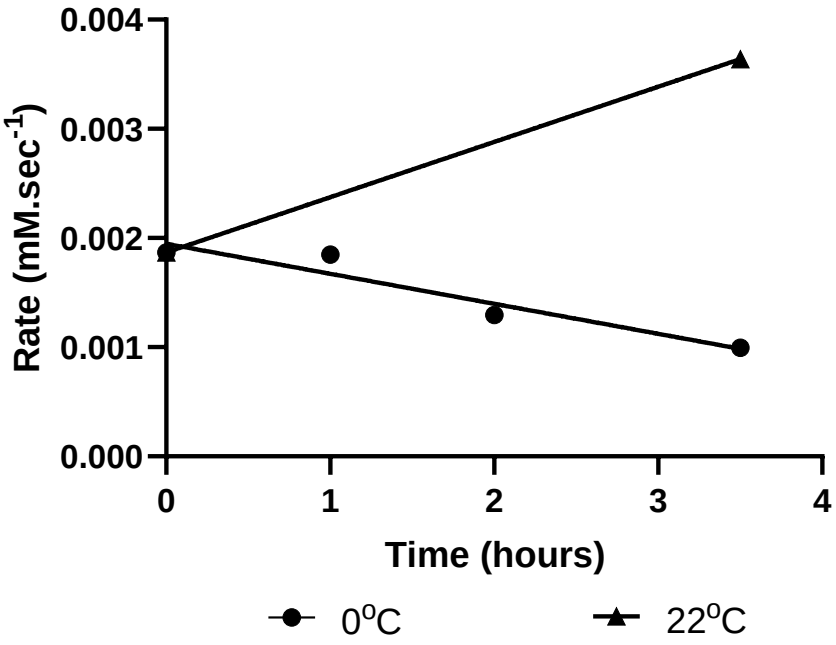

Figure 2.5: Effect of cold inactivation on CysE activity. Rates were measured at constant concentrations of acetyl CoA (0.45 mM) and L-serine (10 mM). CysE enzyme stock was stored on ice (circles) for the duration of the assay, and temperature control enzyme was stored at room temperature (triangles). All assays were carried out at room temperature (22°C). Single replicates are plotted.

Upon interrogation of the literature, it has been reported that CysE homologues lose activity when exposed to low temperatures (0-4°C), a phenomenon known as cold inactivation (Mino *et al.*, 2001; Yi *et al.*, 2013). Cold inactivation occurs in multimeric enzymes and is where hydrophobic interactions between these subunits weaken at cold temperatures, leading to dissociation into smaller oligomeric units (Privalov, 1990). Cold inactivation experiments with CysE homologues report the dissociation of the CysE hexamer into trimers and monomers (Mino *et al.*, 2001). This is in keeping with the CysE trimer-dimer interface and the intra-trimer interface, where the majority of interactions are hydrophobic (Pye *et al.*, 2004; Yi *et al.*, 2013; Kumar *et al.*, 2014). This process is reversible, as activity can be restored by incubating at room temperature, and has been linked to the reformation of hexameric CysE (Mino *et al.*, 2001). With this information we further optimised our purification and assay to reduce the effect of cold inactivation on CysE activity.

To prevent cold inactivation of CysE, we removed all cold storage steps from the purification process, which included protein concentration at 4 °C, storage at 4 °C between IMAC and gel filtration chromatography and storing enzyme stocks at room temperature. Before we realised that CysE was susceptible to cold

inactivation, we had collected a preliminary Michaelis Menten curve for both acetyl CoA (0.1-1.0 mM) and L-serine (as per section 2.2.5.1). This initial data showed rate inhibition at concentrations of acetyl CoA greater than 0.55 mM and was attributed to substrate inhibition (Figure 2.6). Both Michaelis Menten (Figure 2.6a) and substrate inhibition (Figure 2.6b) models were fitted using GraphPad Prism (section 2.2.5.2 and 2.2.5.4). Given that only single replicates were collected for determining the acetyl CoA curve, the curve was used to inform the saturating concentrations for collection of the Michaelis Menten curve for L-serine, which was chosen to be 0.45 mM as it was the highest concentration before substrate inhibition became apparent.

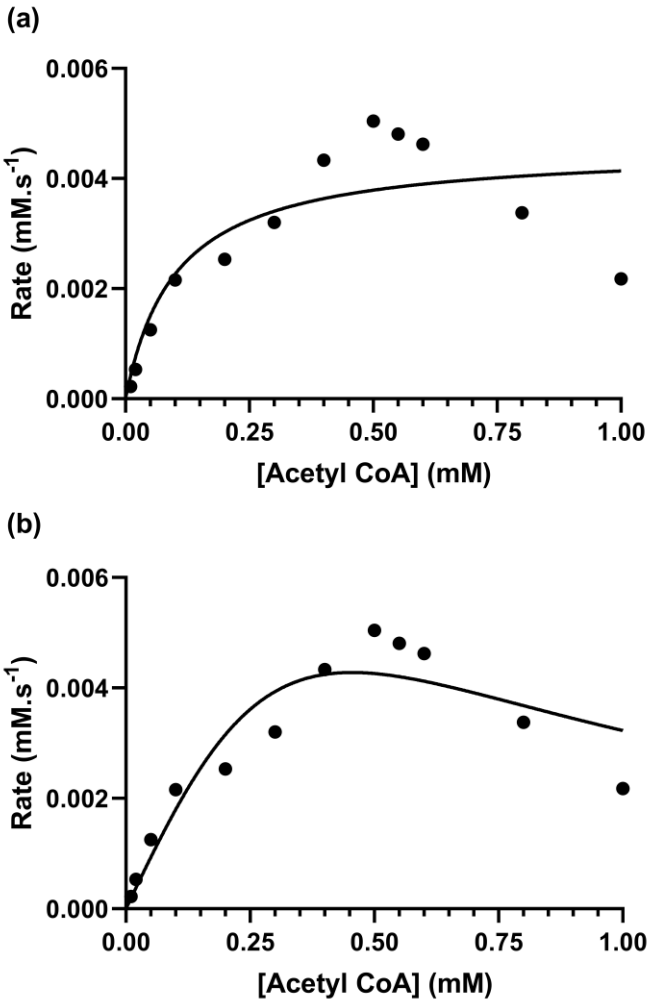

Figure 2.6: Preliminary acetyl CoA Michaelis Menten curve for cold inactivated CysE. (a) Nonlinear regression fit of Michaelis Menten (line). (b) Same as data (a) but nonlinear regression fit of substrate inhibition (line). L-serine was kept at a constant concentration of 1 mM L-serine. CysE was stored on ice for the duration of this assay.

A Michaelis Menten curve was collected for L-serine with cold inactivated CysE (CysE purified with cold exposure steps and stored on ice for duration of the assay). To compare the effect of low temperature on CysE activity we recollected this Michaelis Menten curve with CysE purified and stored at room temperature (Figure 2.7). Both curves were collected at room temperature (i.e. assay buffer at room temperature), saturating concentrations of acetyl CoA (0.45 mM) and using 0.00156 $mg.ml^{-1}$of CysE. Initial velocities were collected for increasing concentrations of L-serine (0.1 to 12 mM) (Figure 2.7). The Michaelis Menten model was fitted (section 2.2.5.2) to each data set. The K_M and V_{max} for cold treated CysE was 0.7728 ± 0.2397 mM and 0.002896 ± 0.0002476 $mM.s^{-1}$ respectively. Room temperature CysE had a K_M of 0.5784 ± 0.2803 mM and a V_{max} of 0.003980 ± 0.0005616 $mM.s^{-1}$. Visual inspection of the plots suggests that the V_{max} of the room temperature CysE is likely greater than reported, as the rate is still increasing linearly with increasing concentrations of L-serine.

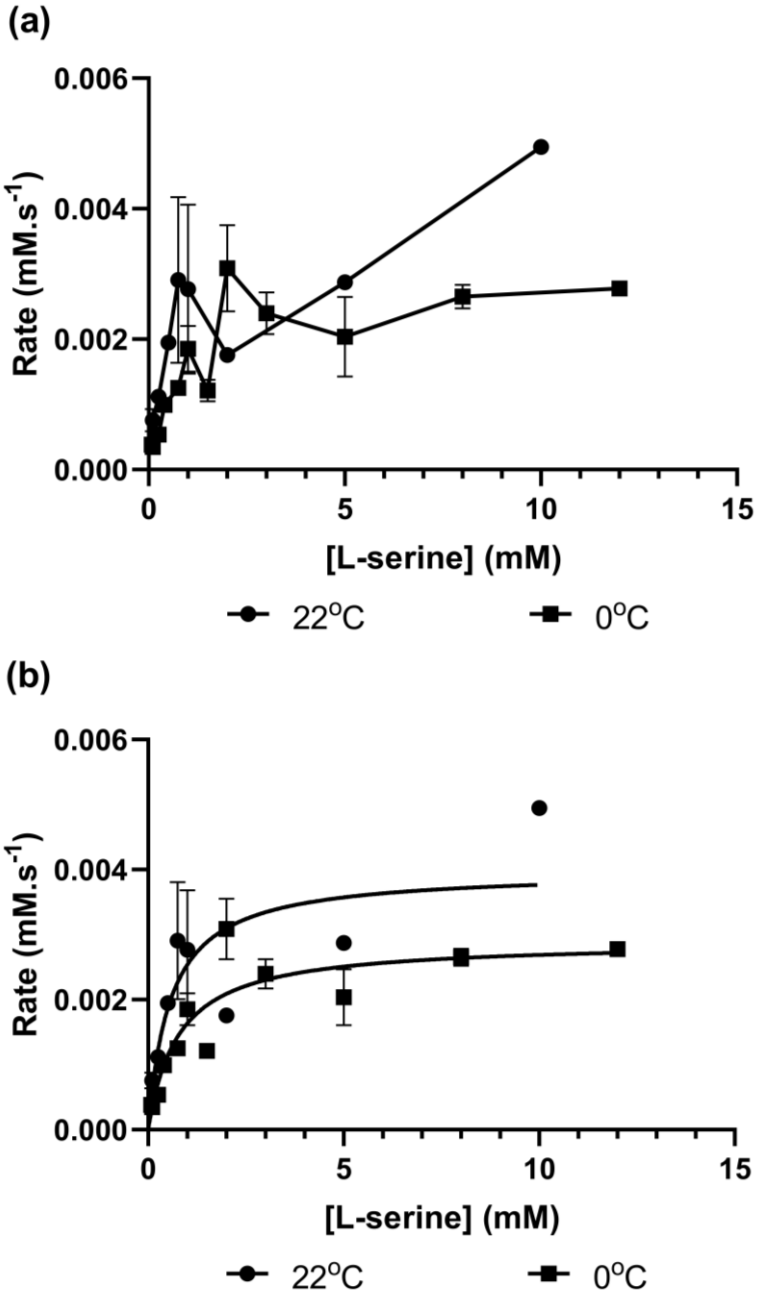

Figure 2.7: Effect of temperature on CysE Michaelis Menten kinetics. (a) Datapoints plotted with connecting lines. (b) Data from (a) with the Michaelis Menten equation (Equation **2.3**) fit (line). All assays were conducted at 22°C. Room temperature dataset is depicted as circles and cold temperature dataset is depicted as squares. Plots were collected at a saturating concentrations of acetyl CoA (0.45 mM) and 0.00156 $mg.ml^{-1}$ of CysE. Each datapoint is the mean calculated from duplicates, and plotted error bars are SEM.

For CysE stored on ice the K_M for L-serine increased, indicating a lower affinity for the substrate and V_{max} decreased, indicating a reduced rate. To explain this difference in activity due to temperature, we investigated whether CysE was dissociating from a hexamer into a lower oligomeric state when exposed to cold temperatures. We analysed samples of cold treated (refrigerated on ice (0°C) overnight) and room temperature CysE by native-PAGE gel electrophoresis as per section 2.2.4.3.

Using native-PAGE electrophoresis we were able to visualise the presence of two extra bands for cold treated CysE (0°C), compared to CysE that was stored at room temperature (22°C). Given that the lowest running band is present for both temperature conditions, this is band is likely the hexameric form of CysE. Given that there are two extra bands present for cold-treated CysE samples, these most likely lower oligomeric states of CysE, consistent with either a trimer, dimer or monomer.

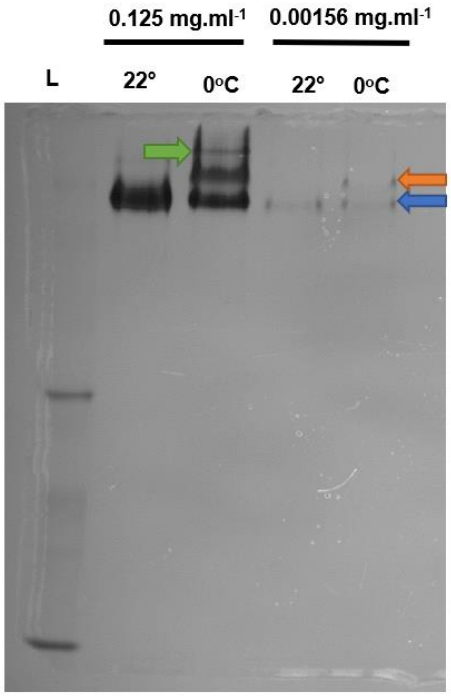

Figure 2.8: Native-PAGE analysis of cold inactivated CysE. Two concentrations of CysE were incubated overnight at room temperature or at 0°C. Hexamer band as indicated by blue arrow, suspected trimer/dimer/monomer are labelled with an orange and green arrow. (L) The ladder could not be visualised and so has not being labelled.

To confirm these results from Figure 2.8, the cold inactivated mixture was prepared again (incubation at 0°C overnight) and analysed by gel filtration chromatography (as per 2.2.4.2). Interestingly, we were only able to visualise a single peak with an elution volume of 12.56 ml (data not shown) that resembled the same elution profile as seen in Figure 2.2a. The cold inactivation seen for CysE homologues has been shown to be reversible and has been attributed to the reassociation of dissociated trimers to form a hexamer (Mino *et al.*, 2001). As our gel filtration purification was conducted at room temperature, with room temperature buffer, we assume the hexamer reformed. Storing CysE at 4°C long term and preincubating at room temperature to restore activity was considered, but it was decided this would introduce a potential source of variability, so these assays were optimised removing exposure of CysE to low temperatures.

Interestingly, we still observed saw the effects of low temperature of CysE in our assays that were carried out at room temperature (assay buffer was kept at room temperature). Although the effects of cold inactivation are reversible, Mino *et al.* (2001) observed that hexamer formation and restoration of enzyme activity occurred after minutes of incubation at room temperature. As assays were initiated with enzyme, there would have been insufficient time for reactivation of CysE and explains the effects of cold inactivation seen during our assays. This would also explain why only a CysE hexamer was seen during gel filtration purification of cold inactivated CysE, as the column takes minutes to run, giving the CysE hexamer time to reform.

2.3.3 CysE stability

After minimising cold exposure, it was observed that enzyme activity dropped after overnight incubation at room temperature. This prompted us to trial the addition of buffer additives to see if we could stabilise enzyme activity.

Loss of activity at room temperature has been observed for diluted CysE (1.3 $\mu g.ml^{-1}$) from *H. influenzae*, which is comparable to the concentrations of CysE used for our assays (0.125 $mg.ml^{-1}$) (Johnson *et al.*, 2004). The authors from this study trialled additives and found that the addition of bovine serum albumin (BSA) (100 $\mu g.ml^{-1}$) improved enzyme stability. We trialled the addition of BSA (100 $\mu g.ml^{-1}$) to purified and diluted CysE (results not shown) (as per section 2.2.4.2), but results were inconclusive.

The addition of reducing agents at low concentrations is known for promoting stability of enzymes, by preventing the unwanted oxidation of cysteine residues (Wingfield, 2001). Using disulphide prediction program DiANNA, CysE was shown to have two cysteines (Cys84 and Cys99) per monomer with a low disulphide prediction score of 0.01681 (where 1 being most likely to form a disulphide bond) (Ferrè & Clote, 2006). To prevent unwanted oxidation of these residues the addition of reducing agents were trialled. Dithiothreitol (DTT) (1 mM) and 2-betamercaptoethanol (1 mM) were added to enzyme stocks directly after purification (prepared as per section 2.2.4.2), but results were inconclusive. Given the amount of time spent on assay optimisation for cold-inactivation it was decided to purify and perform all Michaelis Menten and L-cysteine inhibition assays on the same day to prevent loss of CysE activity affecting results.

2.3.4 Michaelis Menten kinetics of CysE

Michaelis Menten curves were collected for both substrates, L-serine and acetyl CoA. The purpose of collecting this data is to determine K_M and V_{max} for CysE. These kinetic parameters provide insight into the enzyme's affinity for its substrates and can be used to calculate measures of catalytic efficiency including, k_{cat} and k_{cat}/K_M. These kinetic parameters are also needed for collection of inhibition assays.

The Michaelis Menten plot for acetyl CoA was created by plotting initial velocities ($mM.s^{-1}$) against increasing concentrations of acetyl CoA (0.01-1.0 mM) at

saturating concentrations of L-serine (10 mM). The resulting Michaelis Menten plot (Figure 2.9), does not show the classical rate curvature at high concentrations of acetyl CoA (rate plateau at high substrate concentrations), but instead inhibition is present (from 0.55 mM acetyl CoA), suggesting some form of inhibition. Initially, we fitted a substrate inhibition model (Equation 2.4) using GraphPad (Figure 2.9a). Substrate inhibition is where substrate binds to the enzyme to form an unproductive enzyme:product:substrate complex (Fersht, 2017). The model fits the rates plotted relatively well ($R^2 = 0.9145$), but there is some slight deviation from the model at higher concentrations of acetyl CoA, (0.8 -1.0 mM). The K_M and V_{max} values calculated by the substrate inhibition model are 500 mM and 0.01 $mM.s^{-1}$, respectively. Given that these incredibly large values exceeded the concentration range plotted, we deemed this not scientifically relevant and other models were fitted.

To determine the K_M and V_{max} for acetyl CoA, we fitted the Michaelis Menten model (Equation 2.3) calculating the K_M and V_{max} for acetyl CoA to be 0.152 ± 0.05 mM and $5.93 \times 10^{-3} \pm 5.74 \times 10^{-4}$ $mM.s^{-1}$, respectively (Figure 2.9b).

Further comparison of the goodness of fit of the substrate inhibition and Michaelis Menten models, demonstrates that the substrate inhibition model fits the rates better than the Michaelis Menten plot, with R^2 values of 0.9145 and. 0.8375, respectively. So, while the kinetic parameters generated from the substrate inhibition model are not suitable for use, we do believe that substrate inhibition is the cause of inhibition present in our acetyl CoA Michaelis Menten plot.

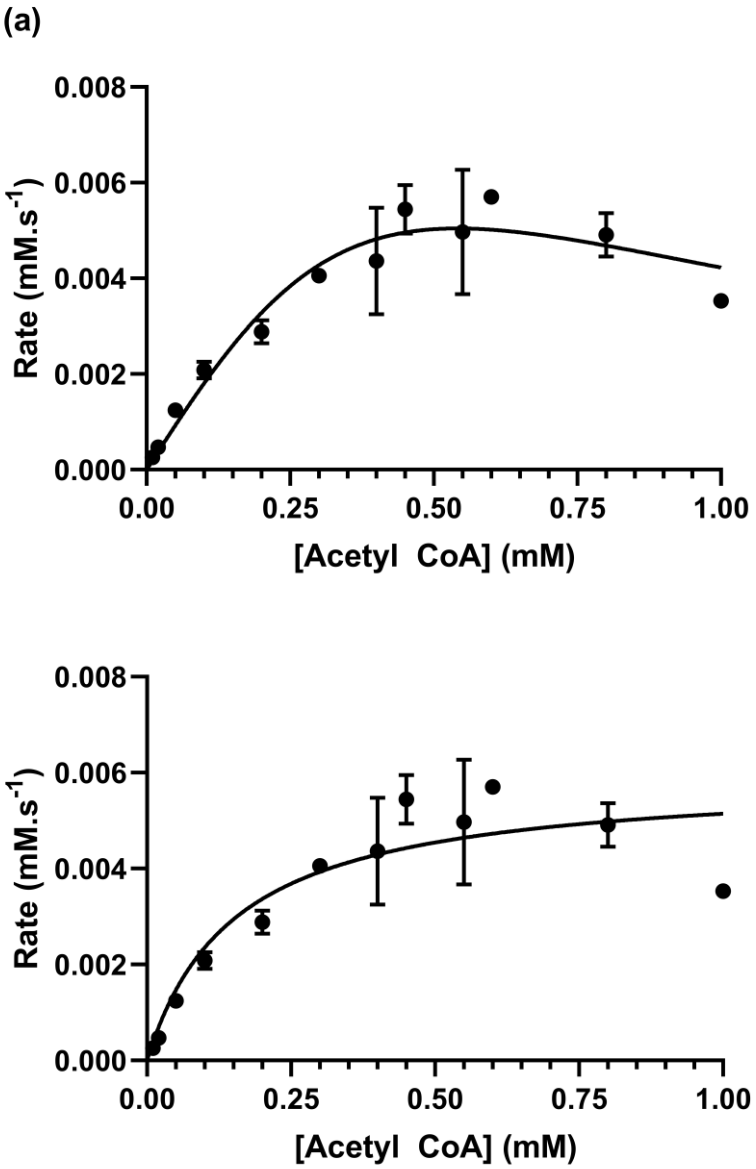

Figure 2.9: Enzyme rate dependent on increasing concentrations of acetyl CoA. (a) Fit of substrate inhibition model (Equation .). (b) Same data as (a) fit with Michaelis Menten equation (Equation). Rates measured at saturating concentrations of L-serine (10 mM). Circles represent mean derived from duplicates and error bars are SEM. Plot was collected at room temperature (22°C).

The substrate inhibition observed for the acetyl CoA Michaelis Menten curve with 10 mM L-serine, is comparable to the acetyl CoA Michaelis Menten curve with 1 mM L-serine (Figure 2.10). The rates appear to be within error, up until substrate inhibition becomes at 0.55 mM acetyl CoA, where the rates deviate. For the 1 mM L-serine plot, the rates are lower at higher concentrations of acetyl CoA, compared to the 10 mM L-serine plot. It is unclear whether this difference in substrate inhibition seen in these two datasets is due to differences in L-serine concentration or temperature treatment of CysE, as both are variables in these datasets. To

determine which factor is responsible, we would recollect the 1 mM L-serine dataset using CysE enzyme purified and stored at room temperature.

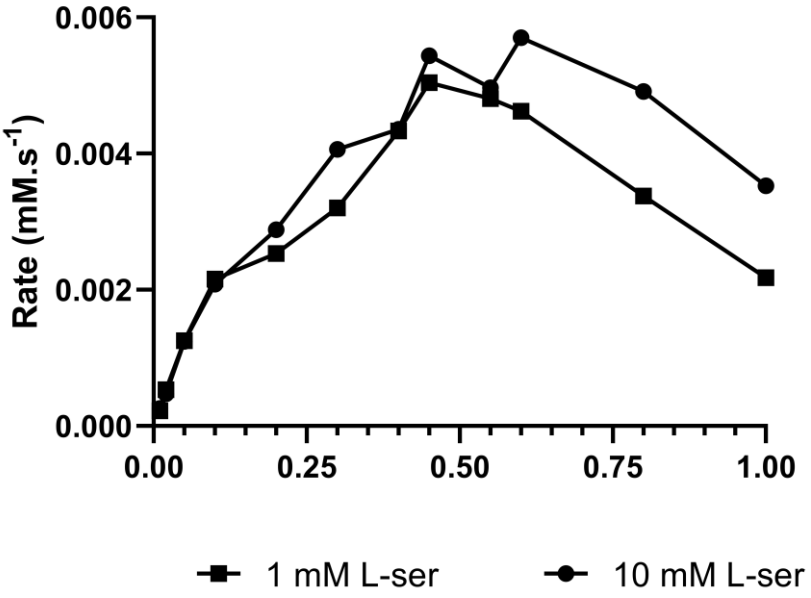

Figure 2.10: Comparison of Michaelis Menten data collected at different concentrations of L-serine. Lines plotted are connecting lines between each data point. All data collected with the same CysE concentration (0.00156 $mg.ml^{-1}$). Plots were collected either at 10 mM L-serine (circles) or 1 mM L-serine (squares). CysE was stored on ice for collection of 1 mM L-serine data. 1 mM L-serine dataset taken from Figure 2.6 and 10 mM L-serine dataset taken from Figure 2.9.

For the collection of Michaelis Menten plots for a dual substrate enzyme, the concentration of one substrate is varied, while the other substrate is kept at saturating conditions to prevent from becoming rate limiting (Fersht, 2017). Often concentrations greater than 2 x K_M are used, but given that substrate inhibition is present, 0.45 mM acetyl CoA was chosen to be the saturating concentration for collection of the L-serine Michaelis Menten plot, as it is the highest concentration of acetyl CoA before the rate becomes affected by substrate inhibition.

The L-serine Michaelis Menten curve was generated by plotting initial velocities ($mM.s^{-1}$) against increasing concentrations of L-serine (0.1-200 mM) (section 2.2.5.2). We observed classical Michaelis Menten behaviour for L-serine, with substrate saturation of the enzyme seen at 20 mM of L-serine (Figure 2.11). The K_M for L-serine was 2.58 ± 0.73 mM and the V_{max} 6.63 x 10^{-3} ± 4.72 x 10^{-4} $mM.s^{-1}$. The difference in K_M values for each substrate (2.58 mM L-serine vs. 0.152 mM acetyl CoA, (Table 2.3), demonstrates that CysE has a greater affinity for acetyl CoA compared to L-serine. K_M values for both L-serine and acetyl CoA are

comparable to those that have been collected for other CysE bacterial homologues, given that these were collected under different experimental conditions (Table 2.4).

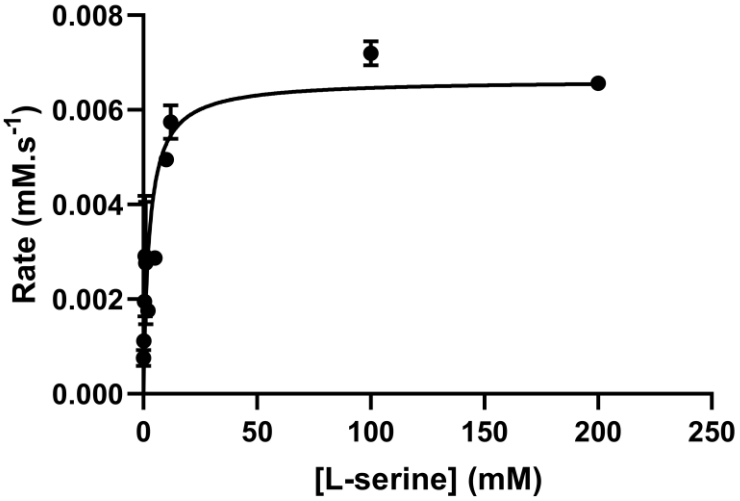

Figure 2.11: L-serine Michaelis Menten-fitted curve. Acetyl CoA kept at saturating concentration (0.45 mM). Circles represent mean derived from duplicates for each datapoint and error bars SEM. Data collected at room temperature (22°C).

The V_{max} values for both substrates are comparable, with 6.63 x 10^{-3} and 5.93 x10^{-3} mM.s^{-1}, for L-serine and acetyl CoA, respectively (Table 2.3). The catalytic turnover (k_{cat}) values were derived from the Vmax as per section 2.2.5.2. The k_{cat} for CysE is 822 ± 59 and 730 ± 70 s^{-1}, for L-serine and acetyl CoA, respectively, treating CysE as a hexamer. The k_{cat} calculation assumed a hexamer of CysE monomers as it is not clear if all active sites are active at the same time, and also for comparison to literature values. The k_{cat} values are within magnitude of values reported for CysE homologues (Table 2.3).

Table 2.3: Summary of Michaelis Menten kinetic parameters for substrates L-serine and acetyl CoA. Values are means calculated from duplicates and are quoted with SEM. k_{cat} values are reported for

Parameter	**L-serine**	**Acetyl CoA**
K_M (mM)	2.58 ± 0.73	0.152 ± 0.05
V_{max} (mM.s^{-1})	6.63 x 10^{-3} ± 4.72 x 10^{-4}	5.93 x 10^{-3} ± 5.74 x 10^{-4}
k_{cat} (s^{-1})	822 ± 59	730 ± 70
k_{cat}/K_M (L-serine)($M^{-1}.s^{-1}$)	3.19*10^5	4.80*10^6

The specificity constant, k_{cat}/K_M, values were calculated by dividing the k_{cat} by the K_M for each substrate The k_{cat}/K_M values for CysE are 3.19 x 10^5 and 4.80 x 10^6 $M^{-1}s^{-1}$ for L-serine and acetyl CoA, respectively. k_{cat}/K_M values of $10^5/10^6$ indicate that the enzyme is not diffusion limited ($k_{cat}/K_M \geq 10^8\ M^{-1}s^{-1}$) (Schurr & Schmitz, 1976). These values are comparable with values calculated for other CysE bacterial homologues (Table 2.3).

Table 2.4: Comparison of CysE kinetic parameters. DTNB = DTNB-coupled assay, A_{232} = monitor depletion of acetyl CoA at 232 nm, Nr = not reported. k_{cat} values are reported for the CysE hexamer.

Organism	**K_M (Ser/AcCoA)**	**k_{cat} (Ser/AcCoA) (s^{-1})**	**k_{cat}/K_M (Ser/AcCoA) ($M^{-1}s^{-1}$)**	**pH, Temperature, Assay method**	**Reference**
N. gonorrhoeae FA1090	2.58/0.152	822/730	$3.19*10^5/4.80*10^6$	8.0, 22°C, A_{232} nm	This thesis
E. coli	1.3/0.3	228/306	$1.34*10^5/2.12*10^5$	7.0, 20°C, A_{232} nm	(Benoni *et al.*, 2017b)
S. typhimurium	3.2/0.4	135/nr	$3.4*10^5$/nr	7.0, 25°C, DTNB	(Leu & Cook, 1994)
H. influenzae	4.7/0.7	2200/nr	$4.70x10^5$/nr	7.5, 25°C, DTNB	(Johnson *et al.*, 2004)

Interestingly there is a 10 fold k_{cat}/K_M increase for acetyl CoA compared to L-serine. This can be attributed to CysE having a greater affinity for acetyl CoA, with a ten fold lower K_M for acetyl CoA (0.152 mM) compared to L-serine (2.58 mM). K_M values tend to reflect concentrations of substrate observed in the intracellular environment. Currently there are no reported values for L-serine or acetyl CoA concentrations for *Neisseria* species. In *E. coli* the intracellular concentrations of acetyl CoA have been reported to vary between 20 – 600 µM as it is dependent on growth phase and nutrient availability (Takamura & Nomura, 1988). The K_M of acetyl CoA being in the middle of that range at 152 µM, would mean that CysE would be saturated with acetyl CoA. For L-serine, intracellular concentrations in *E. coli* have been reported to be 68 µM (Sajed *et al.*, 2015). The acetyl CoA values fits with the observation that K_M values tend to be around intracellular concentration of the substrate ((Bennett *et al.*, 2009)), whereas this is not the case for L-serine as the low intracellular concentration to K_M ratio for L-serine is much lower (68µM vs.

2.58 mM, concentration vs. K_M L-serine). This ratio would suggest that CysE would not be saturated with L-serine, and assuming intracellular concentrations are similar in *N. gonorrhoeae* this undersaturation would limit activity of CysE *in vivo* (Davidi *et al.*, 2016).

Michaelis Menten kinetics of CysE enzymes from other *E. coli* and *H. influenzae* consistently display classical (where at high concentrations of substrate the enzymatic rate plateaus at $\approx V_{max}$) plots for acetyl CoA, but observe substrate inhibition for L serine Michaelis Menten plots (Kredich & Tomkins, 1966; Johnson *et al.*, 2004; Benoni *et al.*, 2017b). Interestingly we observe the opposite where substrate inhibition is present for Michaelis Menten plots for acetyl CoA and not L-serine. Substrate inhibition occurs when a substrate binds to the enzyme to form an unproductive complex. Based on the reaction mechanism for CysE homologues, we predict that CysE most likely has a sequential mechanism, which is in keeping with the proposed formation of the ternary complex during acyl transfer to L-serine (Johnson *et al.*, 2004; Benoni *et al.*, 2017b). CysE from *H. influenzae* has been demonstrated to have an ordered mechanism where acetyl CoA binds and is released first (Johnson *et al.*, 2004). Assuming a sequential mechanism, it is possible at high concentrations of acetyl CoA for CoA to be released from the enzyme:*O*-acetylserine (enzyme:product) complex, only for acetyl CoA bind to the acetyl CoA/CoA binding site forming an unproductive complex, explaining the substrate inhibition we observe for acetyl CoA.

Previously researchers have investigated the design of inhibitors for a CysE related hexapeptide acetyltransferase, GlmU (Olsen *et al.*, 2007). Inhibitors for GlmU targeted the acetyl CoA binding site, instead of the active site (L-serine binding site). For CysE, targeting the acetyl CoA binding site, might prove to be a good target when screening for inhibitors.

Once we had determined the K_M for each substrate, before commencing with the collection of inhibitor assays, we re-confirmed that our rate was still dependent on enzyme concentration at our new saturating concentrations of 10 and 0.45 mM for L-serine and acetyl CoA, respectively (Figure 2.12). The initial velocity was derived from the first ten seconds of the assay. Here, initial velocity increases linearly with enzyme concentration, up until concentrations greater than 0.00156

mg.ml^{-1}. This demonstrates that initial velocity is still dependent on enzyme concentration, and so inhibitor assays were collected using 0.00156 mg.ml^{-1} of CysE.

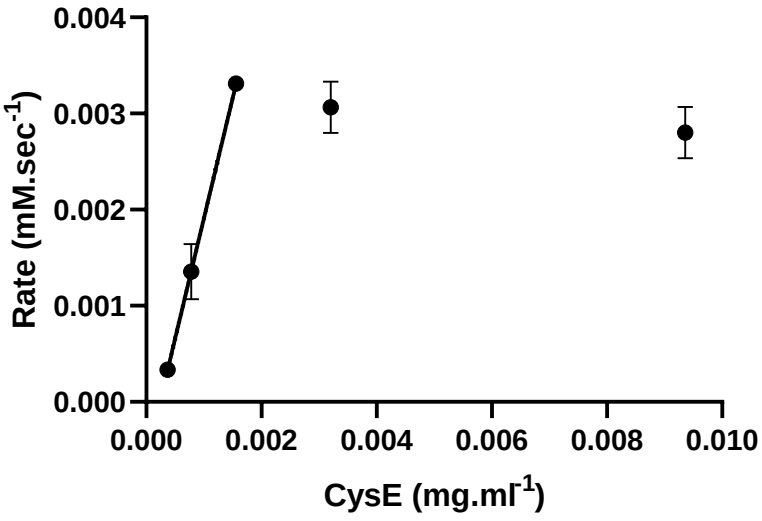

Figure 2.12: Dependence of rate on the concentration of CysE. All data was collected at saturating concentrations of L-serine and acetyl CoA, 10 and 0.45 mM, respectively. Circles represent mean derived from duplicates for each datapoint and error bars are SEM.

2.3.5 Characterising L-cysteine inhibition of CysE

For CysE proteins, feedback inhibition by L-cysteine is well documented across both bacterial and plant species. Here, we characterised L-cysteine inhibition relative to substrate, L-serine, for CysE. To characterise this inhibition, we carried out inhibitor assays to generate IC_{50}, Dixon and Michaelis Menten plots, for the calculation of IC_{50} , K_i and mode-of-inhibition for L-cysteine respectively.

2.3.5.1 L-cysteine IC_{50} assays

Inhibition assays were set up as per section 2.2.5.3. Initial velocity data was collected over a range of L-cysteine concentrations (0.8-40 µM). Substrates were held at saturating conditions for acetyl CoA (0.45 mM, 3 x K_M) and non-saturating conditions of L-serine (1 mM, 0.5x K_M). Enzyme concentration was kept constant at 0.00156 mg.ml^{-1}for all assays. CysE activity is inhibited by increasing concentrations of L-cysteine (Figure 2.13a). To calculate the IC_{50} for L-cysteine, the normalised rate was plotted against the log of L-cysteine concentration and fitted to Equation 2.5 using GraphPad (Section 2.2.5.5) (Figure 2.13b). The calculated IC_{50} for L-cysteine is 5.01 ± 0.403 µM.

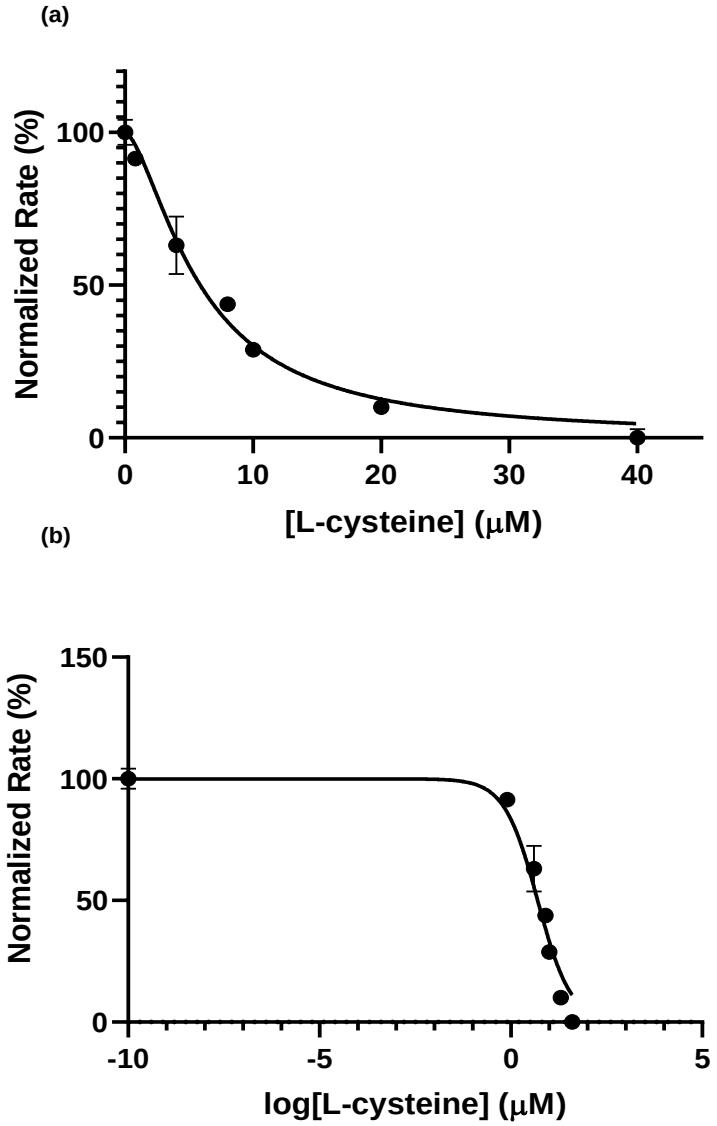

Figure 2.13: IC_{50} plot for L-cysteine. (a) Normalised rate plotted against increasing concentrations of L-cysteine. (b) Normalised rate plotted against $\log_{10}$ of L-cysteine concentrations. Line represents the fit of Equation 2.5. Substrate concentrations were kept constant, at 0.45 mM and 1 mM, for acetyl CoA and L-serine, respectively. The IC_{50} for L-cysteine is 5.01 µM. CysE activity (Rate, $mM.s^{-1}$) was normalised by dividing the rate by rate of the no-inhibitor control. Data points are mean and error bars are SEM derived from two replicates.

To determine the K_i of L-cysteine, the reciprocal rate was plotted against increasing concentrations of L-cysteine (0-80 µM), at fixed concentrations of L-serine (1, 3 and 10 mM, 0.3x, 1x and 4x K_M), to generate a Dixon plot (Dixon, 1953). Concentrations of acetyl CoA were kept at saturating concentrations (0.45 mM). It is possible to determine mode-of-inhibition for an inhibitor by analysing the intersection of the linear regressions for each substrate concentration (Dixon, 1953). For competitive inhibition or mixed inhibition, these linear regressions would be expected to intersect behind the y-axis and above the x-axis. For non-competitive

inhibition, these linear regressions would intersect behind the y-axis but on the x-axis. Finally, for uncompetitive inhibition we would expect to find a series of non-intersecting linear regressions running parallel to each other. Linear regression analysis was fitted for each L-serine concentration dataset. For L-cysteine (Figure 2.14), we see that the intersection of the linear regressions occurs above the y-axis and behind the x-axis, suggesting either competitive or mixed mode inhibition. Based on Equation 2.6, the x co-ordinate of the intercept is $-K_i$. Here the coordinates are -4.095, 58.3, so the calculated K_i of L-cysteine is 4.095 ± 1.081 µM.

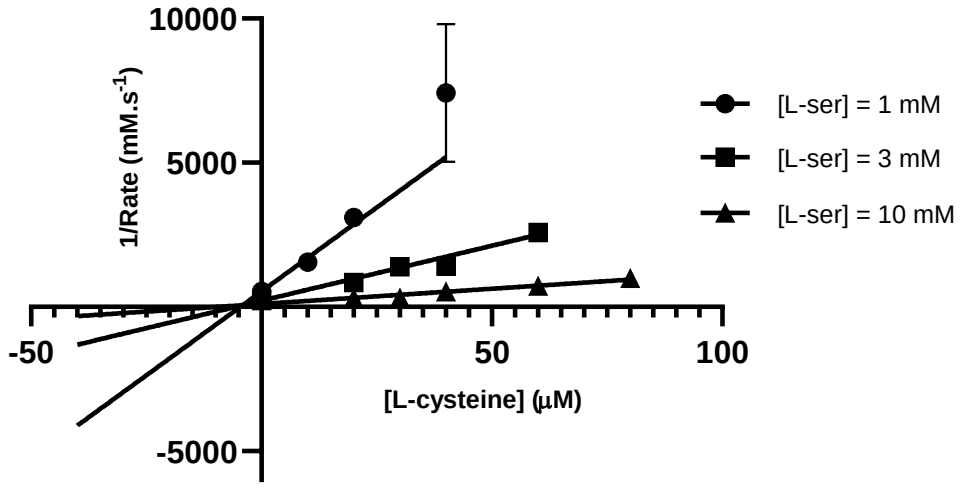

Figure 2.14: Dixon plot showing competitive inhibition. Rates plotted for 1 mM L-serine (circles), 3 mM L-serine (squares) and 10 mM L-serine (triangles). Acetyl CoA was kept at constant saturating conditions of 0.45 mM. Data points represent mean of two replicates and error bars SEM. Lines represent fit of linear regressions.

The calculated K_i for L-cysteine was used to generate Michaelis Menten plots to determine the type of inhibition displayed by L-cysteine relative to L-serine (Figure 2.15). Rates were plotted against increasing concentrations of L-serine at fixed concentrations of L-cysteine. To determine mode-of-inhibition, datasets were fitted using non-competitive, uncompetitive, mixed and competitive inhibition models offered in GraphPad. The competitive model had the best degree of fit, with a R^2 = 0.9183 compared to 0.7325, 0.8325, 0.9183, for uncompetitive, non-competitive and mixed inhibition models, respectively. A mixed mode-of-inhibition was ruled out even though it had good degree of fit (R^2 = 0.9183) as the fit was ambiguous. A K_i of 4.64 ± 1.11 µM was calculated for L-cysteine by fitting the competitive inhibition model. It should be noted that due to time constraints, the datasets used for Dixon plot analysis were also used for Michaelis Menten

inhibition analysis. Hence why there are only a few data points per L-cysteine concentration. In the future these plots will be recollected based on the concentrations used to generate the L-serine Michaelis Menten plot (Figure 2.11), at fixed concentrations of L-cysteine based on the K_i (4.01 µM) calculated from the Dixon plot (0.5-4 x K_i = 2-18 µM)

For competitive inhibition, the inhibitor is competing directly with L-serine for the active site, and therefore it would be expected that at high concentrations of L-serine, inhibitory effects of L-cysteine would be overcome, and that the V_{max} should approximately be the same value for all L-cysteine datasets. It would be expected that the K_M would increase with increasing concentrations of L-cysteine. The inhibition plot (Figure 2.15) does not show this trend, instead the V_{max} values for all data sets are dissimilar and decrease as inhibitor concentration increases. We acknowledge that independent of the graph pad R^2 values, the data below resembles a more non-competitive mode of inhibition i.e. the V_{max} decreases with increasing concentrations of inhibitor. The rates have not plateaued for any of the datasets plotted, and so it is impossible to say with any certainty what the V_{max} values are. Given the results from the Dixon and Michaelis Menten plots and that a competitive inhibition model for L-cysteine relative to L-serine, is well documented for CysE homologues (Hindson, 2003; Johnson *et al.*, 2004; Benoni *et al.*, 2017b), and is supported by crystallographic CysE structures with cysteine bound in the active site (Pye *et al.*, 2004; Yi *et al.*, 2013), we believe that CysE does have a competitive inhibition mechanism relative to L-cysteine.

To confirm this more data needs to be collected including repeating these Michaelis Menten plots and including higher concentrations of L-serine (20, 100 and 200 mM). If a competitive inhibition mechanism is present, the rate inhibition would be overcome at high concentrations of L-serine (V_{max} of inhibitor Michaelis Menten plots ≈ V_{max} of uninhibited plots).

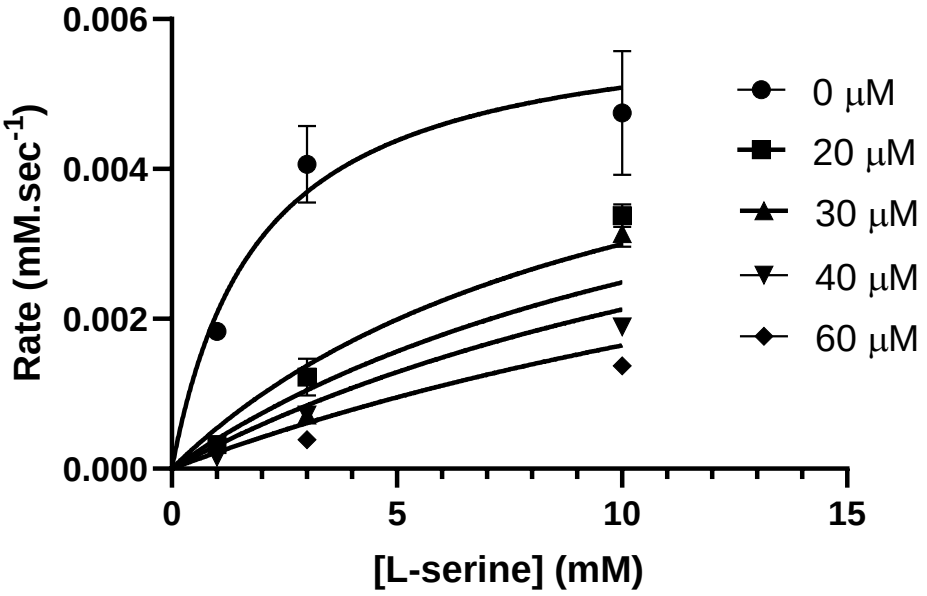

Figure 2.15: Fit of competitive inhibition model for L-cysteine relative to L-serine. Rates were measured over a range of concentrations of L-serine (0-10 μM) at collected at fixed concentrations of L-cysteine (20, 30, 40 and 60 μM), and saturating concentrations of acetyl CoA (0.45 mM). Data points represent the mean derived from two replicates and error bars represent SEM. Lines represent fit of competitive inhibition model Equation 2.7.

2.3.5.2 Analysis of IC_{50} and K_i values for L-cysteine

The IC_{50} value is a measure of the amount of inhibitor required to reduce enzyme activity by half (Fersht, 2017). The calculated IC_{50} for L-cysteine was shown to be 5.01 μM. This value is notably greater than the reported IC50 values for bacterial CysE homologues Table 2.5. It is noted, that there is some variability between IC50 values reported (Table 2.5) and this is likely due to differences in enzyme concentration and concentration of substrates (for competitive inhibitors), which are shown to influence the IC_{50} (Fersht, 2017). A better value for comparison of inhibitor potency is K_i , as it is not influenced by as many factors as IC_{50} values, therefore making them better for comparison to other K_i values.

The K_i for L-cysteine was calculated using different two methods, the Dixon plot (4.1 ± 1.081 μM) and Michaelis Menten inhibition plot (4.643 ± 1.11 μM), producing values that are in good agreeance within each other (Table 2.5). We compared the Ki value calculated from the Dixon plot to literature values, as although the preferred method is to derive the K_i from the Michaelis Menten inhibition plot, the datasets used for this analysis were incomplete (as discussed previously).

CysE from *N. gonorrhoeae* has a K_i of 4.1 µM, which is ten-fold greater than the lowest reported value of 0.4 µM from *S. typhimurium*. The highest K_i reported in Table 2.5 is 10 µM for *H. influenzae* (Johnson *et al.*, 2004). This variation can be partially attributed to differences in assay conditions, most notably pH. pH has been shown to influence both L-serine and L-cysteine binding in CysE homologues. For example, CysE from *H. influenzae* (activity measured at pH 6.5) reports a relatively high K_M for L-serine (17 mM) and K_i for L-cysteine (10 µM)(Johnson *et al.*, 2004), whereas values collected at a pH 7.6 in *S. typhimurium* have a K_M of 3.2 mM and K_i of 0.4 µM (Kredich & Tomkins, 1966).Given that the pH optima for CysE homologues is approximately 7.6 (Qiu *et al.*, 2013), and our assays were collected at pH 8.0, the effect of pH on our reported K_i values is likely minimal and the increased K_i values are due to a genuine reduction in CysE sensitivity to L-cysteine inhibition.

Currently there is no data available for intracellular concentrations of L-cysteine in *N. gonorrhoeae*. Interestingly, the K_i values for L-cysteine for CysE enzymes (Table 2.5), are much lower than reported intracellular concentrations of L-cysteine (204 ± 45 µM) found in *E. coli* (Sajed *et al.*, 2015). It is unclear what the nutrient availability of L-cysteine is in the urogenital tract, but given the high intracellular concentrations of glutathione (Seib *et al.*, 2006) and host-derived oxidative stress, it is possible that these high L-cysteine demands are met by reducing inhibition sensitivity L-cysteine, allowing for continued L-cysteine synthesis at higher L-cysteine concentrations compared to other CysE homologues.

Table 2.5: Comparison of CysE homologue IC_{50} and K_i parameters for L-cysteine. The K_i for *S. typhimurium* is not reported in reference. Nr =not reported All values are mean ± SEM. K_i value for CysE from *N. gonorrhoeae* is calculated from Dixon plot Figure 2.14.

Organism	**K_i (µM)**	**IC_{50} (µM)**	**Condition: pH, Temp, Assay method**	**Reference**
N. gonorrhoeae	4.095 ± 1.081	5.01 ± 0.403	8.0, 22°C, A_{232} nm	This thesis
E. coli	1	0.18 ± 0.02*	7.5, 25°C, DTNB *7.5, 20°C A_{232} nm	(Mino *et al.*, 1999),*(Benoni *et al.*, 2017b)
S. typhimurium	0.4	1.1	7.6, 25°C, DTNB	(Kredich & Tomkins, 1966)
H. influenzae	10±5	Nr	6.5, 25°C, DTNB	(Johnson *et al.*, 2004)

2.4 Conclusions and future directions

In this chapter we present that CysE from *N. gonorrhoeae* is a functional serine acetyltransferase. CysE was shown to be susceptible to cold inactivation, most likely due to hexamer dissociation, in keeping with observations of other CysE homologues (Mino *et al.*, 2001; Benoni *et al.*, 2017b). CysE from *N. gonorrhoeae* differs from other CysE enzymes in that it does not experience substrate inhibition by L-serine (Kredich & Tomkins, 1966; Benoni *et al.*, 2017b), but instead is subject to substrate inhibition by acetyl CoA.

CysE from *N. gonorrhoeae* is sensitive to feedback inhibition by L-cysteine. Calculated IC_{50} and K_i values were shown to be higher than other characterised CysE proteins. L-cysteine displays a competitive mode-of-inhibition, relative to L-serine. This is consistent with reported L-cysteine inhibition of other CysE enzymes (Johnson *et al.*, 2004; Benoni *et al.*, 2017b) and reported crystal structures of CysE proteins with L-cysteine bound in the active site (Figure 1.8) (Olsen *et al.*, 2004; Pye *et al.*, 2004). Combined, this evidence suggests that while CysE is subject to regulation by L-cysteine, it has reduced sensitivity, which would support the idea of *N. gonorrhoeae* having greater intracellular concentrations of L-cysteine, needed to meet high L-cysteine demand for mitigating oxidative stress encountered during host infection.

Future work includes investigation as to the type of inhibition cysteine exhibits on CysE relative to acetyl CoA. In other bacteria it was reported that CysE displays competitive inhibition to both substrates, despite binding in the L-serine binding pocket in the active site (Johnson *et al.*, 2004; Pye *et al.*, 2004). Preliminary inhibitor screening for the CysE-related hexapeptide acyltransferase, GlmU, identified potential inhibitors that target the acetyl CoA binding site (Olsen *et al.*, 2007). To characterise this inhibition, we will collect Dixon and Michaelis Menten based inhibitor plots.

Based on our collected data we hypothesise a sequential mechanism for CysE from *N. gonorrhoeae*. Future work includes collecting kinetic data at varying substrate concentrations for analysis using a Lineweaver-Burke plot to determine reaction mechanism (Fersht, 2017).

The kinetic data, reaction mechanism and mode of inhibition by L-cysteine presented in this chapter are vital pieces of information to understand the reaction mechanism of CysE. Understanding the reaction mechanism is crucial for computational inhibitor screening to identify lead compounds for CysE inhibition. For example, given that L-cysteine is an effective competitive inhibitor of CysE, the active site could be targeted by screening inhibitors that are isostructural to L-cysteine. Using methods developed in this thesis, the lead inhibitor compounds identified by computational screening will be tested *in vitro* to determine the IC_{50}, K_i and mode-of-inhibition.

Chapter 3

Structural and biophysical characterisation of CysE and the cysteine synthase complex

3.1 Introduction

CysE is a serine acetyltransferase (SAT, EC 2.3.1.30) that catalyses the first step of the two-step cysteine biosynthesis pathway. CysE catalyses the acetylation of L-serine, producing *O*-acetylserine. L-cysteine is formed from *O*-acetylserine, by the addition of sulphide and removal of acetate, catalysed by CysK. CysE and CysK bind together to form the cysteine synthase complex (CSC). The CSC is unusual in that most protein complexes are formed to shuttle substrates/products from one enzyme to another. The CSC differs in that the C-terminal tail of CysE binds in the active site of CysK to inhibit its activity (Campanini *et al.*, 2005; Huang *et al.*, 2005; Kumaran *et al.*, 2009). One hypothesis for formation of the CSC is for modulation of sulphur flux in bacterial metabolism (Hell *et al.*, 2002; Wirtz *et al.*, 2012). Alignment of the CysE protein sequence from *N. gonorrhoeae* with other bacterial homologues, demonstrates moderate sequence similarity compared to other proteobacterial species (average 55% sequence similarity), but shows strong conservation of hexapeptide repeat, active site and C-terminal tail residues (**Figure 1.7**). Although structures of CysE from other bacteria have been characterised, there has been no investigation into the structure of CysE or formation of the cysteine synthase complex from *N. gonorrhoeae*.

We propose CysE is a valid drug target for the design of new antimicrobial compounds to treat gonorrhoea. To do this we need a high-resolution structure for CysE (Reichau *et al.*, 2011), with and without substrates bound. These structures can then be used for computational inhibitor screening to identify lead compounds for further development. As there is no structure for CysE from *N. gonorrhoeae*, one of the aims of this thesis is to purify, crystallise and determine the structure of CysE using X-ray crystallography.

3.2 Materials and Methods

3.2.1 Crystallisation of CysE

3.2.1.1 Protein preparation

CysE protein was expressed and purified following methods in section 2.2.2 and section 2.2.4, respectively. Protein concentration was determined by Nanodrop™ as per section 2.2.4.5.

3.2.1.2 High throughput crystallisation screens

High throughput crystallisation screens were set up to identify promising crystallisation conditions that could be further optimised to produce crystals suitable for X-ray diffraction. The following screens: Index™-HR2-144, PEGRx HT™-HR2-086, CrystalHT™-HR2-130 and the SaltRxHT™–HR2-136 (Hampton Research, U.S.A.), were used. Screens were set up in low profile 96-2 well INTELLI-PLATE and were set up using the Mosquito crystallisation robot (TTP LabTech Ltd., USA). Each crystallisation condition had a reservoir solution (crystallisation solution) of 200 µl and 200 nl sitting drops. Protein drops consisted of a 1:1 mixture of reservoir solution and concentrated protein. Screens were checked weekly for crystal formation using a dissection microscope.

3.2.1.3 Hanging drop fine screens

Promising crystallisation conditions from high throughput screens were further optimised through scaling up to hanging drop fine screens. 24 well VDX trays were set up with mother liquor (well reservoir) volumes of 500 µl or 1000 µl from concentrated stock solutions. Hanging drops were prepared by mixing a 1:1 ratio (1:1 µl or 2:2 µl) of mother liquor and concentrated protein solution on a siliconised cover slip, before inverting drop-side down, over a well, lined with silicone grease. For each condition, crystallisation parameters such as pH, drop size and the concentration of protein and precipitant were optimised. Crystallisation drops were checked for crystal growth under a dissection microscope, daily for one week and weekly thereafter.

3.2.1.4 Ligand co-crystallisation

High throughput screens were set up as per protocol (section 3.2.1.2), but with the addition of acetyl CoA or L-cysteine to the concentrated protein stocks (final

concentration of 0.1 mM and 5.5 mM, respectively). Promising conditions were further optimised through setting up fine drop screens as per section 3.2.1.3, with the exception of adding the ligand to the protein stock before setting up the crystallisation drops.

3.2.1.5 Seeding method

Crystal seeding was employed to increase crystal size and improve diffraction quality. This method was used only for hanging drop fine screens, which were set up as per section 3.2.1.3. Before sealing the well, a single cat whisker was dragged across a CysE crystal grown from a previous crystal screen and swiped through the fresh CysE protein drop. The well was sealed as per section 3.2.1.3. Crystallisation drops were checked for crystal growth under a dissection microscope, daily for one week and weekly thereafter.

3.2.1.6 Final structure crystallisation condition

Purified protein was concentrated to 24 $mg.ml^{-1}$ and stored on ice for a short period of time, as prolonged incubation at room temperature lead to precipitation. This optimised tray was based on a condition identified from high throughput crystallisation tray HR2-144 Index^{TM} : 35% Tacsimate^{TM} (v/v) pH 7.0 (Hampton Research, USA). Tacsimate^{TM} is a mixture of seven organic acids and was used both as a precipitant and a buffer in CysE crystallisation (refer to Appendix C for Tacsimate^{TM} composition). Trays were set up as per section 3.2.1.3. The crystals used for X-ray diffraction were grown using whisker seeding. Drop composition was made up with 2:2 µl drops (mother liquor: protein concentrate). All crystals were grown at 18°C.

3.2.1.7 Crystal preparation for X-ray diffraction

Each crystal was transferred using a cryo-loop, to a cryo-protectant solution, consisting of a modified mother liquor solution with the addition of 15% glycerol (v/v) as a cryo-protectant. Crystals were then flash cooled in liquid nitrogen. Crystals were stored short-term in liquid nitrogen (one to two days) before data collection.

3.2.1.8 Ligand soaking

Ligand soaking was employed as an alternative method to obtaining the structure of CysE complexed with either substrates or inhibitors. This was carried out for

both L-serine and L-cysteine. Ligand soaks were prepared by the addition of either L-cysteine (5.5 mM) or L-serine (6 mM) to mother liquor solution. Crystals were grown and prepared for data collection as per section 3.2.1.7., with the addition of an extra soaking step, before transferring to the cryo-protectant solution.

3.2.2 Data collection

X-ray diffraction data was collected at the Australian Synchrotron (Melbourne, Victoria) on the MX2 beamline (McPhillips *et al.*, 2002), equipped with an EIGER x 16M detector (Dectris, Switzerland).

3.2.3 Data processing

3.2.3.1 Indexing, integration and scaling

The CysE dataset diffraction images were indexed, integrated and scaled, using XDS (Kabsch, 2010). Merging of reflections was carried out using AIMLESS (Evans & Murshudov, 2013) from the CCP4 suite (Winn *et al.*, 2011). Data quality was assessed through AIMLESS (Evans & Murshudov, 2013) and through manually viewing diffraction images using ALBULA (Dectris, Switzerland). FreeR flag dataset (5% of dataset reflections not to be used in refinement and used to compute R_{free}) was generated in AIMLESS.

3.2.3.2 Detection of twinning and non-crystallographic symmetry

Data was analysed for evidence of twinning and translational non-crystallographic symmetry (tNCS) in AIMLESS from the CCP4 suite (Winn *et al.*, 2011) (Evans & Murshudov, 2013) and *phenix.xtriage* from PHENIX suite

3.2.4 Structural analysis

3.2.4.1 Matthew's coefficient

The total number of monomers in the asymmetric unit was determined by calculating the solvent content using the Matthew's coefficient (Matthews, 1968) program, as a part of the CCP4 program suite (Winn *et al.*, 2011).

3.2.4.2 Molecular replacement

The structure of CysE from *Y. pestis* (3GVD) was retrieved from the protein data bank (PDB). A single monomer was extracted from this file, in PyMOL (The PyMOL Molecular Graphics System, Version 2.3.2 Schrödinger, LLC). Molecular

replacement was carried out using *phenix.phaser* (McCoy *et al.*, 2007), from the PHENIX suite (Adams *et al.*, 2010).

3.2.4.3 Model building and refinement

The model was initially built and refined using the program *phenix.autobuild* (Terwilliger *et al.*, 2008) from the PHENIX suite (Adams *et al.*, 2010). The resulting structure, was further built manually using the program COOT (Emsley & Cowtan, 2004). For manual building and refinement in COOT, the 2Fo-Fc and Fo-Fc electron density maps, were set to 1σ and 3σ, respectively. After each round of structure manipulation, *phenix.refine* was used to run rounds of real-space refinement (Afonine *et al.*, 2012).

3.2.4.4 Ligand fitting and refinement

We prepared the structure for ligand fitting by building and refining the protein structure and adding in waters using *phenix.refine.* We used the program *phenix.ligandidentification* to screen 200 common ligands. *Phenix.ligandfit* was used to search specifically for ligands of interest (Terwilliger *et al.*, 2006) (Venkatachalam *et al.*, 2003). Visual inspection and manual real space refinement were carried out in COOT.

3.2.4.5 Structural analysis

Assessment of Ramachandran outliers was carried out using *MolProbity* (Chen *et al.*, 2010), from the PHENIX suite (Adams *et al.*, 2010). Images of the model and maps were generated using programs PyMOL (The PyMOL Molecular Graphics System, Version 2.3.2 Schrödinger, LLC) and COOT (Emsley & Cowtan, 2004). Hydrogen bonds were classified as being moderate for distances between 2.5-3.2Å and weak for 3.3-4.0Å (Jeffrey, 1997). Bond distances were measured in PyMOL and COOT. Comparing structures was conducted through calculating root mean square distances (r.m.s.d) using alignment tool in PyMOL. The surface area and buried residue calculations for the trimer/hexamer interfaces were carried out using PDBePISA (Krissinel & Henrick, 2007). ENDscript 3.0 was used to identify secondary structural features (Robert & Gouet, 2014), alongside visual inspection in PyMOL. LigPlot+ was used to visualise ligand-protein interactions (Laskowski & Swindells, 2011).

3.2.5 Formation of the cysteine synthase complex

Protocol for forming the CSC was based on a method by (Benoni *et al.*, 2017b). CysE and CysK were purified individually before being used for CSC formation.

3.2.5.1 Purification of CysK

CysK was purified using IMAC and gel filtration chromatography as per section 2.2.4.1 and 2.2.4.2 by Dr Joanna Hicks with minor modifications. CysK was purified with the addition of CysK co-factor, pyridoxal 5' phosphate (PLP). 250 µl of PLP (final concentration 0.3 mM) was added to cell pellets just before sonication (section 2.2.4). CysK without the addition of PLP was also purified and used to form the CSC.

3.2.5.2 Formation of the cysteine synthase complex

CysE and CysK were combined together (CysE:CysK, molar ratio of 1:1 or 3:2) and were incubated on ice for 15 min (final volume 0.5 ml). After incubation, 20 µl was kept aside for native-PAGE gel electrophoresis. Apparent molecular weights of CysE, CysK and the CSC, were measured using gel filtration chromatography.

3.3 Results and Discussion

3.3.1 Crystallisation of CysE

Before the commencement of this master's research, Dr Joanna Hicks grew diffracting CysE protein crystals and collected datasets from three crystals (2.15, 2.56 and 2.6 Å respectively). All crystals were from the same crystallisation condition; 5% MPD, 10% PEG 6000, 0.1M HEPES (pH 8.0) (Figure 3.1). The data collected was processed in the H32 space group. However, despite many attempts we were unable to solve the structure, with R values not improving during refinement with the best final model having a R_{work}/R_{free} score of 0.29/0.39. Further interrogation of the datasets using *phenix.xtriage* showed that these datasets had a high percentage of twinning. Attempts to detwin the data using *phenix.refine* and DETWIN (CCP4 suite), were unsuccessful. It was decided to screen and optimise alternative crystallisation conditions to produce un-twinned high-quality crystals.

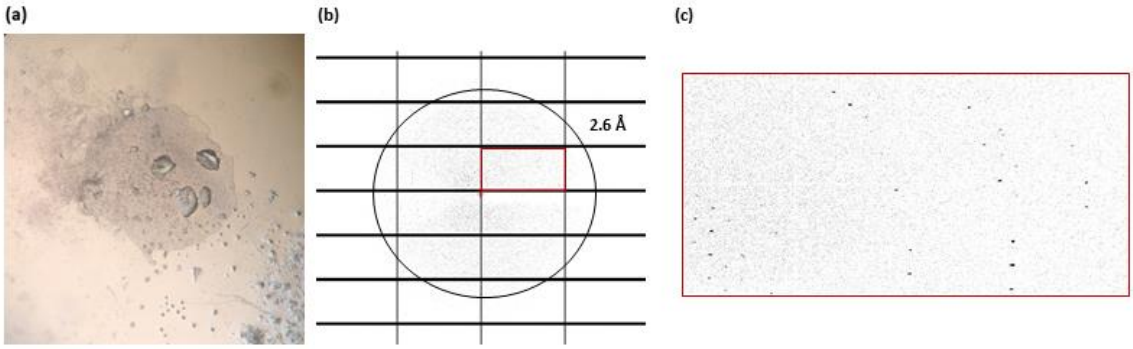

Figure 3.1: Initial crystallisation and diffraction of CysE. (a) Crystallisation condition; 5% MPD (v/v), 10% PEG6000 (v/v), 0.1M HEPES pH 8.0. (b) Example diffraction image of crystal. (c) Close up of diffraction pattern from (b). Diffraction images generated using ALBULA.

High throughput crystallisation screens were trialled (section 3.2.1.2) and we observed several promising crystallisation conditions that produced micro-crystals. Multiple crystallisation conditions were scaled up to fine screen hanging drops, where crystallisation parameters such as pH and precipitant concentration were varied. The best formed crystals grew in 35% (v/v) Tacsimate^{TM} (pH 7.0) and so this condition was further optimised. While some well-formed crystals grew in this condition, the majority of the crystals were poorly formed (Figure 3.2). To improve crystal quality, pH, Tacsimate^{TM} concentration, and drop size were optimised. The shape of the crystal improved if the pH was lowered (7.0 to 6.5) and larger crystals were obtained by increasing the final drop volume from 2 to 4 µl. However, the diffraction quality of these crystals was poor (3.5 - 4.0 Å, data not shown). Therefore, seeding techniques were employed to improve crystal quality.

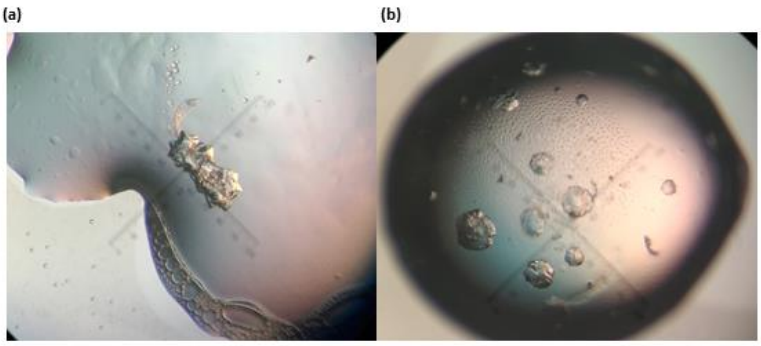

Figure 3.2: CysE crystals grown in Tacsimate$^{TM.}$ (a) Crystal from 35% Tacsimate^{TM} (v/v) pH 6.5. (b) Crystal from 21% Tacsimate^{TM} (v/v) pH 6.6.

Crystallisation drops were whisker seeded (using a crystal pre-grown in the same crystallisation condition) and set up with a 10-20% reduction in both protein and precipitant concentration to prevent spontaneous nucleation events from occurring and promote growth of larger crystals. Crystals grew faster using this method (⩽1 week vs. 2-4 weeks) and produced well-formed single crystals. The best formed crystals grew between 26-28% (v/v) Tacsimate^{TM} and between pH 6.5-6.8.

Crystals were prepared for X-ray diffraction by immersing in a cryoprotectant solution consisting of the crystallisation solution plus 15% (v/v) glycerol, before flash freezing in liquid nitrogen. Diffraction data were collected at the Australian synchrotron on the MX2 beamline, equipped with an EIGER detector, as per section 3.2.2. Diffraction data were collected from a 360° rotation of the crystal, with data collected every 0.5°, at a wavelength of 0.9537 Å. Diffraction data were collected from a single crystal grown in 28% (v/v) Tacsimate^{TM} pH 6.6 at a protein concentration of 24 mg.ml^{-1} (Figure 3.3).

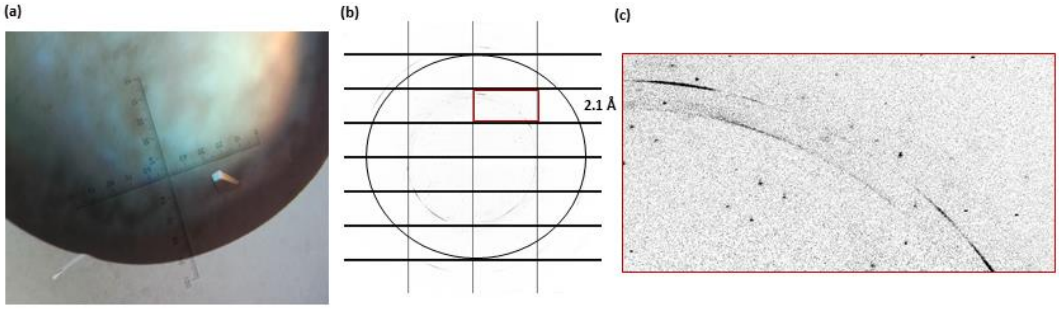

Figure 3.3: Crystallisation and diffraction of CysE apoenzyme. (a) Crystal grown using hanging drop and whisker seeding. Crystallisation condition: 26.25% (v/v) Tacsimate^{TM} pH 6.6, 24 mg.ml^{-1} of protein. (b) example of CysE diffraction from crystal. (c) Close up of diffraction pattern from (b).

3.3.2 CysE data processing

Data was indexed initially in space group $P2_1$, but was determined to have been incorrectly assigned using *zanuda*, (Lebedev & Isupov, 2014) from the CCP4 suite (Winn *et al.*, 2011). The data was subsequently reindexed in space group P2 (based on *zanuda*_output), integrated and scaled using XDS (Kabsch, 2010). Data was merged using AIMLESS from the CCP4 suite (Winn *et al.*, 2011). AIMLESS was also used to generate a FreeR flag dataset for refinement and dataset quality statistics (Table 3.1). The CysE dataset had resolution to 2.01 Å. Data quality statistics demonstrate that the quality of the data is good with parameters meeting the following data quality thresholds; $CC_{1/2} \geqslant 0.3$ (0.917), $I/\sigma I \geqslant 2.0$ (3.5) and $R_{merge} \leqslant 0.8$ (0.490) and overall completeness > 95% (100%) (values in highest resolution shell reported). Resolution was not cut back and data were used for downstream processing.

Table 3.1: Data collection statistics for CysE. Statistics for highest resolution shell are in brackets. Data statistics generated by AIMLESS and *phenix.tableone.*

Data statistic	**Apostructure**	
Space group	P2	
Wavelength (Å)	0.953732	
Cell dimensions **a/b/c (Å)** **α/β/γ (°)**	77.999/94.011/102.158 90.000/91.285/90.000	
Mosaicity	0.05	
Monomers in asymmetric unit	6	
Resolution range (Å)	46.93-2.01	(2.04-2.01)
Numbers of observed reflections	689243	(35091)
Number of unique reflections	97704	(4841)
$\mathbf{R_{merge}}$	0.053	(0.490)
$\mathbf{R_{pim}}$	0.02259	(0.1943)
CC $_{(1/2)}$	0.999	(0.917)
Mean I/σI	17.2	(3.5)
Completeness	100.0	(100.0)
Multiplicity	7.1	(7.2)
Wilson B factor (Ang^2)	30.7	

3.3.3 Solving the structure of CysE

There are homologous CysE structures in the PDB, some of these were identified to be potential candidates for molecular replacement with good sequence similarity (≥ 30%) and conservation of secondary structural features (Figure 1.7 and Figure 3.4). Using this information, we decided to use the CysE structure from *Y. pestis* (3GVD) as our search model for molecular replacement as it exceeded the minimum sequence requirements (57% sequence similarity) (Kim *et al.*, 2006) and the majority of the structure had been built (96%).

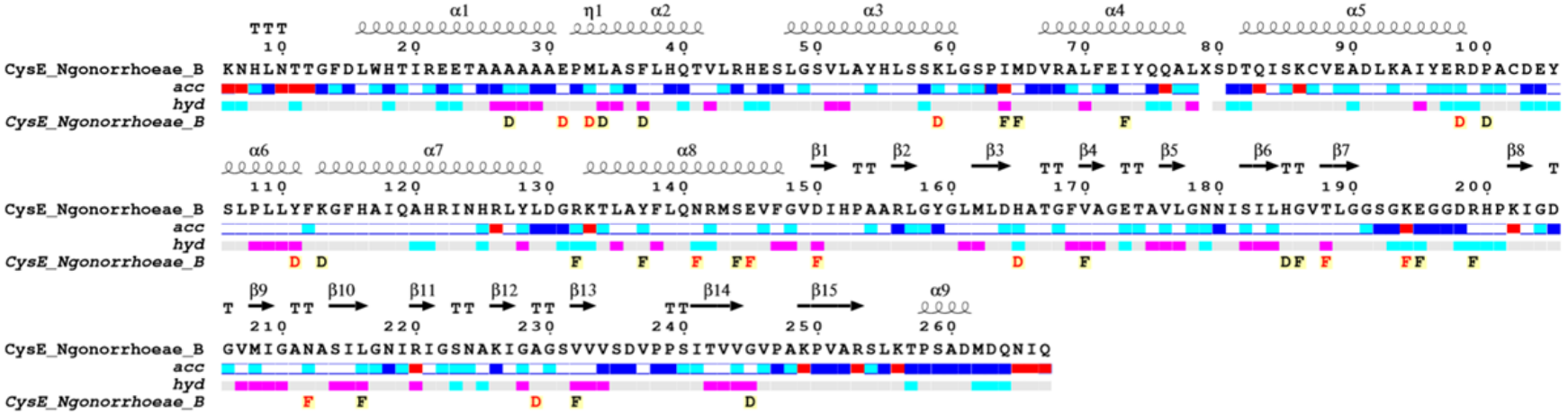

Figure 3.4: ENDscript analysis of the secondary structure of CysE from *N. gonorrhoeae.* For each residue solvent accessibility and hydrophobicity is labelled below the sequence. Solvent accessibility is labelled "acc" and is rated in terms of "Blue" being accessible, "cyan" less accessible, "white" being completely buried, from solvent (red being not calculated). Hydrophobicity is labelled as "hyd" and is ranked as cyan being hydrophilic, purple being hydrophobic and white being neutral. Secondary structure elements are labelled in grey above the peptide sequence, with helices, β-strands, and β-turns, represented by linked loops, arrows and TT, respectively. Letters indicate non-crystallographic interaction with chain denoted by letter. Refer to Appendix C.3. for chain labelling of the monomers in the ASU. Chain B was used for analysis. Figure generated using ENDscript 2.0 (Robert & Gouet, 2014).

The Mathew's co-efficient was used to predict the number of monomers in asymmetric unit (ASU) (Matthews, 1968). The most likely number of monomer copies was determined to be six, calculated with a predicted molecular weight of 31.5 kDa for CysE using Protparam, (section 2.2.4.2). For molecular replacement, the CysE monomer (3GVD) was used as a search model, with six monomers in the ASU (*Phenix.phaser*). Phaser found one solution, which had good TFZ and LLG scores of 37.3 and 5333, respectively (McCoy *et al.*, 2007).

Phenix.xtriage and AIMLESS were used to assess data quality and detection of crystal pathologies. There was strong evidence that the CysE dataset possessed translational non-crystallographic symmetry (tNCS), as indicated by the presence of a large (48%, $p= 8.2*10^{-5}$) non-origin peak of the Patterson function. tNCS can lead to issues during refinement such as high R-values (R_{work}/R_{free}) (Read *et al.*, 2013). Therefore, the structure was refined with tNCS torsion-constraints using *phenix.refine*. The program also detected the presence of two ice rings, which are visible in Figure 3.3. Completeness in resolution shells 2.26-2.22 Å was noticeably lower compared to other low resolution shells (92 vs. 99%) (Appendix C.2.). Given that the level of data completeness was still reasonable ($\geqslant$90%), no data was excluded from downstream analysis.

The CysE model was built using the program *autobuild.phenix*. The program was supplied with the *phenix.phaser* output model and map, reflection file (with FreeR flag dataset) and the CysE amino acid sequence. Default settings were used (Appendix C.4.), with the exception of not placing waters in refinement and rebuild in place set to false. The latter step is to allow the program to edit the structure file sequence based on the sequence file, as well as build outside the model (if there is unmodelled density). The structure went through six iterative building rounds and three cycles of refinement. The resulting structure had a good R_{work}/R_{free} score for a starting model of 0.2413/0.28839. In the asymmetric unit, six monomers were built, with three packed forming a homotrimer, while two of the remaining monomers form two-thirds of a trimer, while the remaining monomer is outside of the trimer. The last trimer can be generated from the repeating crystal symmetry lattice (Appendix C.3.). The majority of each monomer was built (80%) by automated building using *phenix.autobuild*, however there was a large amount of

unmodelled density at both the N and C-terminal ends of each chain. The remaining unbuilt peptide sequence was manually built in COOT.

3.3.3.1 Identification of active site ligand

Visual inspection of the refined CysE model, revealed that the active site had unmodelled density that was too large to be water (Figure 3.5). Initially we screened 200 compounds using *phenix.ligandidentification* (as per section 3.2.4.4), but this was unsuccessful. Using *phenix.ligandFit* we screened the physiologically relevant compounds L-serine and L-cysteine. Once fitted, the model and ligand were refined together using *phenix.refine*. Initially, both L-cysteine and L-serine fitted well, but after refinement, the Fo-Fc map indicated that there was still positive density present, and that the thiol and hydroxyl group did not have enough electron density to support the electron density map. Based on this we screened the buffer compounds malonate and D-malate present in our crystallisation condition (i.e. compounds present in Tacsimate^{TM} , Appendix C.1.). Malonate is a three carbon dicarboxylic acid, and fitted well initially, but there was clearly a side group present on the middle carbon. Finally, we fitted and refined with D-malate, and found that there was no positive or negative density present (Figure 3.5b), indicating a good fit.

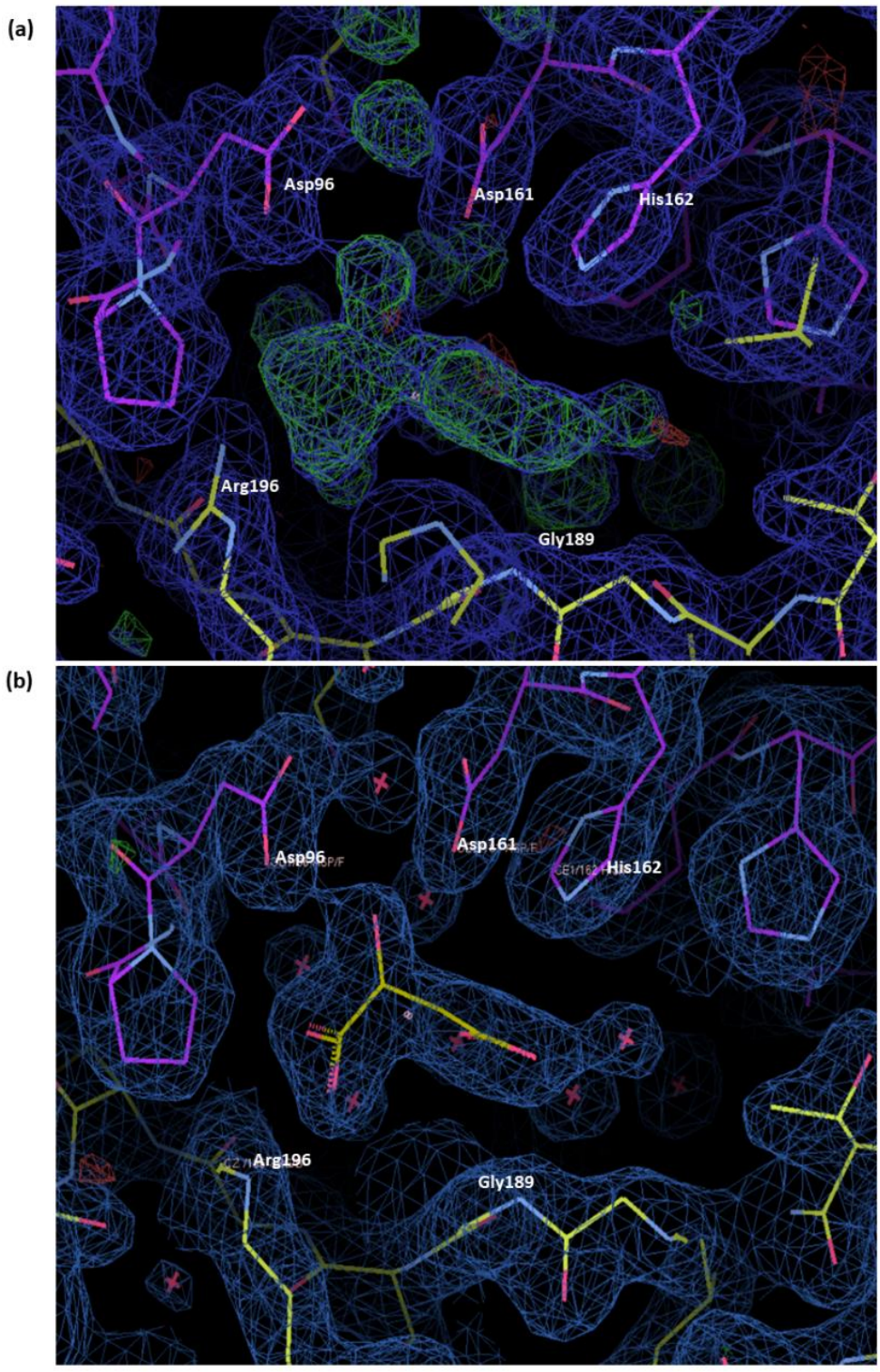

Figure 3.5: COOT electron density maps for fitting of D-malate. (a) Map and model used for fitting ligands. (b) Refined map and model with D-malate. 2Fo-Fc map (blue mesh) is contoured to 1 σ and Fo-Fc map is contoured to 3 σ (green and red mesh). Green mesh = positive density, Red mesh = negative density. Active site residues Asp161, His162, Arg196, Gly189 and Asp96 are labelled. D-malate is denoted as dark yellow sticks. Waters are denoted as red crosses.

3.3.4 Analysis of CysE structure

Our final structural model for CysE has a final R_{work}/R_{free} of 0.1846/0.2174 (Table 3.2). Structure and map files for the CysE model are listed under Appendix C.5. There was no density to support the N-terminal Hexahistidine-tag for any of the chains in the ASU, or the first two residues of each monomer. The overall structure of CysE is well built, with an average monomer length of 260 residues (260/272, 96% built) (Appendix C.6.). The CysE monomer is composed of an N-terminal α-helical domain (Met1-Phe144) and a unique left-handed parallel β-helix (LβH) (Gly145-Ile272) (Figure 3.4 and Figure 3.6,). The alpha helical domain consists of eight α-helices. The domain begins with a meandering loop (Lys3-Asp12). α1 helix spans from Leu13-Ala27. From α1 to α2 there is a sharp $\approx$ 180° turn, which aligns α2 (Pro29-Arg41) and α1, forming an antiparallel hairpin. After α2 an $\approx$ 90° turn occurs before α3 (Leu45-Leu57), breaking away from the α1 and α2 hairpin. After α3, there are two turns, lining up α4 (Val64-Ala74) to run antiparallel to α3. From α4 there is another turn before leading to α5 (Thr79-Arg95). After α5 a turn links to α6 (Tyr102-Tyr108). From α6 there is a turn before transitioning to α7 (Lys110-Asp127) which is followed by the helix α8 (Lys130-Phe144), which then leads onto the beginning of the C-terminal domain.

Table 3.2: CysE final model quality statistics. Statistics generated by *phenix.xtriage* and *phenix.tableone*.

Data statistic	**CysE**
R_{work}	0.1818
R_{free}	0.2159
No. of protein residues	1550
Total number of non-hydrogen atoms	12194
Macromolecules	11465
Ligands	54
Solvent	675
RMS Bonds (Å) **Angles (°)**	0.008 1.018
Average B value (Å)	38.74
Macromolecules	38.64
Ligands	34.97
Solvent	40.86
Ramachandran analysis	
No. of residues in favoured region (%)	97.3
No. of residues in allowed region (%)	2.7
No. of residues in outlier region (%)	0.0
Rotamer outliers (%)	0.09

The C-terminal domain consists of a lefthanded parallel β (LβH) helix, consisting of 15 turns and five distinct coils. The helix contains six β-sheets: β1 (Leu158-Asp161), β2 (Ile178-Leu181), β3 (Thr185-Gly187), β4 (Ile238 -Val241), β5 (Lys246-Arg250), β6 (Lys246-Arg250) (Figure 3.6). The repeating turn-sheet-turn pattern is generated by repetition of a tandem hexapeptide repeat (Figure 1.7 and Figure 3.4). The only deviation from this repeat within the helix is between β3 and β4, which leads to the formation of an extended β-loop. This β-loop extends from

Gly191 to Arg199. This loop forms one half of the active site for CysE, and houses active site residues Arg196, His197, Gly188, where D-malate binds (Figure 3.6). The LβH ends at Pro244, after which the short C-terminal tail breaks away from the helix forming a small helix α9 (Pro255-Asp258).

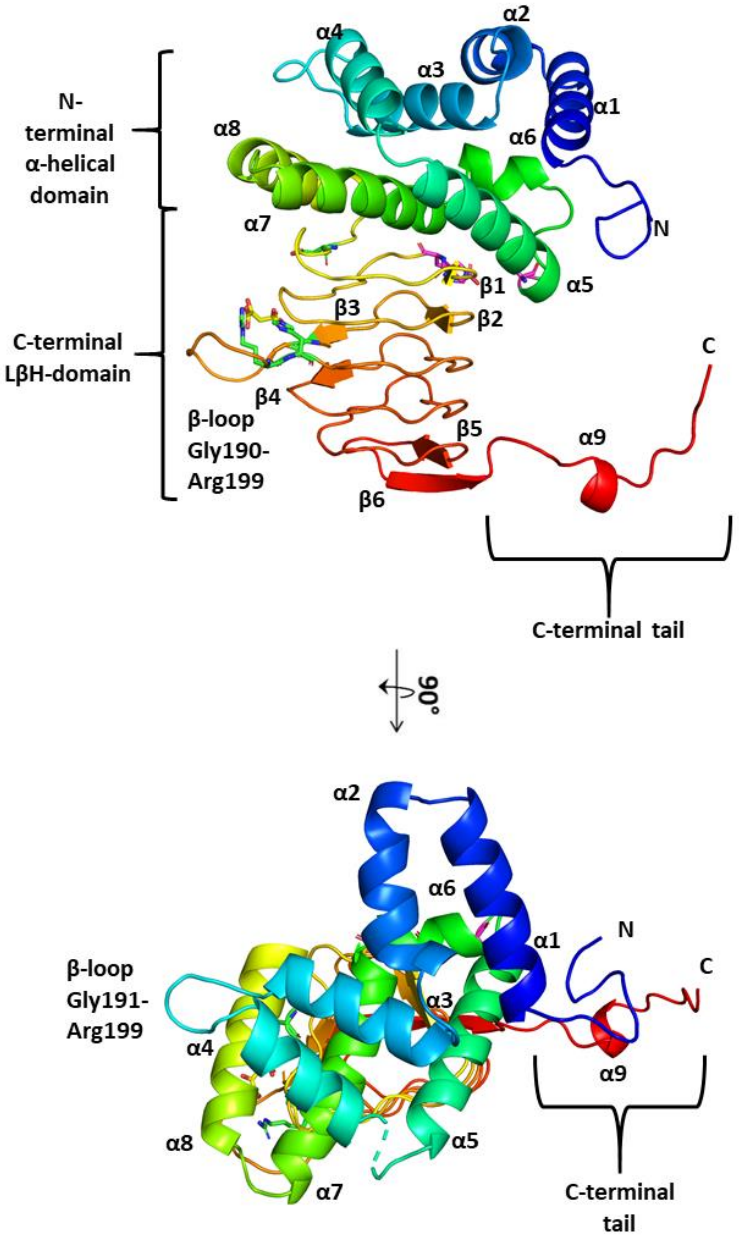

Figure 3.6: CysE monomer from *N. gonorrhoeae*. Protein amino-terminus is coloured blue and carboxyl-terminus is coloured red. All domains are labelled as well as the flexible C-terminal tail. Active site residues and the bound ligand D-malate are represented as sticks, with malate coloured yellow. Active site residues are coloured green and purple to match colour scheme in Figures 3.8 and 3.9. Note active sites are shared across two monomers in the trimer explaining why active site residues are on opposing sides of the monomer. Figure generated in PyMOL.

The C-terminal tail adopts two conformations in our structure. For chains C and D (Appendix C.3), the tail loops upward against the side of the monomer, in the same manner as homologous CysE structures (Figure 1.8c) forming predominantly hydrophobic interactions, as well as a single hydrophilic interaction between the terminal amine group on Lys223 and the hydroxyl groups from tail residues Asp260, Gln261 and Asn262 (Figure 3.7b). For chains A, B, E and F, the tail extends outward away from the trimer and packs against neighbouring CysE monomers, by fitting into the groove where the C-terminal tail would bind (Figure 3.7c, Figure 3.8a and Figure 3.9). We hypothesise this extended C-terminal conformation is formed from domain swapping.

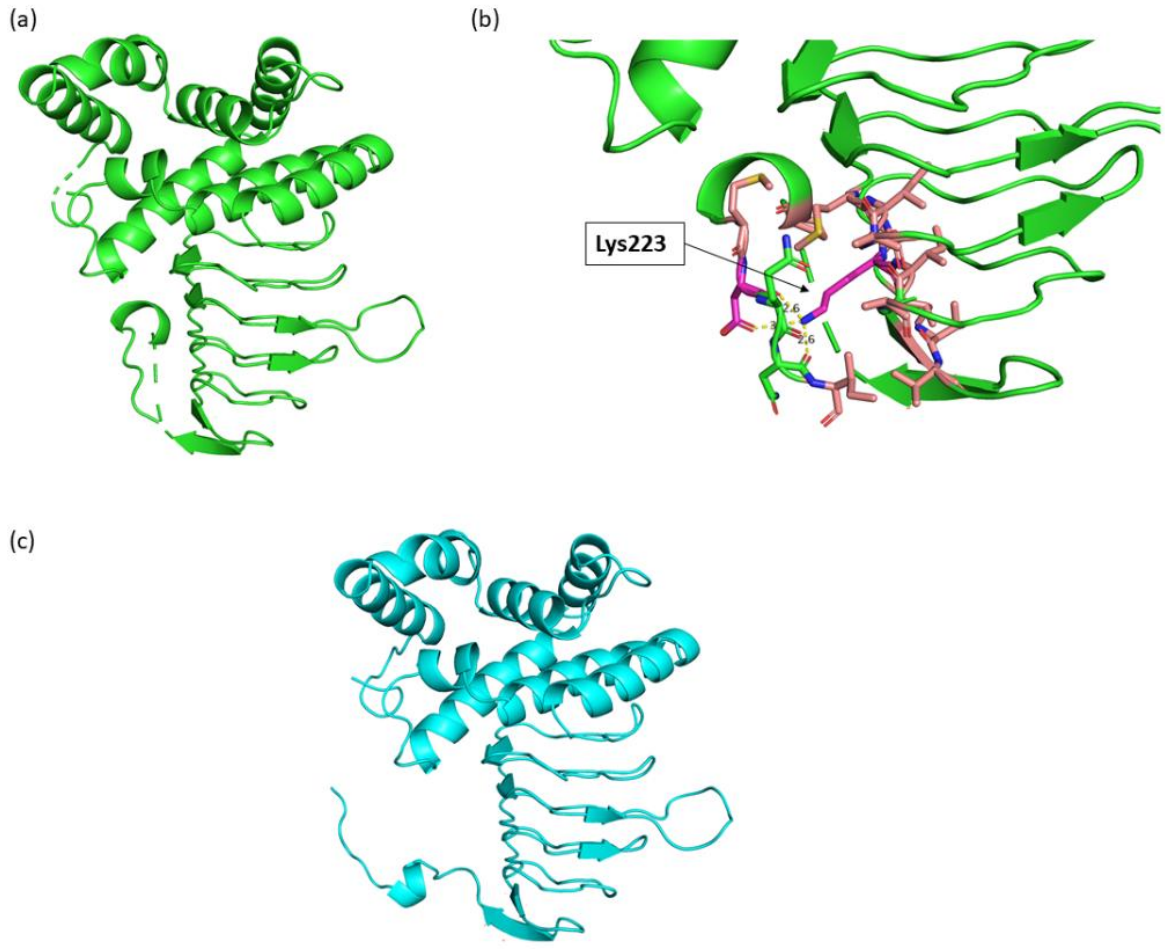

Figure 3.7: Comparison of the two C-terminal tail formations present in CysE. (a) Monomer with folded C-terminal tail. (b) Close up of C-terminal tail from (a) interacting residues are shown as sticks with hydrophobic residues coloured peach, polar residues coloured green and hydrophilic residues coloured magenta. (c) Monomer with the 'domain swapping' C-terminal tail. Images generated in PyMOL.

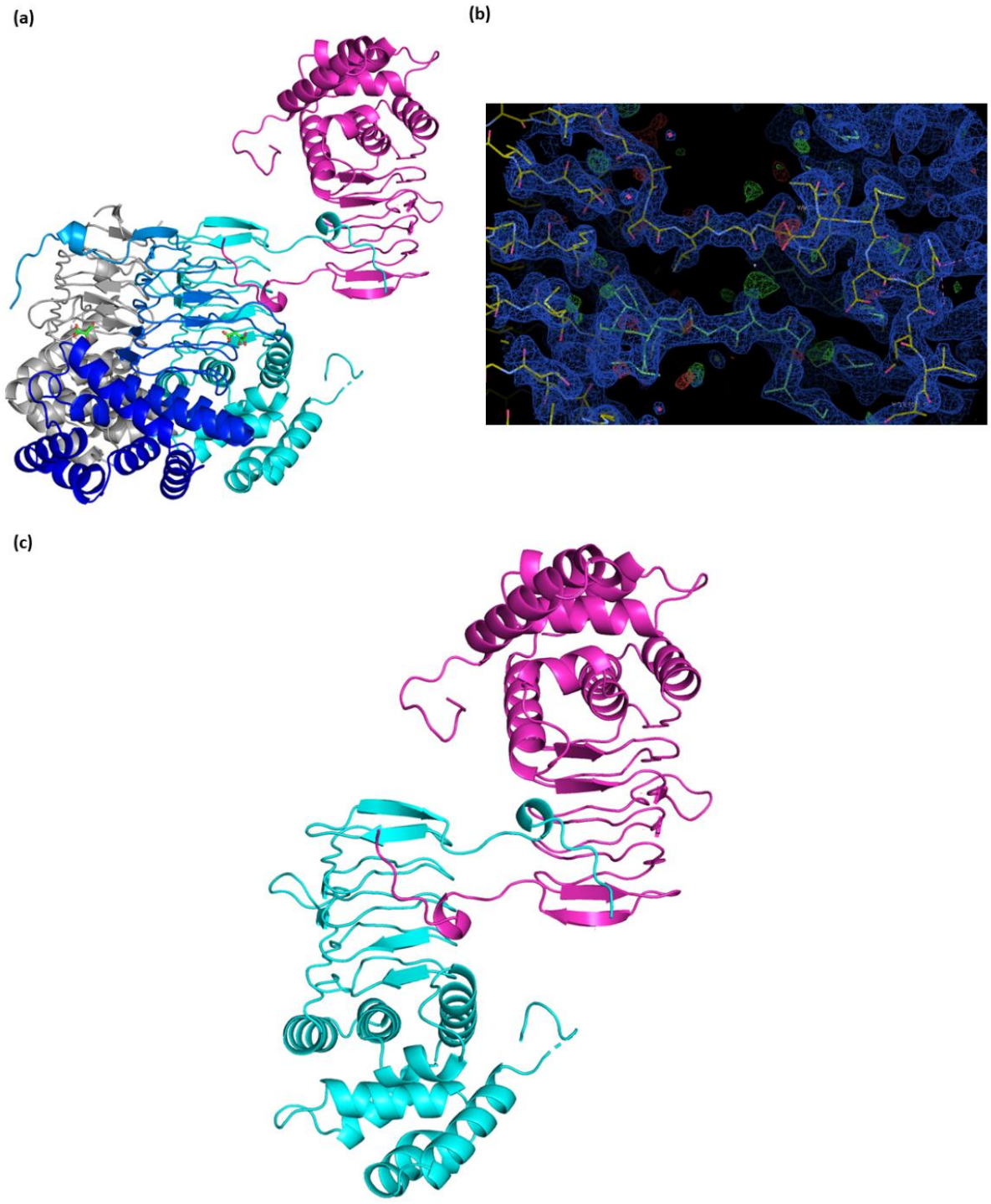

Figure 3.8: Analysis of the domain swapping C-terminal tail in the CysE monomers. (a) Monomer C-terminal domain swapped with monomer in adjacent hexamer. Non-domain swapped monomers in both hexamers have been removed for clarity. (b) COOT electron density map for domain swapped C-terminal tail. 2Fo-Fc and Fo-Fc map contoured at one and three σ, respectively. (c) Domain swapped monomers from (a), with non-interacting monomers removed. Images generated in PyMOL and COOT.

Domain swapping is where two proteins exchange identical structural segments with each other, forming a higher oligomeric conformation (Bennett *et al.*, 1995). The domain swapped C-terminal chains are supported by electron density, for four chains (Figure 3.8b). In domain swapped proteins there is often a hinge loop which is able to adopt a domain swapped conformation (Bennett *et al.*, 1995). In CysE we see that the C-terminal chain deviates from the folded C-terminal conformation at residue Ser251 (Figure 3.9). The C-terminal tail extends away from the monomer from Ser251 to Pro255, and then mimics the interaction of the CysE folded C-terminal tail from Ser256 to Gln264, as demonstrated by alignment of the blue/green C-terminal tail.

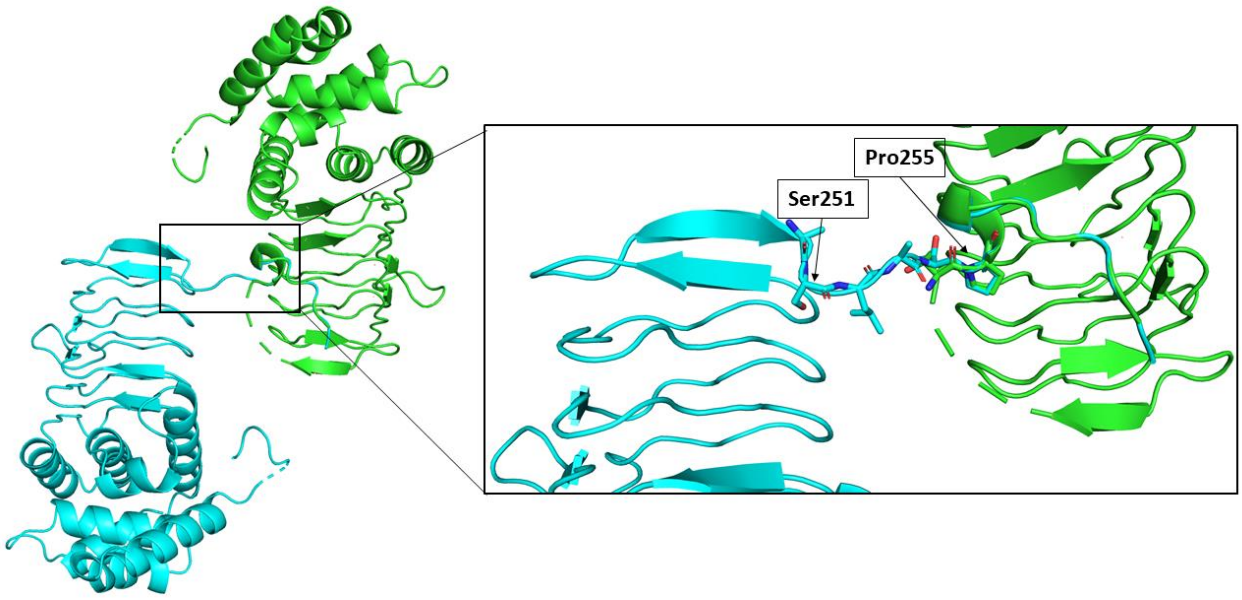

Figure 3.9: Analysis of the domain swapped CysE C-terminal tail. Domain swapped monomer is coloured cyan. The folded C-terminal tail monomer denoted as green. Chain B is coloured cyan, chain C is coloured green. Hinge loop residues labelled and denoted as sticks. Image generated in PyMOL.

For chains C and D, which have the folded C-terminal tail conformation, the monomers are likely capable of domain swapping but are unable to due to crystal packing. In Figure 3.10, the monomers with folded C-terminal tails (yellow/chain C and magenta/chainD) are horizontally displaced from monomers in the neighbouring hexamer (green), preventing the C-terminal tails from being able to physically reach the C-terminal binding region on the adjacent monomer and as a result are unable to undergo domain swapping.

CysE purifies as a hexamer during gel filtration chromatography (Figure 2.2), and SAXS analysis is also consistent with a hexameric protein (data collected by Dr Hicks and not shown), consistent with the majority of CysE homologues. We conclude that the extension of the C-terminal tail leading to domain swapping is an artefact of crystal packing and is not present when CysE is in solution. The C-terminal tail is well built in this structure compared to the many CysE structures in the PDB (Olsen *et al.*, 2004; Pye *et al.*, 2004; Kumar *et al.*, 2011).There are still eight residues missing from the C-terminal tail, but this tail has been reported to be flexible (Pye *et al.*, 2004) and so is likely not visible in the crystal structure.

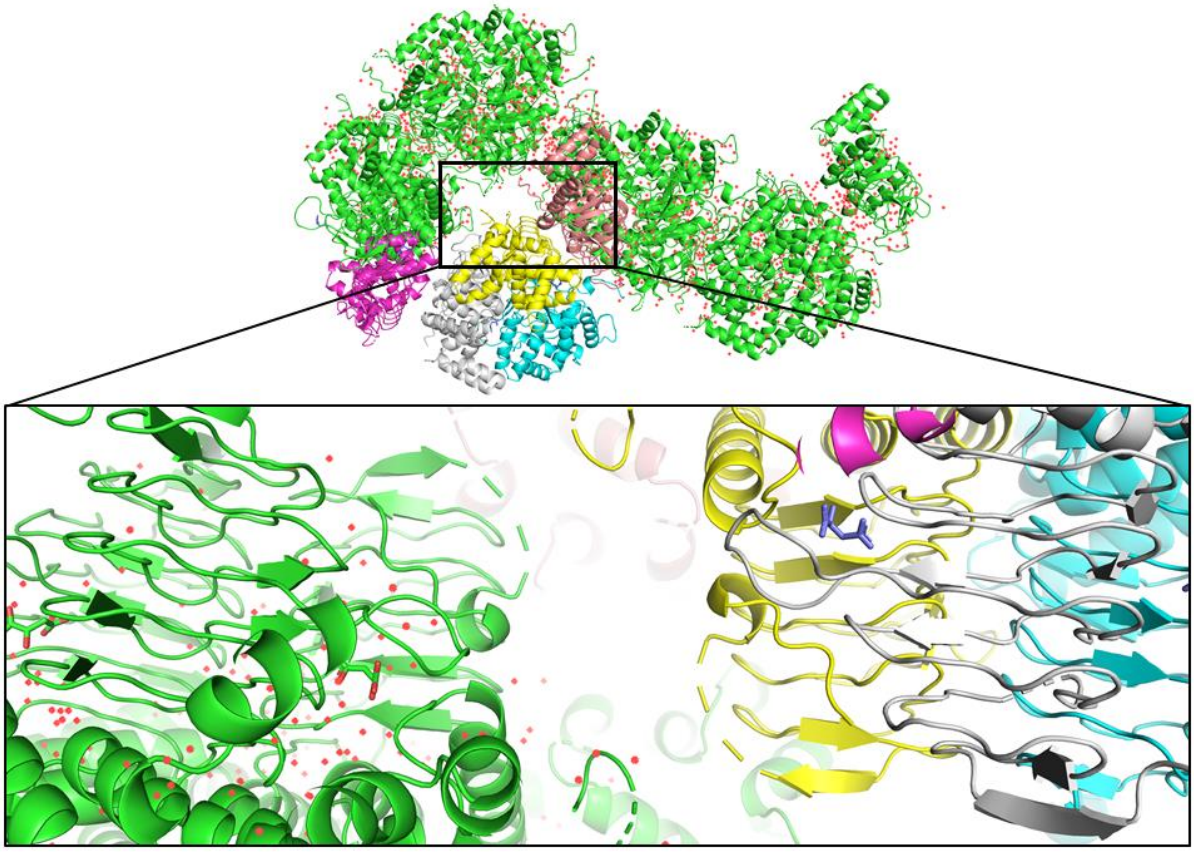

Figure 3.10: Analysis of CysE monomers with no domain swapping. The image contained within the black box is a close up of one of the folded C-terminal monomers (yellow) amongst packed hexamers in the lattice. Here the symmetry generated monomer (green) and folded monomer are displaced vertically as a result of crystal packing.

3.3.4.1 Analysis of the CysE hexamer

In the monomer, each LβH helix is shaped as a triangular barrel, which pack together to form a trimer with three fold symmetry (Figure 3.11a,b). The trimer has a height of 44 Å, and a width of 50 Å at the N-terminus and 48 Å at the C-terminus. The main interactions between monomers in the trimeric arrangement are hydrophobic interactions between the N-terminal helices α2 and α4 on adjacent monomers.

The CysE hexamer is composed of a dimer of trimers and has three and two fold symmetry (Figure 3.11c). The CysE hexamer is 104.2Å long, with the same width dimensions of the trimer. The dimer of trimers forms through interaction of the N-terminal domains between two trimers. A large portion of the trimer surface area is buried at the trimer-trimer interface, with 22410 $Å^2$ buried out of a total hexameric surface area of 50460 $Å^2$ (calculated as per section 3.2.4). The calculated free gibs energy for the dissociation (ΔG^{diss}) of the hexamer is 18.5 kcal/mol, demonstrating that the hexameric arrangement is thermodynamically stable. CysE has been confirmed to elute as a hexamer by gel filtration chromatography (Figure 2.2) This hexameric oligomeric state for CysE, has been demonstrated by Kumar *et al.* (2011), to vital for CSC formation.

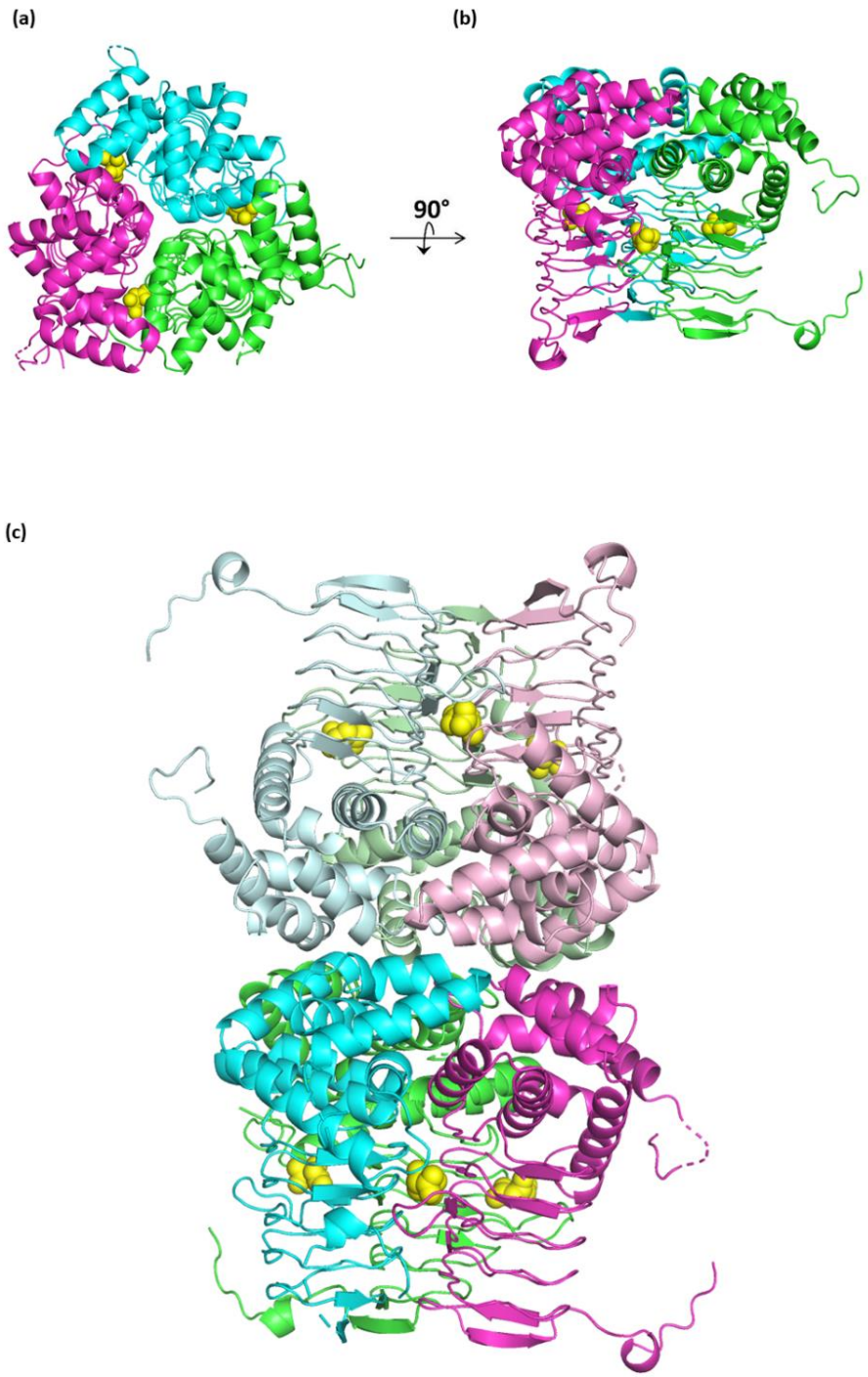

Figure 3.11: Quaternary arrangement of CysE from *N. gonorrhoeae*. (a) CysE trimer. (b) Trimer rotated by 90°C. (c) Dimer of trimers, hexameric arrangement. Peptide chain is displayed as cartoon and D-malate is shown as yellow spheres bound in the active sites. Figure generated using PyMOL.

3.3.4.2 The CysE active site

Active sites are formed between each monomer in a trimeric arrangement, with six actives site per hexamer. Active site residues are distributed between neighbouring monomers (Figure 3.11, Figure 3.12 and Figure 3.14). These active site residues have been identified through sequence alignment (Figure **1.7**) and are labelled in

Figure 3.13 and Figure 3.14. One half of the active site is on the β-extended loop (Arg196, His197, Gly188B, green) of one monomer, while the other residues (Asp96, Asp161 and His162,magenta) are situated on the linking turn between the α5 and α6 helices (Figure 3.12). Hydrogen bonds between D-malate and residues were determined using the measurement wizard tool in LigandPlot (Figure 3.14) and PyMOL (Figure 3.13).

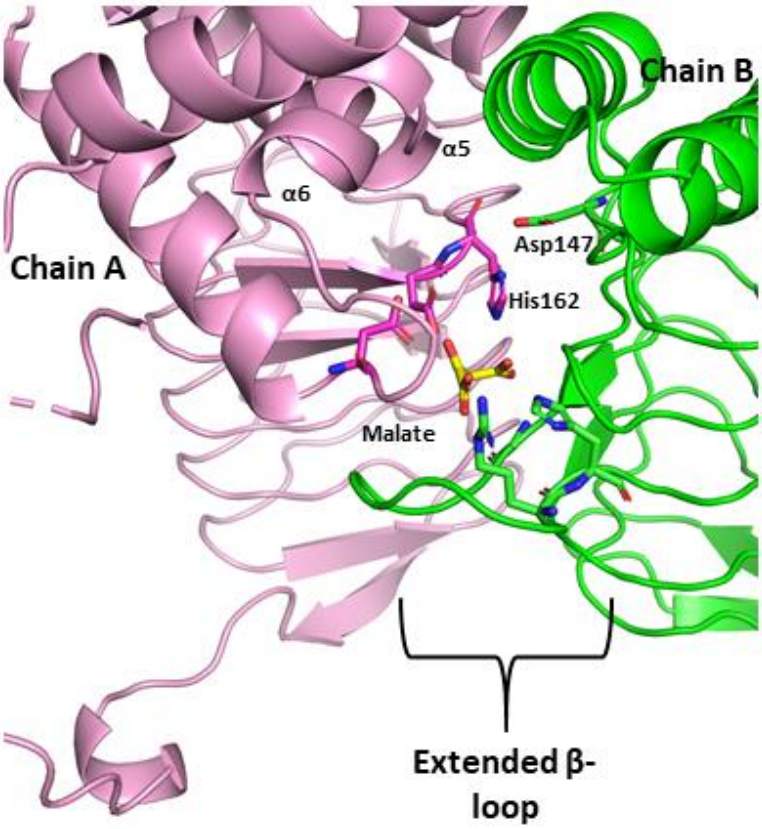

Figure 3.12: D-malate bound in the active site between two CysE monomers. D-malate and active site residues represented as sticks. Catalytic residues Asp147 and His162 are labelled. Figure generated using PyMOL.

The Arg196 terminal amine and amide form strong hydrogen bonds (2.7 and 2.8 Å) with the C1 carboxylic group (Figure 3.14). The α-hydroxyl group interacts with a water (3.1 Å), which is co-ordinated by negatively charged groups from Asp96 and Asp161. The C4 carboxylic acid group is wedged between two flanking histidines, His162 and His189. The carboxyl group is bent away from catalytic residues His162 (3.6 Å, distance not shown), and hydrogen bonds to the Nϵ2 from the imidazole ring of His197 (2.8 Å) and peptide backbone amide of Gly188 (2.6 Å) (Figure 3.13 and Figure 3.14).

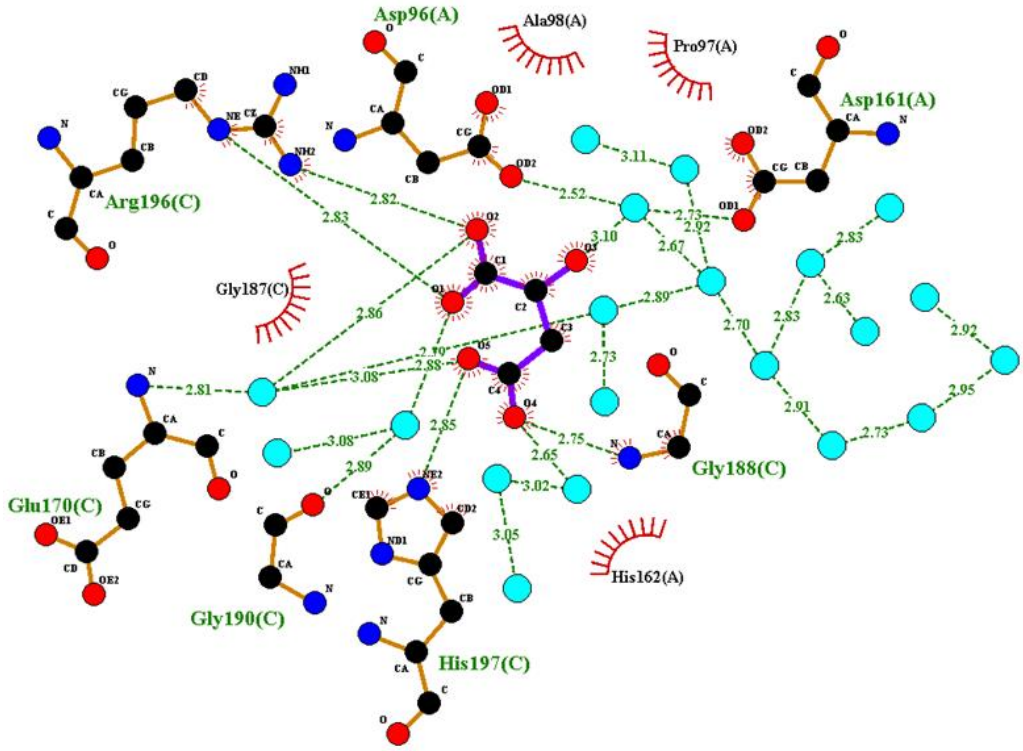

Figure 3.13: LigPlot representation of D-malate interaction in CysE active site. Only hydrophobic interactions between catalytic triad residue His162 and D-malate are observed. Figure created using LigPlot+ .

The formation of the catalytic triad is present in the *N. gonorrhoeae* CysE structure with the co-ordination and interactions of D-malate and active site residues comparable to those seen with L-cysteine bound in the *E. coli* CysE structure (Figure 3.14b, c). The major differences regarding interactions is between the carboxylic acid group and the flanking histidine residues. In *E. coli*, the thiol group from L-cysteine interacts with both of these histidine residues.

Catalytic triad residues, His162 and Asp147, are equivalent to His158 and Asp143 in *E. coli* (1T3D) (Figure 3.14). Likewise, the *N. gonorrhoeae* active site residues Asp161, Asp96, Arg196, His197 are equivalent to Asp153, Asp88, Arg188 and His189, respectively, in *E. coli.* The majority of hydrophilic interactions between *N. gonorrhoeae* CysE and D-malate are the same as *E. coli* CysE (1T3D) and L-cysteine. The only differences are the interactions between the active site histidines and the terminal carboxylic acid/β-thiol group (*N. gonorrhoeae*/*E. coli*). In our CysE structure the carboxylic group is bent away from His162, and instead is co-ordinated to the amine of the His197 imidazole ring and the peptide amine group of Gly187 on the Chain C side of the active site.

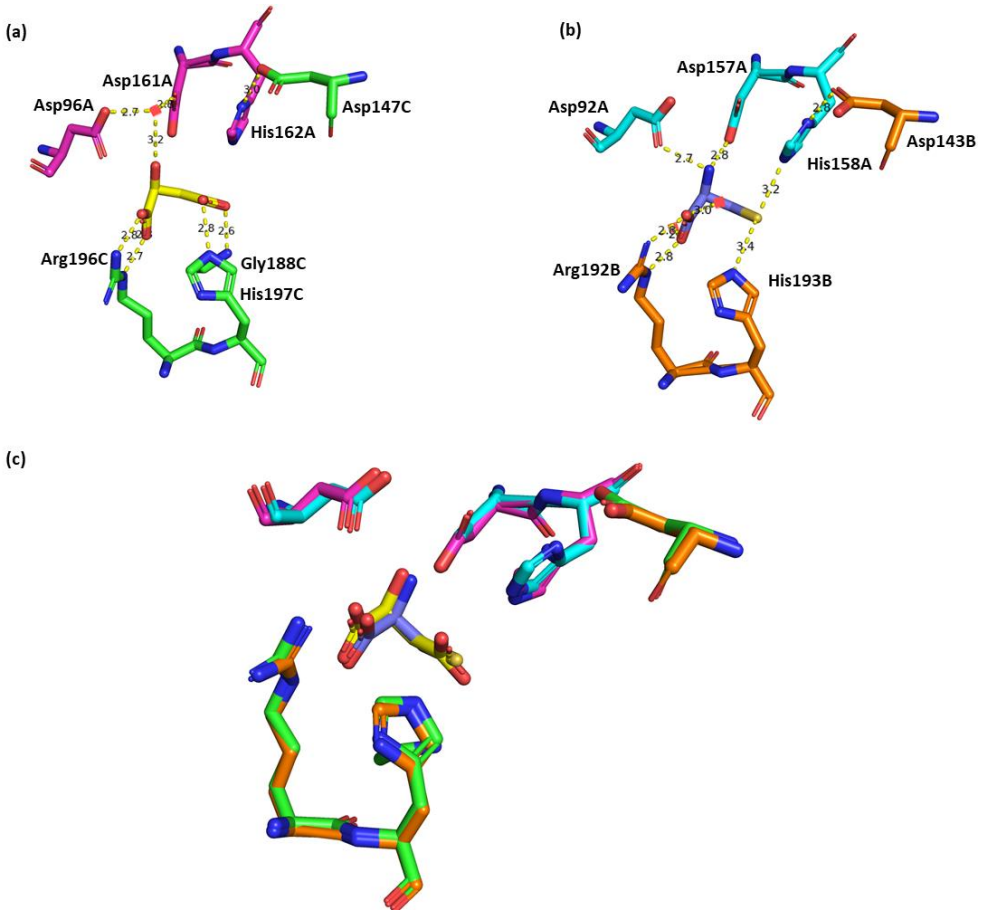

Figure 3.14: Comparison of active sites from *N. gonorrhoeae* with D-malate bound and CysE with L-cysteine bound from *E. coli* (1T3D). D-malate, L-cysteine and active site residues represented as sticks. (a) Chain A and chain B active site residues have been coloured pink and green to represent belonging to each adjacent monomer. Malate is coloured purple. (b) Chain A and chain B active site residues have been coloured pink and green to represent belonging to each adjacent monomer. Cysteine is coloured purple. (c) Overlay of CysE with 1T3D. Dashed lined represent hydrophiclic interactions. Bond distances are in Angstroms. Figure created using PyMOL.

Equivalent residues involved in CoA binding, from the soybean CysE structure were identified using structural alignment in PyMOL. Here, residues Ala215, Ala233 and Gly195, are equivalent to residues Ala208, Ala226 and Gly188 from *N. gonorrhoeae* (Figure 3.15). Superposition of the CysE structure from soybean complexed with CoA (4N6B) and our CysE structure, show a high degree of similarity (r.m.s.d = 0.682). We subsequently modelled CoA into the active site of our CysE structure, to examine CoA interactions. CoA binds in the cleft between neighbouring monomers (Figure 3.15). The major interactions between CoA and the CysE monomer are hydrogen bonding interactions. On one monomer, the amine groups from Ala208 (2.8Å) and Ala226 (3.1Å), hydrogen bond with hydroxyl groups of the CoA pantothenic arm. Given that there are no structures with acetyl CoA bound in the active site of CysE and given that CoA is isostructural for acetyl

CoA, the interaction between CysE and CoA presented here are presumed the same as interactions between CysE and acetyl CoA.

On the neighbouring monomer the Gly188 hydroxyl group hydrogen bonds to the amine located on the pantothenic arm of CoA. Upon closer examination of our structure with CoA modelled in the active site, the thioester group of CoA is present in the active site and located in close proximity to the catalytic His162 (Figure 3.14) . If acetyl CoA were bound in CysE where CoA is modelled, the acetyl group would be able to participate in the transferase reaction.

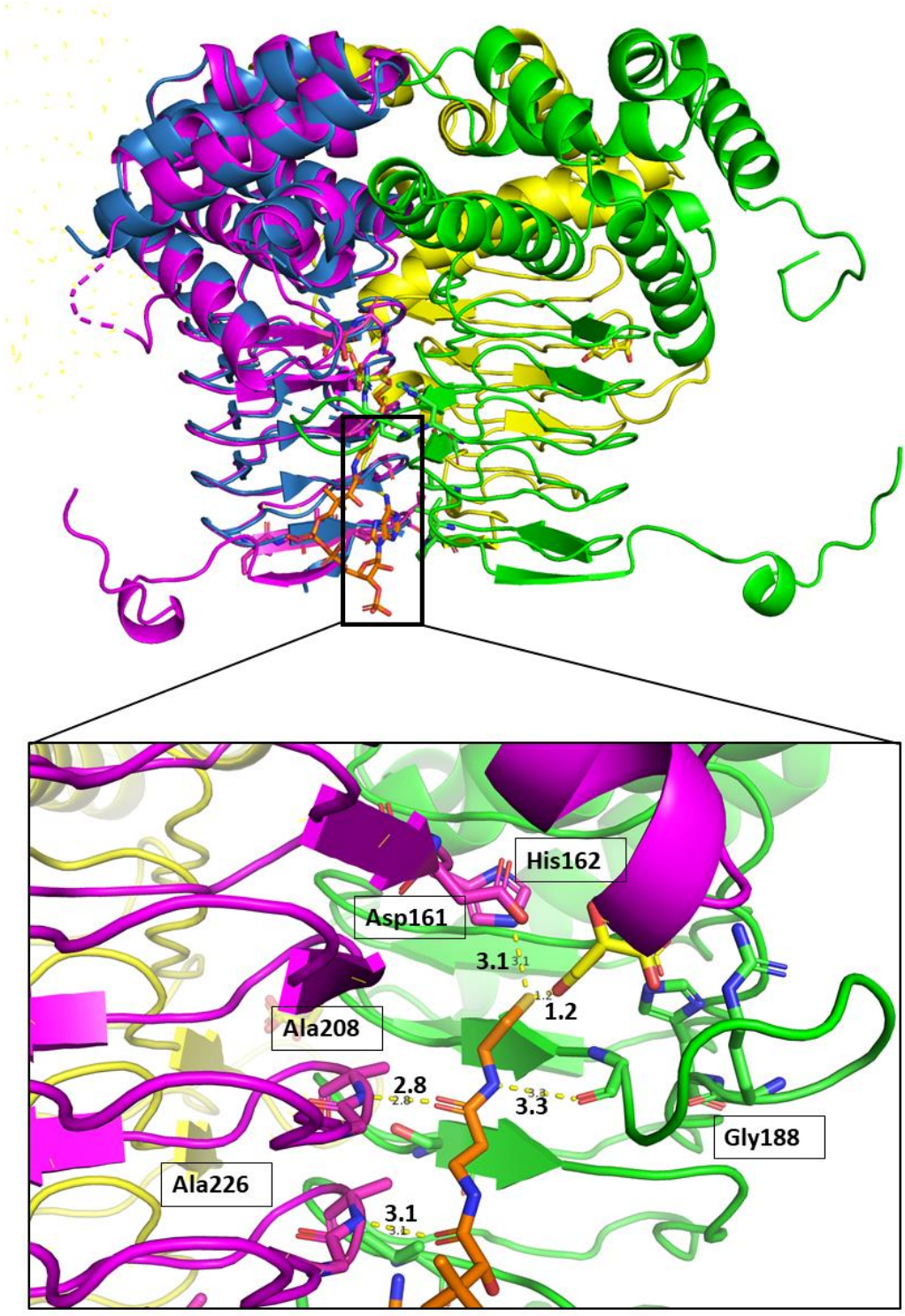

Figure 3.15: Overlay of CysE with CysE and CoA from soybean (4N6B). Soybean CysE is coloured blue and CoA is denoted as orange sticks. CysE trimer from *N. gonorrhoeae* is coloured yellow, magenta and green. Hydrogen bonding residues are labelled for Ala208, 226 and Gly188. Hydrophilic interactions are denoted as dashed yellow lines. All distances measured in Angstroms. Image generated in PyMOL.

While the Ramachandran analysis reported no outliers, active site residues His162 and Arg196, as well as Ala163, were consistently in the allowed region, but not favoured region, for all six monomers (Figure 3.16), suggesting that the residues are in an energetically strained conformation. This strained conformation for these active site residues is supported by electron density (Figure 3.5) and in keeping with observations from studies of CysE homologue from *H. influenzae* (Olsen *et al.*, 2004). Given that these residues are part of the active site, this conformation is likely related to catalysis.

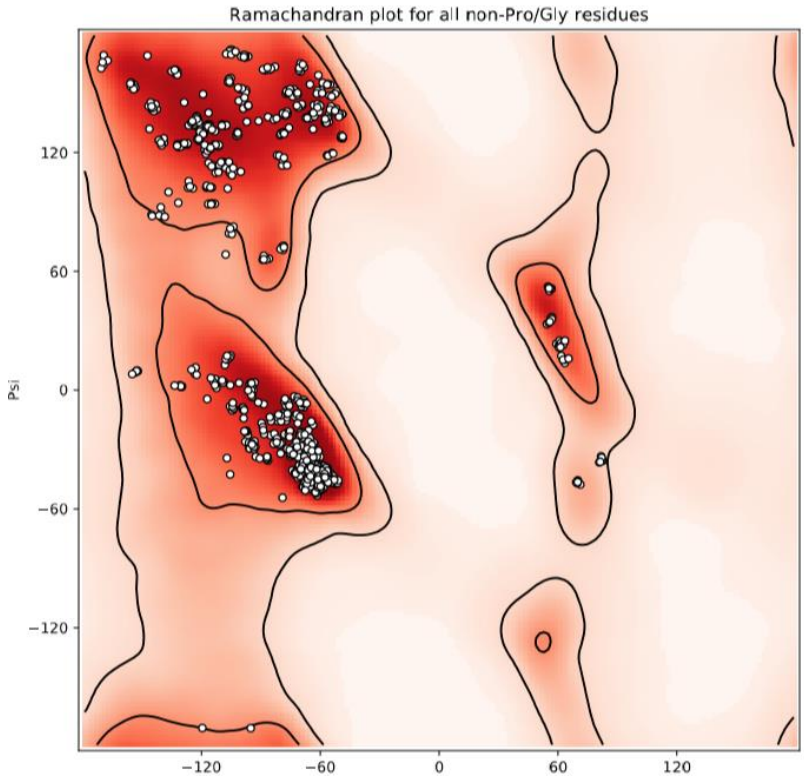

Figure 3.16: Ramachandran analysis of non-proline/glycine residues from the CysE structure. Dots represent the phi and psi angles for a single residue. Favoured, allowed and disallowed regions are outlined on the graph. Favoured regions are within the innermost blobs (dark red). Allowed regions is the area between the innermost and outermost blobs (pink). Disallowed region is the area outside the outermost blobs (light pink/white). Analysis was generated using Molprobity.

Ligand soaks were performed with CysE crystals with substrates acetyl CoA and L-serine as per section 3.2.1.8. Datasets were collected for each substrate respectively, but intial analysis indicated that neither L-serine nor acetyl CoA were present at their respective substrate binding sites. Futthermore, deterioration of crystal quality was visible during soaks and was confirmed through smearing of diffraction spots (data not shown). Based on these results, future attempts to obtain the crystal structure of CysE bound to substrate will be through co-crystallisaiton.

Attempts were made to co-crystallise substrates L-serine, acetyl CoA and inhibitor L-cysteine with CysE (as per section 3.2.1.4). However, we found that our crystallisation drops were mainly precipitate, and any crystals that formed were determined by X-ray diffraction to be small molecule compounds, being most likely the ligand added. Further optimisation of the crystallisation conditions will be carried out.

3.3.5 Formation of the cysteine synthase complex

Cloning, expression and purification of CysK with and without the PLP cofactor was carried out by Dr Joanna Hicks as per section 2.3. Both CysE and CysK were purified using IMAC and gel filtration chromatography as per section 2.2.4., using the same IMAC buffers as previously mentioned (section 2.2.4) and a modified gel filtration buffer (50 mM Tris pH 8.0, 200 mM NaCl). Both proteins were purified individually using gel filtration chromatography, using an ENrich 650 column, for use in CSC experiments.

CysE was shown to have an elution volume of 12.56 ml, consistent with a CysE hexamer, and is in keeping with results from section 2.3.1 (Figure 3.17a). The elution profile of CysK purified in the absence of PLP (Figure 3.17b) presents as two peaks, at 9.5 and 14.35 ml, with the latter of an approximate molecular weight of 47 kDa (calculated as per section 2.2.4.4), consistent with a CysK dimer. The 9.5 ml peak occurs before the void volume of the column (10.56 ml) and is most likely aggregated protein. CysK purified in the presence of PLP shows little aggregated protein in the column void volume and elutes as a single peak at 14.6 ml consistent with a dimer (Figure 3.18b), with a small peak eluting at 18.55 ml, likely corresponding to free PLP. CysE and CysK proteins purified in the expected multimeric forms of a hexamer and dimer, respectively (Figure 3.18a, b). It is important to confirm and check the stoichiometries of the two proteins that constitute the CSC, prior to attempting to form the CSC.

To form the complex we trialled combining CysE and CysK at monomeric molar ratios (CysE:CysK) of 1:1 (CysK purified in the absence of PLP) and 3:2 (CysK purified with PLP) and incubating for 15 minutes on ice. A sample was removed for native-PAGE gel electrophoresis before loading onto a gel filtration column (Enrich 650).

No elution peak corresponding to the CSC was observed on the gel filtration chromatograms. Each shows only two peaks, corresponding with a CysE hexamer and CysK dimer, respectively (Figure 3.17c and Figure 3.18c). Based on observations from homologous CSCs (Benoni *et al.*, 2017b), the CSC is composed of one hexamer and two CysK dimers, and for *N. gonorrhoeae* the CSC would have a predicted molecular weight of ~ 332 kDa. This would correspond with a peak with an elution volume of 11.9 ml, which is absent from both Figure 3.17c and Figure 3.18c.

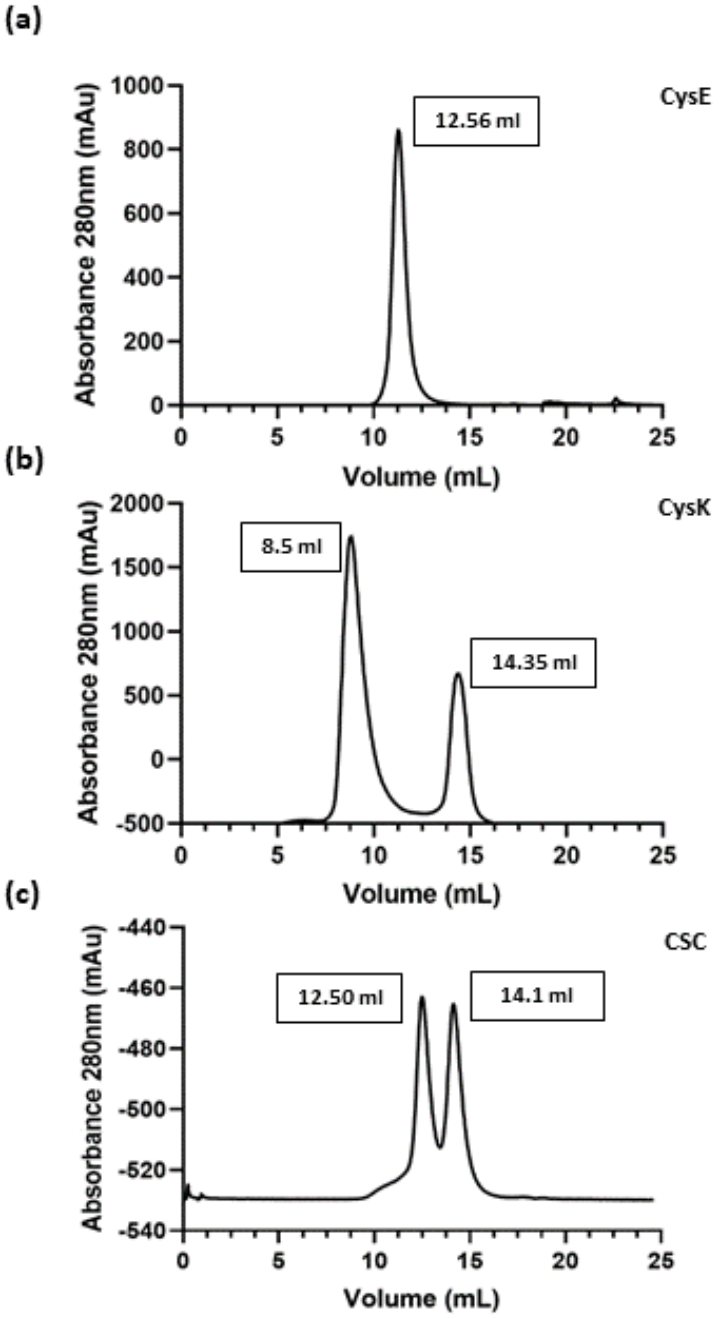

Figure 3.17: Gel filtration chromatogram of CysE, CysK and cysteine synthase complex formation attempt without PLP. (a) Gel filtration chromatogram of CysE. (b) Gel filtration chromatogram of CysK (b). (c) Cysteine synthase complex attempt, 1:1 CysE:CysK. All peaks are labelled with elution volumes.

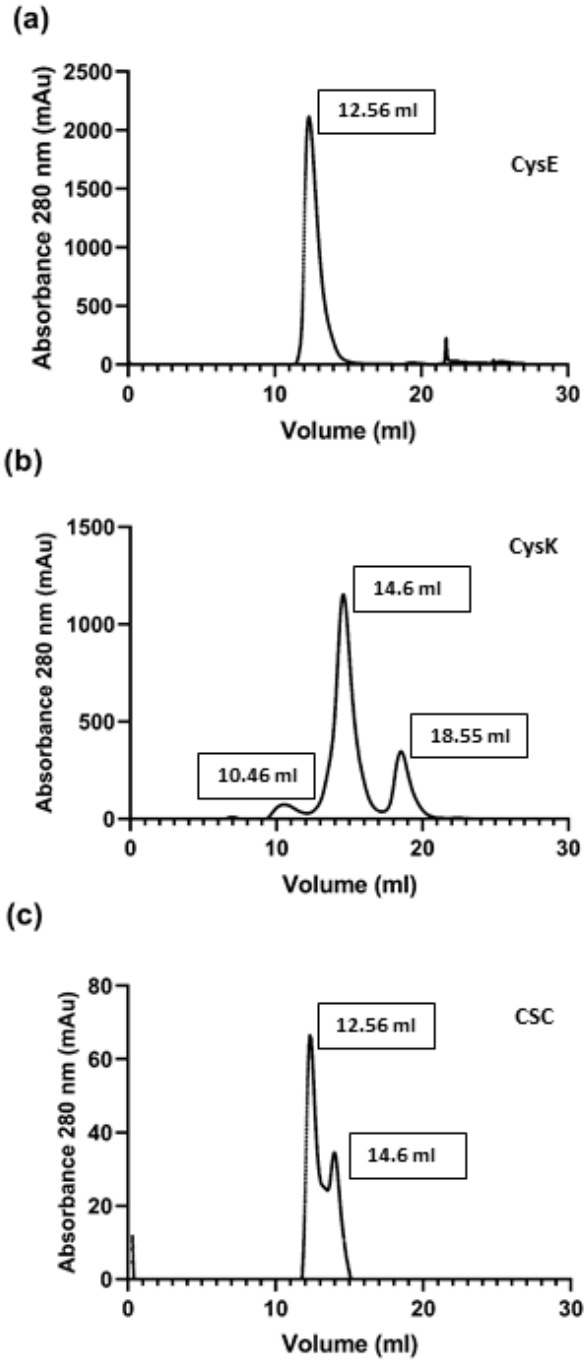

Figure 3.18: Gel filtration chromatogram of CysE, CysK and cysteine synthase complex formation attempt with PLP. (a) Gel filtration chromatogram of CysK with PLP. (b) Gel filtration chromatogram of CysE. (c) Cysteine synthase complex attempt, 3:2 CysE:CysK. All peaks are labelled with elution volumes.

The lack of CSC formation was confirmed by native-PAGE gel electrophoresis (Figure 3.19). Both CysE and CysK stocks were ran alongside the CSC mixture for comparison. CysE runs as a single band near the top of the native-PAGE gel, whereas for CysK there are five thin bands that have migrated halfway through the gel (Figure 3.19). It is not clear why five bands are present, but these bands are likely differently charged forms of CysK, which have migrated at different rates during electrophoresis. Different bands could also represent PLP-bound and unbound forms of CysK. The CSC mixture has bands on the native-PAGE gel that are equivalent to the individual CysE and CysK samples, as would be expected, however there are no extra bands present. If a small amount of CSC had formed, we would expect an extra band not present in the CysE and CysK lanes to present in the CSC mixture. These results from native-PAGE gel electrophoresis confirm the gel filtration chromatography results, that the CSC was not formed.

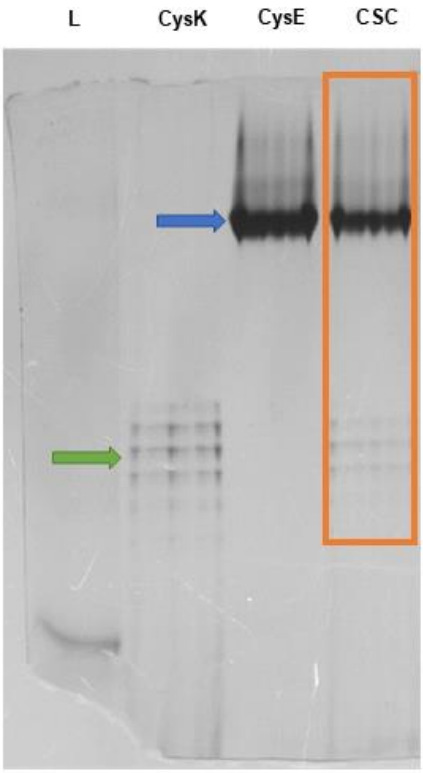

Figure 3.19: Native-PAGE gel electrophoresis of the 3:2 cysteine synthase complex formation attempt with PLP. (a) Native-PAGE gel electrophoresis of CysE, CysK and CSC. L= Precision Plus Ladder. CysE protein bands are labelled with blue arrows, CysK protein bands are labelled with green arrows, and CSC is highlighted in orange. Molecular weights of Precision Plus Protein Standards (L) in KDa are not labelled as standards could not be visualised.

The cysteine synthase complex is well conserved across bacterial and plant species, but there are exceptions. The most well studied example is from the enteric

protozoan, *E. histolytica*. Here authors demonstrated using peptide binding assays that although the CSC could not form, the C-terminal CysE fragment could bind to CysK from *E. histolytica*. The inability of the CSC to form was attributed to the rare trimeric conformation of CysE (Kumar *et al.*, 2011). CysE from *N. gonorrhoeae* exists as hexamer and includes residues essential for CSC formation, including the C-terminal tail isoleucine residue (Huang *et al.*, 2005), and suggesting that it should form the CSC.

One possible explanation for why we could not form the CSC, is the presence of *O*-acetylserine. *O*-acetylserine at millimolar concentrations (10 – 1000 mM), dissociates the CSC (Benoni *et al.*, 2017a). *O*-acetylserine is a common metabolite in *E. coli* (Sajed *et al.*, 2015), and so it is possible that *O*-acetylserine from *E. coli* expression strain BL21(DE3) could co-purify with CysK or CysE, and prevent formation of the CSC. However, this can be ruled out as *O*-acetylserine, has been shown to be unstable at pHs greater than 7.6 (Kredich & Tomkins, 1966), where it will non-enzymatically form the isoform *N*-acetylserine, which is unable to bind to CysK (Kredich & Tomkins, 1966). Given that the purification of CysK was conducted at room temperature in buffers with a constant pH of 8.0, there was likely no O-acetylserine present, and can be ruled out.

It is possible that the CSC forms in *N. gonorrhoeae*, but the rate of formation might be substantially slower than other CSC complexes. Benoni *et al.* (2017b) were able to form the *E. coli* CSC using nanomolar concentrations of CysE (7 nM) and CysK (23 nM) (monomer concentrations). Formation of the CSC for *E. coli* has been reported to have a dissociation constant (K_d) of 5 nM (Benoni *et al.*, 2017a). This value suggests that the CysE and CysK subunits have a strong affinity for each other and the formation of the CSC is strongly favoured. It was assumed when planning the CSC experiments in this research, that the CysE and CysK from *N. gonorrhoeae* would have a similar affinity and form the CSC. We have demonstrated that even when using more concentrated stocks (micromolar) of CysE and CysK, we were unable to form the CSC. To investigate this theory, future work will involve incubating the CSC mixture for longer periods of time and trial a low CysE/CysK ratio (1:10 or 1:100) to increase the chances of CSC formation.

It is possible that the CSC is unable to form in *N. gonorrhoeae*. The evolutionary advantage for organisms that have lost the ability to form the CSC would be that CysK activity is no longer inhibited, which leads to increased L-cysteine production and gene expression of sulphate assimilatory genes would be subsequently down regulated, due to unregulated consumption of *O*-acetylserine by CysK. In this research we have shown that CysE from *N. gonorrhoeae* is sensitive to feedback inhibition by L-cysteine (Chapter 2). Given that *N. gonorrhoeae* has a high demand for cysteine, primarily for the production of large amounts of reducing compounds, like glutathione (Seib *et al.*, 2006), there might be an advantage to not being able to form the CSC. However, further investigation and method optimisation is needed before we can fully rule out CSC formation.

One possibility is that the lack of CSC formation is linked to the inability of *N. gonorrhoeae* to reduce sulphate to sulphide, and that two of the deleted genes from this pathway would be under operon control by the transcriptional regulator CysB. Sequence alignments by Hicks and Mullholland (2018) demonstrated that the OASS present in *N. gonorrhoeae* has the greatest homology to the OASS-A isoform (CysK). This isoform utilises sulphide as a thiol donor, whereas OASS-B isoform (CysM) utilises directly imported thiosulphate. Given that CysK is able to form the CSC, while CysM cannot (Zhao *et al.*, 2006), it would be expected that we would be able to form the CSC in *N. gonorrhoeae*. However, biochemical characterisation studies of CysK from *N. gonorrhoeae* are required to investigate this further.

3.4 Conclusions & future directions

We have obtained a high-resolution structure of CysE from *N. gonorrhoeae* at a resolution of 2.01 Å. The structure is composed of two domains: an N-terminal α-helical domain and a C-terminal LβH domain. We describe the first evidence of a domain swapping in a CysE structure, where the flexible C-terminal tails domain swap with neighbouring monomers. In the active site, D-malate is bound and interacts through extensive hydrogen binding with the active site residues.

One remaining challenge is to obtain a co-crystallised structure of CysE and its substrates. Co-crystallisation will be further optimised for substrates L- serine and acetyl CoA. These substrate-protein structures will provide essential information

on the residues needed for substrate binding and allow us to screen inhibitors to target these substrate binding sites. The tentative screening of two other CysE datasets obtained from crystals grown in Tacsimate^{TM}, all have D-malate bound in the active site. For future crystallisation attempts, a new crystallisation condition will be optimised to prevent the interference by D-malate.

CysE active site residues are conserved in our CysE structure. Inspection of the active site shows conservation of the 3D arrangement around our buffer compound D-malate. The arrangement of the catalytic triad residues, His162 and Asp147 with L-serine, suggests that CysE from *N. gonorrhoeae* shares the same chemical mechanism as other CysE homologues.

We are the first to demonstrate evidence of domain swapping for a CysE structure. The C-terminal tail, which is involved in the formation of the CSC, was able to domain swap with the C-terminal tail on a neighbouring monomer in the crystal lattice. Although this is an artefact of crystallisation, this provides some insight into the degree of flexibility of the C-terminal tail and the residues required for cysteine synthase complex formation.

Attempts to form the CSC with CysE and CysK from *N. gonorrhoeae* were unsuccessful, but we will continue this research and explore other methods of measuring CSC formation. To confirm whether the CysE C-terminal tail can bind to CysK, we will use a fluorometric-based peptide binding assay using a decapeptide that mimics the C-terminal tail (Campanini *et al.*, 2005). We will also trial the addition of sulphide, as it has been shown to promote the reassociation of the CSC in CysE homologues (Wirtz & Hell, 2006), and may help with CSC formation.

The CysE structure presented here is a significant step towards developing inhibitors for CysE. However, for computational inhibitor screening high resolution structures with substrates bound are needed. If co-crystallisation of CysE and each substrate is unsuccessful, we can dock the substrates L-serine and acetyl CoA (based on other CysE structures) into our apo structure for inhibitor screening. The apo structure is extensively built (96%) and is solved at a high resolution (2.01 Å). Promising inhibitors identified using this method, will be ordered and tested using

the inhibition assays developed during this thesis. The ultimate goal would be to identify a potent inhibitor that shows good specificity for CysE.

While outside the scope of this master's thesis, future research will characterise CysK from *N. gonorrhoeae*. Dharavath *et al.* (2017) demonstrated that *Brucella abortus* was unable to form the CSC, even though CysE had C-terminal residues shown to be important for CSC formation. This was attributed to two CysK residues occupying the active site, preventing the binding of the C-terminal tail from CysE. Hence, characterising CysK may reveal any structural differences in CysK that could explain why we were unable to form the CSC in *N. gonorrhoeae*.

Chapter 4

Conclusions and Future Research

N. gonorrhoeae is the causative organism of the sexually transmitted infection, gonorrhoea. Over decades of antibiotic use the rapid emergence of antibiotic-resistant strains has created a demand for new antimicrobial treatments (Wi *et al.*, 2017). The targeting of amino acid biosynthesis is a promising new field of antimicrobial research. The cysteine biosynthetic pathway has been shown to be important for pathogenicity and virulence in *Neisseria* species.

N. gonorrhoeae encounters oxidative stress throughout pathogenesis. Furthermore, the ability of *N. gonorrhoeae* to spread to new hosts hinges on the ability of gonorrhoea to survive oxidative stress from commensal *Lactobacilli* in the urogenital tract and within the phagosome of a neutrophil (Hill *et al.*, 1985; Seib *et al.*, 2006). The ability to mitigate these stressors relies on reducing systems to mitigate these host derived oxidative stresses. Given that L-cysteine-derived compounds are necessary for the synthesis of antioxidants, including glutathione, as well as essential cellular compounds such as CoA, iron-sulphur cluster proteins, the pathway for *de novo* synthesis of L-cysteine is an ideal target for developing new treatments for *N. gonorrhoeae*. However, the function and regulation of cysteine synthesis is poorly understood in *N. gonorrhoeae*. In this thesis we have biochemically and structurally characterised one of the key cysteine biosynthetic enzymes, CysE.

CysE is a serine acetyltransferase that catalyses the first step in cysteine biosynthesis. CysE catalyses the acetylation of L-serine, forming *O*-acetylserine, which then undergoes a condensation reaction with sulphide via *O*-acetylserine sulfhydrylase (CysK), to form L-cysteine (Pye *et al.*, 2004). Multiple levels of regulation act on the sulphur assimilation and cysteine biosynthetic pathways in response to sulphur flux (Wirtz *et al.*, 2012). This is primarily carried our via the feedback inhibition of CysE by L-cysteine and formation of the CysE:CysK cysteine synthase complex (CSC) (Benoni *et al.*, 2017b).

In this thesis, we have successfully characterised the catalytic activity of CysE from *N. gonorrhoeae*. We show CysE has serine acetyltransferase activity, with Michaelis constants (K_M) of 2.58 and 0.152 mM, for L-serine and acetyl CoA, respectively, which are comparable to values seen for other CysE homologues. These differences in enzyme affinity for each substrate reflects the intracellular concentrations of these substrates in the cell (Sajed *et al.*, 2015) We also demonstrate the first evidence of substrate inhibition by acetyl CoA for a CysE enzyme. Interestingly, substrate inhibition by L-serine for CysE is well documented. The reason why substrate inhibition is present for acetyl CoA instead of L-serine, could be due to the presence of an ordered mechanism, similar to that seen for CysE from *H. influenzae* (Johnson *et al.*, 2004).

We have solved the structure of CysE from *N. gonorrhoeae* FA1090 at a high resolution of 2.01 Å. In our structure, key active site residues, His162 and Asp146, are conserved. D-malate is bound in the active site and interacts with the same residues as the inhibitor L-cysteine. These residues and the co-ordination of L-serine/L-cysteine (or the isostructural compound D-malate in our structure) confirm formation of the catalytic triad, the essential mechanism of CysE (Pye *et al.*, 2004). We present the first CysE structure to show domain swapping. Here we observed the swapping of the C-terminal tail with neighbouring monomers in the crystal lattice. While this is an artefact from crystallisation, this demonstrates the flexibility of the C-terminal tail, which is thought to be essential for the formation of the cysteine synthase complex (Huang *et al.*, 2005).

We were unable to form the cysteine synthase complex using purified CysE and CysK from *N. gonorrhoeae*. Based on the presence of the essential isoleucine at the end of the C-terminal tail of CysE (Huang *et al.*, 2005), and confirmation of the flexible nature of the C-terminal tail, we expected the CSC to form. The primary purpose of the CSC is to promote the upregulation of the sulphate assimilation pathway in response to low sulphate conditions (Wirtz & Hell, 2006; Kumar *et al.*, 2011). Given that *N. gonorrhoeae* has lost the ability to reduce sulphate to sulphide but is able to grow using thiosulphate as a sole sulphur source (Le Faou, 1984), there may be no advantage to forming the CSC. The CSC also had drawbacks such as halting L-cysteine formation (via inhibition of CysK) (Huang *et al.*, 2005; Benoni *et al.*, 2017b), under low sulphate conditions, therefore in *N. gonorrhoeae*

the lack of formation of the CSC would allow the continuous production of L-cysteine synthesised from thiosulphate. In *E. histolytica*, CysE is unable to form the CSC complex with CysK (Kumar *et al.*, 2011). This lack of formation was attributed to CysE conformation of a trimer and not a hexamer and the C-terminal tail, even though a terminal isoleucine is present. The intracellular demands for this protozoan are quite high considering its inability to store glutathione, instead relying on high concentrations of cysteine to act as a reducing system (Kumar *et al.*, 2011). *N. gonorrhoeae* differs here as it documented to have high concentrations of glutathione, but both organisms would require large amounts of L-cysteine to maintain these high metabolite concentrations. Given that *cysE* is an essential gene in *N. gonorrhoeae*, even when *cysE* deletion strains are cultured in the presence of L-cysteine (Remmele *et al.*, 2014), suggests that *de novo* cysteine synthesis is essential for *N. gonorrhoeae* and that L-cysteine/cystine importation alone is not enough to meet the L-cysteine demands of *N. gonorrhoeae*.

One interesting difference between the CSC forming CysE proteins from other bacteria and CysE from *N. gonorrhoeae* is substrate inhibition. It is well documented that the CSC forming CysE proteins are subject to substrate inhibition by L-serine (Kredich & Tomkins, 1966; Johnson *et al.*, 2004), whereas we show CysE from *N. gonorrhoeae* experiences acetyl CoA inhibition (at concentrations of acetyl CoA above physiological concentrations). The formation of CSC also increases CysE activity via increasing the K_i / K_M for L-serine (Benoni *et al.*, 2017b), The mechanism for this is unclear and given that there is no crystal structure for the CSC, it is hard to determine if CysE in the CSC undergoes conformational changes that could explain this difference in L-serine affinity. Considering CysE from *N. gonorrhoeae* and CysE in the CSC do not experience L-serine inhibition, CysE from *N. gonorrhoeae* may have slight structural differences that are more like the CysE conformation in the CSC, which would prevent L-serine substrate inhibition.

An alternative reason for the inability of CysE and CysK from *N. gonorrhoeae* to form the CSC is the CysK (OASS-A) protein. The OASS identified in *N. gonorrhoeae* has higher sequence homology to CysK (can form the CSC) (Benoni *et al.*, 2017b) and not the thiosulphate utilising isoform CysM (cannot form the CSC) (Nakamura *et al.*, 1983; Tai *et al.*, 1993). Given that *N. gonorrhoeae* can grow on thiosulphate as a sole sulphur source (Le Faou, 1984), CysK must be able

to utilise thiosulphate as a thiol donor. It is possible that CysK may share some characteristics of CysM, including the inability to form the CSC. CysK remains uncharacterised in *N. gonorrhoeae*, however, biochemical and structural analysis may provide insight into the formation of the CSC and regulation of cysteine synthesis in *N. gonorrhoeae*.

To confirm CysE and CysK from *N. gonorrhoeae* cannot form the CSC, future efforts will employ a more rigorous method of measuring CSC formation using a fluorometric assay, monitoring emission of the CysK co-factor, PLP (Campanini *et al.*, 2005). Sequence alignments show that residues essential for CysE binding to the CysK active site are present in the ten carboxyl terminus residues from CysE, suggesting that CysE would be able to form the complex. The fluorometric assay to monitor binding of CysE to CysK will also be used to investigate the CSC, using a CysE C-terminus mimicking peptide.

While the cysteine biosynthetic and sulphate assimilation pathway is regulated directly by sulphur availability, *cysE* is the exception as it is constitutively expressed (Jones-Mortimer *et al.*, 1968). To confirm the essentiality of *cysE* in *N. gonorrhoeae*, a *cysE* knockdown strain in *N. gonorrhoeae* strain, MS11 will be created. The promoter of *cysE* in *N. gonorrhoeae* MS11 will be replaced with a tetracycline-inducible promoter. This will confirm essentiality by *in vitro* growth experiments in the presence and absence of tetracycline.

Neisseria meningitidis is the leading cause of bacterial meningitis, with New Zealand having some of the highest rates globally (Lopez & Sexton, 2013). There is a high level of sequence similarity 97% between CysE homologues from *N. gonorrhoeae* and *N. meningitidis*. CysE is also essential for growth of *N. meningitidis* (Capel *et al.*, 2016). Given the importance of these two pathogenic *Neisseria* species and the sequence homology between CysE homologues, the results of this thesis are broadly applicable to CysE from *N. meningitidis*.

The results presented in this thesis represent a major leap forward in our understanding of cysteine biosynthesis in *N. gonorrhoeae*. These results are also the basis for future work to identify potential CysE inhibitors using computational inhibitor screening. Computational inhibitor screening streamlines the inhibitor discovery process via the ability to screen hundreds of thousands of inhibitors

versus thousands of inhibitors using typical *in vitro* laboratory based screening. However, computational inhibitor screening relies on a detailed understanding of kinetic mechanism and high-resolution protein structures with and without substrates bound. Ongoing research based on the crystallisation of CysE presented here will attempt to obtain CysE structures with L-serine, acetyl CoA and L-cysteine bound respectively. However, if this is unsuccessful the high-resolution structure of CysE presented here can be used to dock substrates and inhibitors for use in computational inhibitor screening. Promising inhibitor compounds can be tested *in vitro* using assays developed in this thesis. Overall, this research has contributed to a greater understanding of a previously uncharacterised essential enzyme for a key metabolic pathway within *N. gonorrhoeae* and paved the way for the development of new inhibitors targeting the promising new antimicrobial target in *N. gonorrhoeae*, CysE.

References

Adams, P. D., Afonine, P. V., Bunkóczi, G., Chen, V. B., Davis, I. W., Echols, N., Headd, J. J., Hung, L.-W., Kapral, G. J., Grosse-Kunstleve, R. W., McCoy, A. J., Moriarty, N. W., Oeffner, R., Read, R. J., Richardson, D. C., Richardson, J. S., Terwilliger, T. C., & Zwart, P. H. (2010). PHENIX: a comprehensive Python-based system for macromolecular structure solution. *Acta crystallographica. Section D, Biological crystallography, 66*(Pt 2), 213-221.

Afonine, P. V., Grosse-Kunstleve, R. W., Echols, N., Headd, J. J., Moriarty, N. W., Mustyakimov, M., Terwilliger, T. C., Urzhumtsev, A., Zwart, P. H., & Adams, P. D. (2012). Towards automated crystallographic structure refinement with phenix.refine. *Acta crystallographica. Section D, Biological crystallography, 68*(Pt 4), 352-367.

Archibald, F. S., & Duong, M. N. (1986). Superoxide dismutase and oxygen toxicity defenses in the genus Neisseria. *Infection and immunity, 51*(2), 631-641.

Bennett, B. D., Kimball, E. H., Gao, M., Osterhout, R., Van Dien, S. J., & Rabinowitz, J. D. (2009). Absolute metabolite concentrations and implied enzyme active site occupancy in Escherichia coli. *Nature Chemical Biology, 5*(8), 593-599.

Bennett, M. J., Schlunegger, M. P., & Eisenberg, D. (1995). 3D domain swapping: a mechanism for oligomer assembly. *Protein science : a publication of the Protein Society, 4*(12), 2455-2468.

Benoni, R., Beck, C. M., Garza-Sánchez, F., Bettati, S., Mozzarelli, A., Hayes, C. S., & Campanini, B. (2017a). Activation of an anti-bacterial toxin by the biosynthetic enzyme CysK: mechanism of binding, interaction specificity and competition with cysteine synthase. *Scientific Reports, 7*(1), 8817.

Benoni, R., De Bei, O., Paredi, G., Hayes, C. S., Franko, N., Mozzarelli, A., Bettati, S., & Campanini, B. (2017b). Modulation of Escherichia coli serine acetyltransferase catalytic activity in the cysteine synthase complex. *FEBS letters, 591*(9), 1212-1224.

Billker, O., Popp, A., Brinkmann, V., Wenig, G., Schneider, J., Caron, E., & Meyer, T. F. (2002). Distinct mechanisms of internalization of Neisseria gonorrhoeae by members of the CEACAM receptor family involving Rac1- and Cdc42-dependent and -independent pathways. *The EMBO Journal, 21*(4), 560-571.

Borregaard, N. (2010). Neutrophils, from Marrow to Microbes. *Immunity, 33*(5), 657-670.

Brunner, K., Maric, S., Reshma, R. S., Almqvist, H., Seashore-Ludlow, B., Gustavsson, A.-L., Poyraz, Ö., Yogeeswari, P., Lundbäck, T., Vallin, M.,

Sriram, D., Schnell, R., & Schneider, G. (2016). Inhibitors of the Cysteine Synthase CysM with Antibacterial Potency against Dormant Mycobacterium tuberculosis. *Journal of Medicinal Chemistry, 59*(14), 6848-6859.

Bulut, H., Moniot, S., Licht, A., Scheffel, F., Gathmann, S., Saenger, W., & Schneider, E. (2012). Crystal Structures of Two Solute Receptors for l-Cystine and l-Cysteine, Respectively, of the Human Pathogen Neisseria gonorrhoeae. *Journal of Molecular Biology, 415*(3), 560-572.

Campanini, B., Pieroni, M., Raboni, S., Bettati, S., Benoni, R., Pecchini, C., Costantino, G., & Mozzarelli, A. (2015). Inhibitors of the Sulfur Assimilation Pathway in Bacterial Pathogens as Enhancers of Antibiotic Therapy. *Current Medicinal Chemistry, 22*(2), 187-213.

Campanini, B., Speroni, F., Salsi, E., Cook, P. F., Roderick, S. L., Huang, B., Bettati, S., & Mozzarelli, A. (2005). Interaction of serine acetyltransferase with O-acetylserine sulfhydrylase active site: evidence from fluorescence spectroscopy. *Protein science : a publication of the Protein Society, 14*(8), 2115-2124.

Capel, E., Zomer, A. L., Nussbaumer, T., Bole, C., Izac, B., Frapy, E., Meyer, J., Bouzinba-Ségard, H., Bille, E., Jamet, A., Cavau, A., Letourneur, F., Bourdoulous, S., Rattei, T., Nassif, X., & Coureuil, M. (2016). Comprehensive Identification of Meningococcal Genes and Small Noncoding RNAs Required for Host Cell Colonization. *mBio, 7*(4), e01173-16.

Carmel-Harel, O., & Gisela., S. (2000). Roles of the Glutathione- and Thioredoxin-Dependent Reduction Systems in the Escherichia Coli and Saccharomyces Cerevisiae Responses to Oxidative Stress. *Annual Review of Microbiology, 54*(1), 439-461.

CDC (Compiler) (2016). *Addressing the Threat of Drug-Resistant Gonorrhea*: CDChttps://www.cdc.gov/nchhstp/newsroom/docs/factsheets/drug-resistant-gonorrhea.PDF.

Chen, V. B., Arendall, W. B., 3rd, Headd, J. J., Keedy, D. A., Immormino, R. M., Kapral, G. J., Murray, L. W., Richardson, J. S., & Richardson, D. C. (2010). MolProbity: all-atom structure validation for macromolecular crystallography. *Acta crystallographica. Section D, Biological crystallography, 66*(Pt 1), 12-21.

Chronis, D., & Krishnan, H. B. (2004). Sulfur assimilation in soybean (Glycine max [L.] Merr.): molecular cloning and characterization of a cytosolic isoform of serine acetyltransferase. *Planta, 218*(3), 417-426.

Criss, A. K., Kline, K. A., & Seifert, H. S. (2005). The frequency and rate of pilin antigenic variation in Neisseria gonorrhoeae. *Molecular microbiology, 58*(2), 510-519.

Davidi, D., Noor, E., Liebermeister, W., Bar-Even, A., Flamholz, A., Tummler, K., Barenholz, U., Goldenfeld, M., Shlomi, T., & Milo, R. (2016). Global characterization of in vivo enzyme catalytic rates and their correspondence to in vitro kcat measurements. *Proceedings of the National Academy of Sciences of the United States of America, 113*(12), 3401-3406.

Dharavath, S., Raj, I., & Gourinath, S. (2017). Structure-based mutational studies of O-acetylserine sulfhydrylase reveal the reason for the loss of cysteine synthase complex formation in Brucella abortus. *Biochemical Journal, 474*(7), 1221-1239.

Dixon, M. (1953). The determination of enzyme inhibitor constants. *Biochemical Journal, 55*(1), 170-171.

Droux, M., Ruffet, M.-L., Douce, R., & Job, D. (1998). Interactions between serine acetyltransferase and O-acetylserine (thiol) lyase in higher plants. *European Journal of Biochemistry, 255*(1), 235-245.

Edwards, J., & Butler, E. (2011). The Pathobiology of Neisseria gonorrhoeae Lower Female Genital Tract Infection. *Frontiers in Microbiology, 2*(102).

El-Benna, J., Hurtado-Nedelec, M., Marzaioli, V., Marie, J. C., Gougerot-Pocidalo, M. A., & Dang, P. M. (2016). Priming of the neutrophil respiratory burst: role in host defense and inflammation. *Immunol Rev, 273*(1), 180-93.

Emsley, P., & Cowtan, K. (2004). Coot: model-building tools for molecular graphics. *Acta Crystallographica Section D, 60*(12 Part 1), 2126-2132.

Eschenbach, D. A., Davick, P. R., Williams, B. L., Klebanoff, S. J., Young-Smith, K., Critchlow, C. M., & Holmes, K. K. (1989). Prevalence of hydrogen peroxide-producing Lactobacillus species in normal women and women with bacterial vaginosis. *Journal of Clinical Microbiology, 27*(2), 251-256.

ESR. (2019). *Sexually transmitted infections in New Zealand: Annual surveillence report 2016.* ESR, Porirua, New Zealand.

Evans, P. R., & Murshudov, G. N. (2013). How good are my data and what is the resolution? *Acta Crystallographica Section D, 69*(7), 1204-1214.

Eyre, D. W., Sanderson, N. D., Lord, E., Regisford-Reimmer, N., Chau, K., Barker, L., Morgan, M., Newnham, R., Golparian, D., Unemo, M., Crook, D. W., Peto, T. E., Hughes, G., Cole, M. J., Fifer, H., Edwards, A., & Andersson, M. I. (2018). Gonorrhoea treatment failure caused by a Neisseria gonorrhoeae strain with combined ceftriaxone and high-level azithromycin resistance, England, February 2018. *Euro surveillance : bulletin Europeen sur les maladies transmissibles = European communicable disease bulletin, 23*(27), 1800323.

Ferrè, F., & Clote, P. (2006). DiANNA 1.1: an extension of the DiANNA web server for ternary cysteine classification. *Nucleic acids research, 34*(Web Server issue), W182-W185.

Fersht, A. (2017). *Structure and mechanism in protein science : a guide to enzyme catalysis and protein folding*. Series in Structural Biology (Vol. 9). World Scientific Publishing.

Fifer, H., Cole, M., Hughes, G., Padfield, S., Smolarchuk, C., Woodford, N., Wensley, A., Mustafa, N., Schaefer, U., Myers, R., Templeton, K., Shepherd, J., & Underwood, A. (2018). Sustained transmission of high-level azithromycin-resistant Neisseria gonorrhoeae in England: an observational study. *The Lancet Infectious Diseases, 18*(5), 573-581.

Gasteiger, E., Hoogland, C., Gattiker, A., & Duvaud, S. (2005). Protein Identification and Analysis Tools in the ExPASy Server. In *The Proteomics Protocols Handbook* (pp. 571-607). Totowa, NJ: Humana Press.

George, C. R. R., Enriquez, R. P., Gatus, B. J., Whiley, D. M., Lo, Y.-R., Ishikawa, N., Wi, T., & Lahra, M. M. (2019). Systematic review and survey of Neisseria gonorrhoeae ceftriaxone and azithromycin susceptibility data in the Asia Pacific, 2011 to 2016. *PloS one, 14*(4), e0213312-e0213312.

Guan, R., Roderick, S. L., Huang, B., & Cook, P. F. (2008). Roles of histidines 154 and 189 and aspartate 139 in the active site of serine acetyltransferase from Haemophilus influenzae. *Biochemistry, 47*(24), 6322-6328.

Guédon, E., & Martin-Verstraete, I. (2007). Cysteine Metabolism and Its Regulation in Bacteria. In V. F. Wendisch (Ed.), *Amino Acid Biosynthesis ~ Pathways, Regulation and Metabolic Engineering* (pp. 195-218). Berlin, Heidelberg: Springer Berlin Heidelberg.

Haggerty, C. L., & Ness, R. B. (2006). Epidemiology, pathogenesis and treatment of pelvic inflammatory disease. *Expert Review of Anti-infective Therapy, 4*(2), 235-247.

Heffernan, H., Woodhouse, R., & Williamson, D. (2015). *Antimicrobial resistance and molecular epidemiology of gonococci in New Zealand.* Institute of Environmental Science and Research Limited. 1-19p.

Hell, R., Jost, R., Berkowitz, O., & Wirtz, M. (2002). Molecular and biochemical analysis of the enzymes of cysteine biosynthesis in the plant Arabidopsis thaliana. *Amino Acids, 22*(3), 245-257.

Henikoff, S., Haughn, G. W., Calvo, J. M., & Wallace, J. C. (1988). A large family of bacterial activator proteins. *Proc Natl Acad Sci U S A, 85*(18), 6602-6.

Hicks, J. L., & Mullholland, C. V. (2018). Cysteine biosynthesis in Neisseria species. *Microbiology, 164*(12), 1471-1480.

Hill, S. A., Masters, T. L., & Wachter, J. (1985). Gonorrhea – an evolving disease of the new millennium. *Microbial Cell, 3*(9), 371-389.

Hindson, V. J. (2003). Serine acetyltransferase of Escherichia coli: substrate specificity and feedback control by cysteine. *The Biochemical journal, 375*(Pt 3), 745-752.

Hindson, V. J., & Shaw, W. V. (2003). Random-Order Ternary Complex Reaction Mechanism of Serine Acetyltransferase from Escherichia coli. *Biochemistry, 42*(10), 3113-3119.

Hryniewicz, M. M., & Kredich, N. M. (1991). The cysP promoter of Salmonella typhimurium: characterization of two binding sites for CysB protein, studies of in vivo transcription initiation, and demonstration of the anti-inducer effects of thiosulfate. *J Bacteriol, 173*(18), 5876-86.

Huang, B., Vetting, M. W., & Roderick, S. L. (2005). The active site of O-acetylserine sulfhydrylase is the anchor point for bienzyme complex formation with serine acetyltransferase. *Journal of bacteriology, 187*(9), 3201-3205.

Jagura-Burdzy, G., & Hulanicka, D. (1981). Use of gene fusions to study expression of cysB, the regulatory gene of the cysteine regulon. *Journal of Bacteriology, 147*(3), 744-751.

Jeffrey, G. A. (1997). *An introduction to hydrogen bonding*. New York: Oxford University Press.

Jennison, A. V., Whiley, D., Lahra, M. M., Graham, R. M., Cole, M. J., Hughes, G., Fifer, H., Andersson, M., Edwards, A., & Eyre, D. (2019). Genetic relatedness of ceftriaxone-resistant and high-level azithromycin resistant Neisseria gonorrhoeae cases, United Kingdom and Australia, February to April 2018. *Euro surveillance : bulletin Europeen sur les maladies transmissibles = European communicable disease bulletin, 24*(8), 1900118.

Johnson, C. M., Huang, B., Roderick, S. L., & Cook, P. F. (2004). Kinetic mechanism of the serine acetyltransferase from Haemophilus influenzae. *Archives of Biochemistry and Biophysics, 429*(2), 115-122.

Johnson, C. M., Roderick, S. L., & Cook, P. F. (2005). The serine acetyltransferase reaction: acetyl transfer from an acylpantothenyl donor to an alcohol. *Archives of Biochemistry and Biophysics, 433*(1), 85-95.

Jones-Mortimer, M. C., Wheldrake, J. F., & Pasternak, C. A. (1968). The control of sulphate reduction in Escherichia coli by O-acetyl-L-serine. *Biochem J, 107*(1), 51-3.

Kabsch, W. (2010). XDS. *Acta crystallographica. Section D, Biological crystallography, 66*(Pt 2), 125-132.

Kawasaki, T., & Kawai, T. (2014). Toll-like receptor signaling pathways. *Frontiers in immunology, 5*, 461-461.

Kertesz, M. A. (2001). Bacterial transporters for sulfate and organosulfur compounds. *Research in Microbiology, 152*(3), 279-290.

Kim, Y., Zhou, M., Peterson, S., Anderson, W. F., & Joachimiak, A. (2006). Crystal Structure of Serine Acetyltransferase CysE from Yersinia pestis.

Kredich, N. (2008). Biosynthesis of Cysteine. *EcoSal Plus*.

Kredich, N. M. (1971). Regulation of l-Cysteine Biosynthesis in Salmonella typhimurium : Effects of Growth on Varying Sulphur Sources and O-acetyl-L-serine on Gene Expression. *Journal of Biological Chemistry, 246*(11), 3474-3484.

Kredich, N. M., Becker, M. A., & Tomkins, G. M. (1969). Purification and Characterization of Cysteine Synthetase, a Bifunctional Protein Complex, from Salmonella typhimurium. *Journal of Biological Chemistry, 244*(9), 2428-2439.

Kredich, N. M., & Tomkins, G. M. (1966). The Enzymic Synthesis of l-Cysteine in Escherichia coli and Salmonella typhimurium. *Journal of Biological Chemistry, 241*(21), 4955-4965.

Krissinel, E., & Henrick, K. (2007). Inference of Macromolecular Assemblies from Crystalline State. *Journal of Molecular Biology, 372*(3), 774-797.

Kumar, S., Kumar, N., Alam, N., & Gourinath, S. (2014). Crystal structure of serine acetyl transferase from Brucella abortus and its complex with coenzyme A. *Biochimica et Biophysica Acta (BBA) - Proteins and Proteomics, 1844*(10), 1741-1748.

Kumar, S., Raj, I., Nagpal, I., Subbarao, N., & Gourinath, S. (2011). Structural and Biochemical Studies of Serine Acetyltransferase Reveal Why the Parasite Entamoeba histolytica Cannot Form a Cysteine Synthase Complex. *Journal of Biological Chemistry, 286*(14), 12533-12541.

Kumaran, S., Yi, H., Krishnan, H. B., & Jez, J. M. (2009). Assembly of the cysteine synthase complex and the regulatory role of protein-protein interactions. *J Biol Chem, 284*(15), 10268-75.

Laskowski, R. A., & Swindells, M. B. (2011). LigPlot+: Multiple Ligand–Protein Interaction Diagrams for Drug Discovery. *Journal of Chemical Information and Modeling, 51*(10), 2778-2786.

Le Faou, A. (1984). Sulphur nutrition and metabolism in various species of Neisseria. *Annales de l'Institut Pasteur / Microbiologie, 135*(1, Supplement B), 3-11.

Lebedev, A. A., & Isupov, M. N. (2014). Space-group and origin ambiguity in macromolecular structures with pseudo-symmetry and its treatment with the program Zanuda. *Acta Crystallographica Section D, 70*(9), 2430-2443.

Lee, R. S., Seemann, T., Heffernan, H., Kwong, J. C., Gonçalves da Silva, A., Carter, G. P., Woodhouse, R., Dyet, K. H., Bulach, D. M., Stinear, T. P., Howden, B. P., & Williamson, D. A. (2018). Genomic epidemiology and antimicrobial resistance of Neisseria gonorrhoeae in New Zealand. *The Journal of antimicrobial chemotherapy, 73*(2), 353-364.

Leu, L. S., & Cook, P. F. (1994). Kinetic Mechanism of Serine Transacetylase from Salmonella typhimurium. *Biochemistry, 33*(9), 2667-2671.

Liu, X., Mosoian, A., Li-Yun Chang, T., Zerhouni-Layachi, B., Snyder, A., Jarvis, G. A., & Klotman, M. E. (2006). Gonococcal lipooligosaccharide suppresses HIV infection in human primary macrophages through induction of innate immunity. *J Infect Dis, 194*(6), 751-9.

Lopez, L., & Sexton, K. (2013). *The Epidemiology of Meningococcal Disease in New Zealand in 2012*. Institute of Environmental Science and Research Ltd (ESR), Wellington, New Zealand.

Madeira, F., Park, Y. M., Lee, J., Buso, N., Gur, T., Madhusoodanan, N., Basutkar, P., Tivey, A. R. N., Potter, S. C., Finn, R. D., & Lopez, R. (2019). The EMBL-EBI search and sequence analysis tools APIs in 2019. *Nucleic acids research, 47*(W1), W636-W641.

Masi, A. T., & Eisenstein, B. I. (1981). Disseminated gonococcal infection (DGI) and gonococcal arthritis (GCA): II. Clinical manifestations, diagnosis, complications, treatment, and prevention. *Seminars in Arthritis and Rheumatism, 10*(3), 173-197.

Matthews, B. W. (1968). Solvent Content of Protein Crystals. *Journal of Molecular Biology, 33*(2), 491-497.

McClure, R., Nudel, K., Massari, P., Tjaden, B., Su, X., Rice, P. A., & Genco, C. A. (2015). The Gonococcal Transcriptome during Infection of the Lower Genital Tract in Women. *PLOS ONE, 10*(8), e0133982.

McCoy, A. J., Grosse-Kunstleve, R. W., Adams, P. D., Winn, M. D., Storoni, L. C., & Read, R. J. (2007). Phaser crystallographic software. *Journal of applied crystallography, 40*(Pt 4), 658-674.

McPhillips, T. M., McPhillips, S. E., Chiu, H.-J., Cohen, A. E., Deacon, A. M., Ellis, P. J., Garman, E., Gonzalez, A., Sauter, N. K., Phizackerley, R. P., Soltis, S. M., & Kuhn, P. (2002). Blu-Ice and the Distributed Control System: software for data acquisition and instrument control at macromolecular crystallography beamlines. *Journal of Synchrotron Radiation, 9*(6), 401-406.

Meister, A., & Anderson, M. E. (1983). Glutathione. *Annual Review of Biochemistry, 52*(1), 711-760.

Merz, A. J., & So, M. (2000). Interactions of Pathogenic Neisseriae with Epithelial Cell Membranes. *Annual Review of Cell and Developmental Biology, 16*(1), 423-457.

Mino, K., Imamura, K., Sakiyama, T., Eisaki, N., Matsuyama, A., & Nakanishi, K. (2001). Increase in the Stability of Serine Acetyltransferase from Escherichia coli against Cold Inactivation and Proteolysis by Forming a Bienzyme Complex. *Bioscience, Biotechnology, and Biochemistry, 65*(4), 865-874.

Mino, K., Yamanoue, T., Sakiyama, T., Eisaki, N., Matsuyama, A., & Nakanishi, K. (1999). Purification and Characterization of Serine Acetyltransferase from Escherichia coli Partially Truncated at the C-Terminal Region. *Bioscience, Biotechnology, and Biochemistry, 63*(1), 168-179.

Nakamura, T., Kon, Y., Iwahashi, H., & Eguchi, Y. (1983). Evidence that thiosulfate assimilation by Salmonella typhimurium is catalyzed by cysteine synthase B. *Journal of Bacteriology, 156*(2), 656-662.

Ochman, H., Lawrence, J. G., & Groisman, E. A. (2000). Lateral gene transfer and the nature of bacterial innovation. *Nature, 405*(6784), 299-304.

Ohtsu, I., Wiriyathanawudhiwong, N., Morigasaki, S., Nakatani, T., Kadokura, H., & Takagi, H. (2010). The L-cysteine/L-cystine shuttle system provides reducing equivalents to the periplasm in Escherichia coli. *J Biol Chem, 285*(23), 17479-87.

Olsen, L., B., H., Vetting, M., & Roderick, S. (2004). Structure of serine acetyltransferase in complexes with CoA and its cysteine feedback inhibitor. *Biochemistry, 43*(20), 6013-9.

Olsen, L. R., Vetting, M. W., & Roderick, S. L. (2007). Structure of the E. coli bifunctional GlmU acetyltransferase active site with substrates and products. *Protein science : a publication of the Protein Society, 16*(6), 1230-1235.

Ostrowski, J., & Kredich, N. M. (1989). Molecular characterization of the cysJIH promoters of Salmonella typhimurium and Escherichia coli: regulation by cysB protein and N-acetyl-L-serine. *J Bacteriol, 171*(1), 130-40.

Ostrowski, J., & Kredich, N. M. (1991). Negative autoregulation of cysB in Salmonella typhimurium: in vitro interactions of CysB protein with the cysB promoter. *J Bacteriol, 173*(7), 2212-8.

Pabo, C. O., & Sauer, R. T. (1984). Protein-DNA recognition. *Annu Rev Biochem, 53*, 293-321.

Privalov, P. (1990). Cold Denaturation of Protein. *Critical Reviews in Biochemistry and Molecular Biology, 25*(5), 281-306.

Pye, V. E., Tingey, A. P., Robson, R. L., & Moody, P. C. E. (2004). The Structure and Mechanism of Serine Acetyltransferase from Escherichia coli. *Journal of Biological Chemistry, 279*(39), 40729-40736.

Qiu, J., Wang, D., Ma, Y., Jiang, T., & Xin, Y. (2013). Identification and characterization of serine acetyltransferase encoded by the Mycobacterium tuberculosis Rv2335 gene. *International Journal of Molecular Medicine, 31*, 1229-1233.

Quillin, S. J., & Seifert, H. S. (2018). Neisseria gonorrhoeae host adaptation and pathogenesis. *Nature reviews. Microbiology, 16*(4), 226-240.

Quinn, D., & Sutton, L. (2011). *Enzyme mechanism from isotope effects*. Boca Raton, FL: CRC Press.

Raetz, C. R. H., & Roderick, S. L. (1995). A Left-Handed Parallel β Helix in the Structure of UDP-N-Acetylglucosamine Acyltransferase. *Science, 270*(5238), 997-1000.

Ramsey, K. H., Schneider, H., Cross, A. S., Boslego, J. W., Hoover, D. L., Staley, T. L., Kuschner, R. A., & Deal, C. D. (1995). Inflammatory Cytokines Produced in Response to Experimental Human Gonorrhea. *The Journal of Infectious Diseases, 172*(1), 186-191.

Read, R. J., Adams, P. D., & McCoy, A. J. (2013). Intensity statistics in the presence of translational noncrystallographic symmetry. *Acta crystallographica. Section D, Biological crystallography, 69*(Pt 2), 176-183.

Reichau, S., Jiao, W., Walker, S. R., Hutton, R. D., Baker, E. N., & Parker, E. J. (2011). Potent inhibitors of a shikimate pathway enzyme from Mycobacterium tuberculosis: combining mechanism- and modeling-based design. *The Journal of biological chemistry, 286*(18), 16197-16207.

Remmele, C. W., Xian, Y., Albrecht, M., Faulstich, M., Fraunholz, M., Heinrichs, E., Dittrich, M. T., Müller, T., Reinhardt, R., & Rudel, T. (2014). Transcriptional landscape and essential genes of Neisseria gonorrhoeae. *Nucleic acids research, 42*(16), 10579-10595.

Robert, X., & Gouet, P. (2014). Deciphering key features in protein structures with the new ENDscript server. *Nucleic Acids Research, 42*(W1), W320-W324.

Rowley, J., Vander Hoorn, S., Korenromp, E., Low, N., Unemo, M., Abu-Raddad, L. J., Chico, R. M., Smolak, A., Newman, L., Gottlieb, S., Thwin, S. S., Broutet, N., & Taylor, M. M. (2019). Chlamydia, gonorrhoea, trichomoniasis and syphilis: global prevalence and incidence estimates, 2016. *Bulletin of the World Health Organization, 97*(8), 548-562P.

Rusniok, C., Vallenet, D., Floquet, S., Ewles, H., Mouzé-Soulama, C., Brown, D., Lajus, A., Buchrieser, C., Médigue, C., Glaser, P., & Pelicic, V. (2009). NeMeSys: a biological resource for narrowing the gap between sequence and function in the human pathogen Neisseria meningitidis. *Genome biology, 10*(10), R110-R110.

Saito, K., Yokoyama, H., Noji, M., & Murakoshi, I. (1995). Molecular Cloning and Characterization of a Plant Serine Acetyltransferase Playing a Regulatory Role in Cysteine Biosynthesis from Watermelon. *Journal of Biological Chemistry, 270*(27), 16321-16326.

Sajed, T., Marcu, A., Ramirez, M., Pon, A., Guo, A. C., Knox, C., Wilson, M., Grant, J. R., Djoumbou, Y., & Wishart, D. S. (2015). ECMDB 2.0: A richer resource for understanding the biochemistry of E. coli. *Nucleic Acids Research, 44*(D1), D495-D501.

Salsi, E., Campanini, B., Bettati, S., Raboni, S., Roderick, S. L., Cook, P. F., & Mozzarelli, A. (2010). A two-step process controls the formation of the bienzyme cysteine synthase complex. *The Journal of biological chemistry, 285*(17), 12813-12822.

Sandstrom, I. (1987). Etiology and diagnosis of neonatal conjunctivitis. *Acta Paediatr Scand, 76*(2), 221-7.

Schurr, J. M., & Schmitz, K. S. (1976). Orientation constraints and rotational diffusion in bimolecular solution kinetics. A simplification. *The Journal of Physical Chemistry, 80*(17), 1934-1936.

Seib, K. L., Wu, H.-J., Kidd, S. P., Apicella, M. A., Jennings, M. P., & McEwan, A. G. (2006). Defenses against oxidative stress in Neisseria gonorrhoeae: a system tailored for a challenging environment. *Microbiology and molecular biology reviews : MMBR, 70*(2), 344-361.

Simons, M. P., Nauseef, W. M., & Apicella, M. A. (2005). Interactions of Neisseria gonorrhoeae with adherent polymorphonuclear leukocytes. *Infection and immunity, 73*(4), 1971-1977.

Spyrakis, F., Singh, R., Cozzini, P., Campanini, B., Salsi, E., Felici, P., Raboni, S., Benedetti, P., Cruciani, G., Kellogg, G. E., Cook, P. F., & Mozzarelli, A. (2013). Isozyme-Specific Ligands for O-acetylserine sulfhydrylase, a Novel Antibiotic Target. *PLOS ONE, 8*(10), e77558.

St Amant, D. C., Valentin-Bon, I. E., & Jerse, A. E. (2002). Inhibition of Neisseria gonorrhoeae by Lactobacillus species that are commonly isolated from the female genital tract. *Infection and immunity, 70*(12), 7169-7171.

Stern, A., Brown, M., Nickel, P., & Meyer, T. F. (1986). Opacity genes in Neisseria gonorrhoeae: Control of phase and antigenic variation. *Cell, 47*(1), 61-71.

Stevens, J. S., & Criss, A. K. (2018). Pathogenesis of Neisseria gonorrhoeae in the female reproductive tract: neutrophilic host response, sustained infection, and clinical sequelae. *Current opinion in hematology, 25*(1), 13-21.

Tai, C. H., Nalabolu, S. R., Jacobson, T. M., Minter, D. E., & Cook, P. F. (1993). Kinetic mechanisms of the A and B isozymes of O-acetylserine sulfhydrylase from Salmonella typhimurium LT-2 using the natural and alternate reactants. *Biochemistry, 32*(25), 6433-6442.

Takahashi, H., Watanabe, H., Kim, K. S., Yokoyama, S., & Yanagisawa, T. (2018). The Meningococcal Cysteine Transport System Plays a Crucial Role in Neisseria meningitidis Survival in Human Brain Microvascular Endothelial Cells. *mBio, 9*(6), e02332-18.

Takamura, Y., & Nomura, G. (1988). Changes in the intracellular concentration of acetyl-CoA and malonyl-CoA in relation to the carbon and energy metabolism of Escherichia coli K12. *J Gen Microbiol, 134*(8), 2249-53.

Terwilliger, T. C., Grosse-Kunstleve, R. W., Afonine, P. V., Moriarty, N. W., Zwart, P. H., Hung, L. W., Read, R. J., & Adams, P. D. (2008). Iterative model building, structure refinement and density modification with the PHENIX AutoBuild wizard. *Acta crystallographica. Section D, Biological crystallography, 64*(Pt 1), 61-69.

Terwilliger, T. C., Klei, H., Adams, P. D., Moriarty, N. W., & Cohn, J. D. (2006). Automated ligand fitting by core-fragment fitting and extension into density. *Acta crystallographica. Section D, Biological crystallography, 62*(Pt 8), 915-922.

Thomas, D., & Surdin-Kerjan, Y. (1997). Metabolism of sulfur amino acids in Saccharomyces cerevisiae. *Microbiology and molecular biology reviews : MMBR, 61*(4), 503-532.

Turnbull, A. L., & Surette, M. G. (2010). Cysteine biosynthesis, oxidative stress and antibiotic resistance in Salmonella typhimurium. *Research in Microbiology, 161*(8), 643-650.

Unemo, M., & Nicholas, R. A. (2012). Emergence of multidrug-resistant, extensively drug-resistant and untreatable gonorrhea. *Future Microbiol, 7*(12), 1401-22.

Unemo, M., & Shafer, W. M. (2014). Antimicrobial resistance in Neisseria gonorrhoeae in the 21st century: past, evolution, and future. *Clinical microbiology reviews, 27*(3), 587-613.

Venkatachalam, C. M., Jiang, X., Oldfield, T., & Waldman, M. (2003). LigandFit: a novel method for the shape-directed rapid docking of ligands to protein active sites. *Journal of Molecular Graphics and Modelling, 21*(4), 289-307.

Wang, T., & Leyh, T. S. (2012). Three-stage assembly of the cysteine synthase complex from Escherichia coli. *The Journal of biological chemistry, 287*(6), 4360-4367.

Weston, E., Workowski, K., Torrone, E., Weinstock, H., & Stenger, M. (2018). *Adherence to CDC Recommendations for the Treatment of Uncomplicated Gonorrhea — STD Surveillance Network, United States, 2016.* 473–476p.

WHO (Compiler) (2017). *World Health Organization (WHO) Global Priority List of Antibiotic-Resistant Bacteria to Guide Research, Discovery, and Development of New Antibiotics.* Genenva: WHO http://www.who.int/medicines/publications/WHO-PPL-Short_Summary_25Feb-ET_NM_WHO.pdf.

Wi, T., Lahra, M. M., Ndowa, F., Bala, M., Dillon, J.-A. R., Ramon-Pardo, P., Eremin, S. R., Bolan, G., & Unemo, M. (2017). Antimicrobial resistance in Neisseria gonorrhoeae: Global surveillance and a call for international collaborative action. *PLOS Medicine, 14*(7), e1002344.

Wingfield, P. T. (2001). Use of protein folding reagents. *Current protocols in protein science, Appendix 3*, Appendix-3A.

Winn, M. D., Ballard, C. C., Cowtan, K. D., Dodson, E. J., Emsley, P., Evans, P. R., Keegan, R. M., Krissinel, E. B., Leslie, A. G. W., McCoy, A., McNicholas, S. J., Murshudov, G. N., Pannu, N. S., Potterton, E. A., Powell, H. R., Read, R. J., Vagin, A., & Wilson, K. S. (2011). Overview of the CCP4 suite and current developments. *Acta crystallographica. Section D, Biological crystallography, 67*(Pt 4), 235-242.

Wirtz, M., Beard, K. F. M., Lee, C. P., Boltz, A., Schwarzländer, M., Fuchs, C., Meyer, A. J., Heeg, C., Sweetlove, L. J., Ratcliffe, R. G., & Hell, R. (2012). Mitochondrial Cysteine Synthase Complex Regulates O-Acetylserine Biosynthesis in Plants. *Journal of Biological Chemistry, 287*(33), 27941-27947.

Wirtz, M., & Hell, R. (2006). Functional analysis of the cysteine synthase protein complex from plants: Structural, biochemical and regulatory properties. *Journal of Plant Physiology, 163*(3), 273-286.

Workowski, K., & Berman, S. (2010). *Sexually Transmitted Diseases Treatment Guidelines.* CDC. 1-110.

Yi, H., Dey, S., Kumaran, S., Lee, S. G., Krishnan, H. B., & Jez, J. M. (2013). Structure of soybean serine acetyltransferase and formation of the cysteine regulatory complex as a molecular chaperone. *The Journal of biological chemistry, 288*(51), 36463-36472.

Zhao, C., Moriga, Y., Feng, B., Kumada, Y., Imanaka, H., Imamura, K., & Nakanishi, K. (2006). On the interaction site of serine acetyltransferase in the cysteine synthase complex from Escherichia coli. *Biochemical and Biophysical Research Communications, 341*(4), 911-916.

Appendices

Appendix A: Cloning information for CysE

A.1. Sequences for CysE (NG0_1423)

CysE (NG0_1423) | *Neisseria gonorrhoeae (strain ATCC 700825 / FA* 1090)

location

CysE FA1090 nucleotide sequence | NC_022240.1| NC_022240.1

(1458601..1459419)

ATGAAAAAAAACCATTTGAACACAACCGGTTTCGACCTCTGGCACACC
ATCCGCGAAGAAACCGCGGCCGCTGCCGCCGCCGAACCGATGCTGGC
AAGTTTTTTGCACCAAACCGTGTTGCGCCACGAGTCCCTCGGCTCCGTC
CTTGCCTACCACCTTTCCAGCAAACTCGGCAGCCCGATTATGGACGTG
CGCGCGCTGTTTGAAATTTACCAGCAGGCATTGGGCAGCGACACCCAA
ATCAGCAAATGTGTCGAAGCAGACTTAAAAGCCATCTACGAACGCGAT
CCCGCCTGCGACGAATATTCGCTGCCGCTTTTATATTTCAAAGGCTTCC
ACGCGATTCAGGCACACCGCATCAACCACCGGCTGTATCTCGACGGAC
GCAAAACGCTGGCGTATTTCCTACAAAACCGTATGTCCGAAGTATTCG
GCGTGGACATCCATCCCGCCGCCCGTTTAGGATACGGGCTGATGCTCG
ACCACGCCACCGGCTTTGTTGCCGGAGAAACCGCCGTGTTGGGCAACA
ATATTTCGATTTTGCACGGCGTAACGCTCGGCGGTTCGGGCAAAGAAG
GCGGCGACCGCCACCCCAAAATCGGCGACGGCGTGATGATCGGCGCA
AACGCCTCGATATTGGGCAATATCCGCATCGGCAGCAATGCCAAAATC
GGCGCGGGCAGCGTCGTGGTTTCAGACGTGCCGCCGTCCATCACGGTT
GTCGGCGTACCCGCCAAACCCGTGGCGCGATCGCTCAAAACCCCGTCG
GCGGATATGGATCAAAATATCCAGTTTGCCGAAATCGACTTTATGATT
TGA

CysE peptide sequence| 29.3 kDa| EC:2.3.1.30

MKKNHLNTTGFDLWHTIREETAAAAAAEPMLASFLHQTVLRHESLGSVL
AYHLSSKLGSPIMDVRALFEIYQQALGSDTQISKCVEADLKAIYERDPACD
EYSLPLLYFKGFHAIQAHRINHRLYLDGRKTLAYFLQNRMSEVFGVDIHP
AARLGYGLMLDHATGFVAGETAVLGNNISILHGVTLGGSGKEGGDRHPK
IGDGVMIGANASILGNIRIGSNAKIGAGSVVVSDVPPSITVVGVPAKPVARS
LKTPSADMDQNIQFAEIDFMI

CysE peptide sequence | N-terminal HexaHis-tag and leader sequence (underlined)

293 residues| 31.6/189.6 kDa (monomer/hexamer)| theoretical pI 6.83

MGSSHHHHHHSSGLVPRGSHMMKKNHLNTTGFDLWHTIREETAAAAAA
EPMLASFLHQTVLRHESLGSVLAYHLSSKLGSPIMDVRALFEIYQQALGSD
TQISKCVEADLKAIYERDPACDEYSLPLLYFKGFHAIQAHRINHRLYLDGR
KTLAYFLQNRMSEVFGVDIHPAARLGYGLMLDHATGFVAGETAVLGNNI
SILHGVTLGGSGKEGGDRHPKIGDGVMIGANASILGNIRIGSNAKIGAGSV
VVSDVPPSITVVGVPAKPVARSLKTPSADMDQNIQFAEIDFMI

pET28b description

Vector	**Description**
pET28b	*E.coli* expression vector, 5368 bps, N-terminal thrombin cleavage site, Kanamycin resistance, C and N-terminal His-tags, T7-promoter.

GMO approval numbers:

E. coli: GMD101146

N. gonorrhoeae: GMD102338

A.2 Luria Bertani (LB) Agar (1 L)

Combine the following:

5 g Peptone

10 g NaCl

5 g Yeast extract

5 g Agar

1 L of distilled water

Autoclave at 121°C before use.

LB Broth

Same method as LB agar, but no addition of agar.

Appendix B: Protein purification and kinetic information

B.1. Purification buffers for CysE kinetics and crystallography

	Chemical Composition
Lysis buffer	50 mM Tris (pH 8.0) 200 mM NaCl 20 mM imidazole
Elution buffer	50 mM Tris (pH 8.0) 200 mM NaCl 1 M imidazole
Gel filtration buffer	50 mM Tris (pH 8.0) 100 mM NaCl

SDS-PAGE and native-PAGE gel buffers compositions

Quenching buffer (Q4)

250 mM Tris (pH 6.8)

20% glycerol (w/v)

4% SDS (w/v)

10% beta-2-mercaptoethanol (w/v)

0.025% bromophenol blue (w/v)

Tris-glycine SDS buffer

25 mM Tris (pH 8.5)

250 mM glycine

0.1% SDS (w/v)

Fairbanks staining solution

0.05% coomasie blue

25% isopropanol

10% acetic acid

Destaining solution

10% acetic acid

B.2. Gel filtration calibration curve for ENrich 650

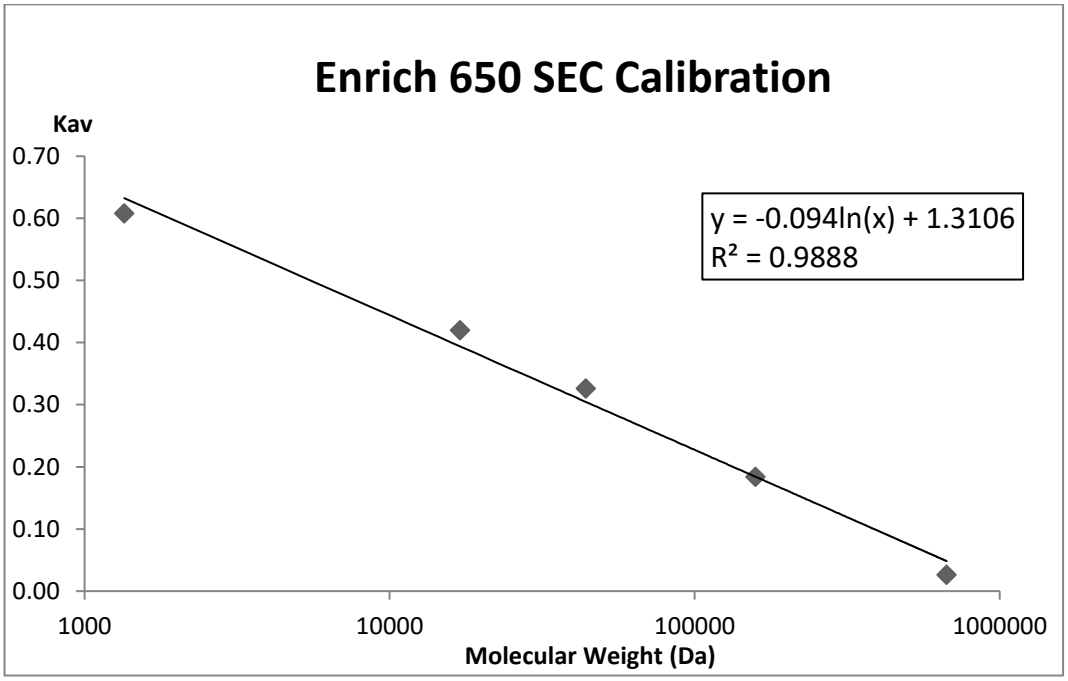

Calibration curve for gel filtration column Enrich650. Calibration curved was used to calculate the approximate molecular weight and oligomeric state of CysE. Column was calibrated in 50 mM Tris (pH 8.0), 200 mM NaCl.

B.3. Raw data used in method optimization, Michaelis Menten and inhibition assays

Link to google drive folder:
https://drive.google.com/drive/folders/1lOYqVibWfbxrQQ3OePha1swaKVvIH_25?usp=sharing

B.4. Initial enzyme concentration trials.

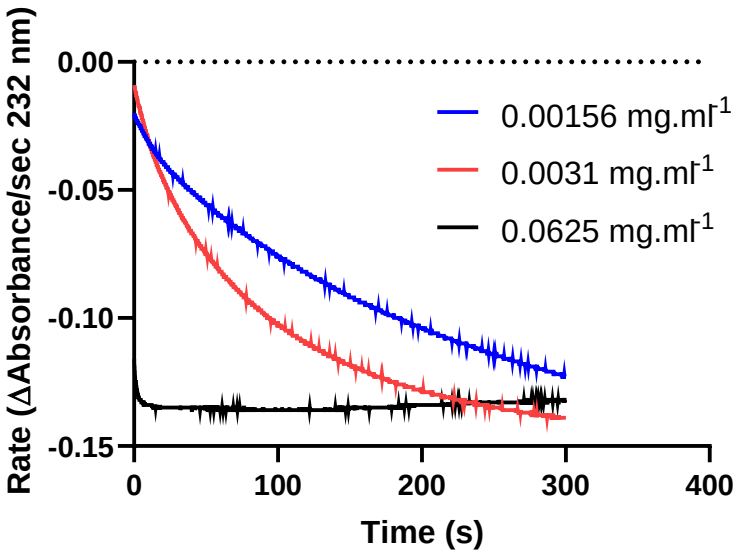

Monitoring CysE activity via depletion of total absorbance at 232 nm over time with varying concentrations of enzyme. Final enzyme concentrations trialled 0.00156, 0.0031 and 0.0625 $mg.ml^{-1}$. Data plotted here was divided by -1 (to get rate of *O*-acetylserine (product) formation, section 2.2.1.8), to generate plot in Figure 2.3a.

Appendix C: Crystallisation and Structure solving information

C.1. Tacsimate™ composition (100% (v/v), pH 7.0) - HR2-755

1.8305 M Malonic acid

0.25 M Ammonium citrate tribasic

0.12 M Succinic acid

0.3 M DL-Malic acid

0.4 M Sodium acetate trihydrate

0.5 M Sodium formate

0.16 M Ammonium tartrate dibasic

C.2. Statistics by resolution shell

Configure | Refine_48

Results | MolProbity | Real-space correlation | Atomic properties | Sequence check

	R-work	R-free	%complete	FOM	Phase error	Scale factor	#work	#test
43.1196 - 6.2395	0.1657	0.2038	98.0%	0.84	24.39	1.00	3159	150
6.2395 - 4.9548	0.1741	0.2181	99.9%	0.84	25.42	0.99	3124	164
4.9548 - 4.3292	0.1412	0.1690	99.4%	0.89	17.31	1.01	3094	164
4.3292 - 3.9336	0.1504	0.1710	100.0%	0.88	16.01	0.99	3068	201
3.9336 - 3.6518	0.1610	0.1995	99.7%	0.87	18.04	1.00	3070	202
3.6518 - 3.4366	0.1823	0.2206	99.9%	0.85	18.09	1.03	3150	139
3.4366 - 3.2646	0.1928	0.1828	99.9%	0.84	21.22	1.02	3120	130
3.2646 - 3.1225	0.1898	0.2391	100.0%	0.85	23.60	0.99	3073	170
3.1225 - 3.0023	0.1981	0.2233	99.9%	0.84	24.78	0.96	3113	154
3.0023 - 2.8988	0.1995	0.2404	99.9%	0.83	23.75	0.97	3097	153
2.8988 - 2.8081	0.1980	0.2187	100.0%	0.83	23.69	1.01	3098	168
2.8081 - 2.7279	0.1957	0.2541	100.0%	0.82	25.50	1.01	3102	163
2.7279 - 2.6561	0.1942	0.2172	100.0%	0.82	22.32	1.02	3071	166
2.6561 - 2.5913	0.1910	0.2225	99.9%	0.84	24.79	1.00	3074	161
2.5913 - 2.5324	0.1854	0.2468	99.9%	0.84	23.99	0.99	3090	169
2.5324 - 2.4785	0.1807	0.2094	99.9%	0.84	22.28	1.00	3099	156
2.4785 - 2.4289	0.1925	0.2135	99.9%	0.83	22.24	0.99	3016	194
2.4289 - 2.3831	0.1890	0.2260	99.9%	0.84	23.70	0.98	3109	169
2.3831 - 2.3405	0.1845	0.2154	100.0%	0.84	24.66	0.99	3099	135
2.3405 - 2.3009	0.1898	0.2547	99.9%	0.83	25.04	1.00	3072	160
2.3009 - 2.2638	0.2044	0.2470	99.9%	0.79	25.59	1.01	3115	147
2.2638 - 2.2289	0.2962	0.3810	92.0%	0.74	30.17	1.01	2838	121
2.2289 - 2.1961	0.2097	0.2900	100.0%	0.76	31.91	1.01	3104	169
2.1961 - 2.1652	0.2128	0.2720	100.0%	0.77	28.77	1.00	2999	174
2.1652 - 2.1360	0.2155	0.2610	100.0%	0.78	27.35	1.00	3100	166
2.1360 - 2.1082	0.2180	0.2577	99.9%	0.78	27.08	1.00	3122	131
2.1082 - 2.0819	0.2201	0.2948	100.0%	0.78	28.56	1.01	3111	148
2.0819 - 2.0568	0.2199	0.2675	99.9%	0.78	28.34	1.01	3101	137
2.0568 - 2.0329	0.2145	0.2659	100.0%	0.79	29.05	1.00	3093	147
2.0329 - 2.0100	0.2225	0.2693	100.0%	0.78	28.40	0.99	3097	140

Idle

Dataset completeness for each resolution shell. Values generated by *phenix.refine*.

C.3. Contents of the asymmetric unit for CysE.

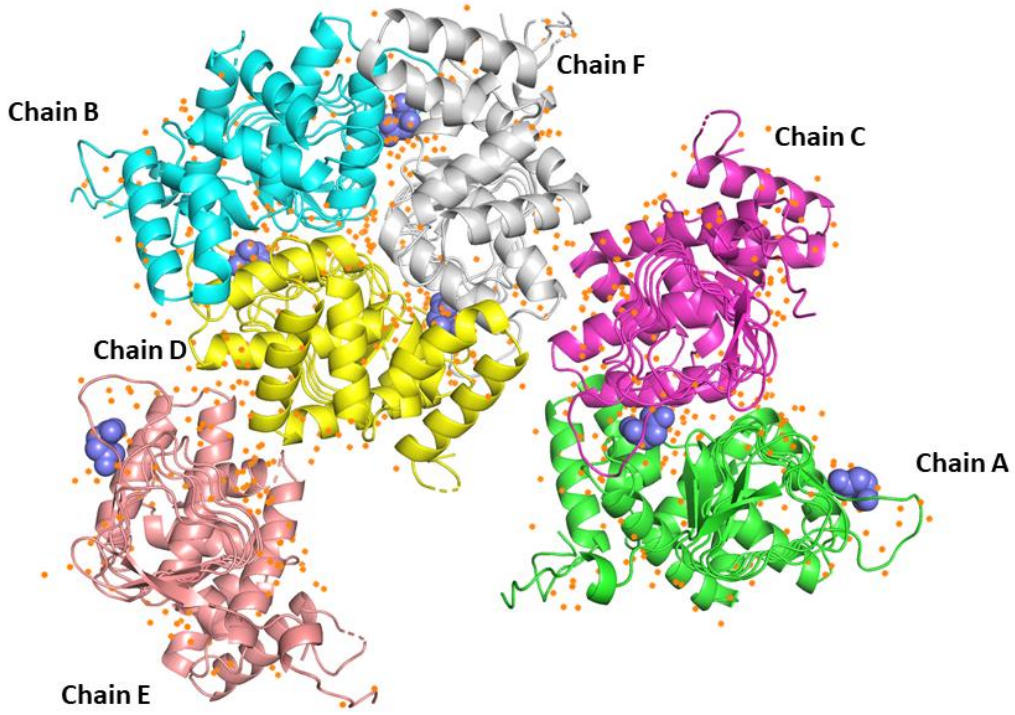

Contents of the asymmetric unit for CysE model. Space group P2. Waters are represented as red crosses. Ligand D-malate is bound in the active site and is represented as purple spheres. Figure generated in PyMOL.

C.4. Input settings for *phenix.autobuild*.

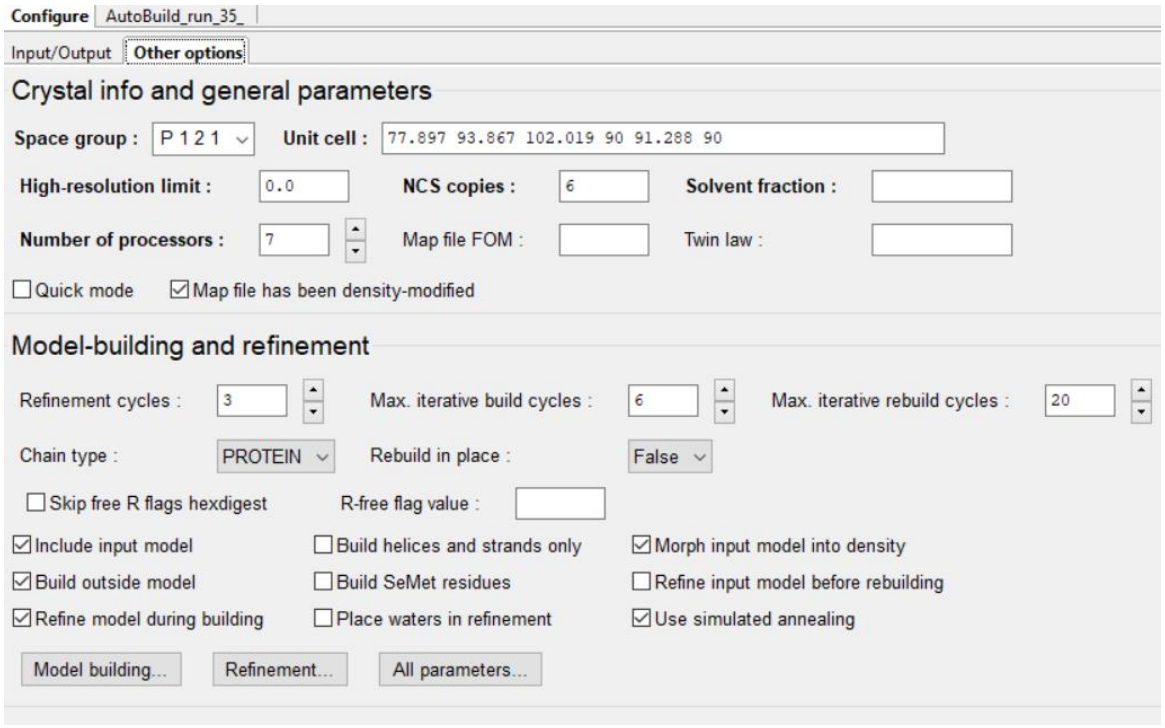

Screenshot of input settings for *phenix.autobuild* used for building the model of CysE.

C.5. CysE structural files

Link to google drive folder:

https://drive.google.com/drive/folders/1lOYqVibWfbxrQQ3OePha1swaKVvIH_25?usp=sharing

C.6. CysE chain statistics

CysE structure statistics for each monomer in the asymmetric unit. Fold of C-terminal tail is reported for each chain.

Chain	Residue chain built	Residues missing	Total built	C-terminal tail
A	Asn4-Gln264	11	261/272	Extended
B	Lys3-Gln264	11	261/272	Extended
C	His5-Gln264	17	256/272	Folded
D	Asn4-Ile263	19	253/272	Folded
E	Asn4-Gln264	12	260/272	Extended
F	Lys3-Gln264	12	260/272	Extended